Utrecht Studies in Earth Sciences 023

Biota-hydrology interactions during the Holocene in Florida

Emmy I. Lammertsma

Utrecht 2012

Utrecht Studies in Earth Sciences

This research was funded by the 'High Potential' stimulation program of the Utrecht University granted to F. Wagner-Cremer, S.C. Dekker and G.-J. Reichart, and financially supported by the LPP Foundation.

USES No. 023
LPP Contribution Series No. 37
ISBN 978-90-6266-311-8
ISSN 2211-4335

Cartography and figures:
Communication & Marketing (8310), Faculty of Geosciences, Utrecht University

Cover: Paynes Prairie Preserve State Park, Florida. Photo by Anneke Wegman.

Printed in the Netherlands by WPS, Zutphen.

Biota–hydrology interactions during the Holocene in Florida

De wisselwerking tussen biota en hydrologie gedurende het Holoceen in Florida

(met een samenvatting in het Nederlands)

Proefschrift

ter verkrijging van de graad van doctor aan de Universiteit Utrecht op gezag van de rector magnificus, prof. dr. G.J. van der Zwaan, ingevolge het besluit van het college voor promoties in het openbaar te verdedigen op vrijdag 26 oktober 2012 des middags te 2.30 uur

door

Emmeline Ilse Lammertsma

geboren op 11 oktober 1982 te Haarlem

Promotoren:	**Prof. dr. H. Middelkoop** **Prof. dr. A.F. Lotter**
Co-promotoren:	**Dr. F. Wagner-Cremer** **Dr. S.C. Dekker**

Members of the dissertation committee

Prof. dr. E.E. Gaiser (Florida International University, USA)
Prof. dr. T.E. Törnqvist (Tulane University, USA)
Prof. dr. J.T.A. Verhoeven (Utrecht University, the Netherlands)
Prof. dr. M.J. Wassen (Utrecht University, the Netherlands)
Dr. D.A. Willard (US Geological Survey, USA)

170 x 240 mm

Contents

General introduction and synopsis

Since the start of the Industrial Revolution in the 19th century the concentration of atmospheric carbon dioxide (CO_2) has been increasing at unprecedented rates, primarily due to the burning of fossil fuel and large-scale land use changes. The concurrent enhanced radiative forcing has already led to altered weather patterns and a global average rising sea level, and these trends will likely continue under ongoing societal and industrial activities (IPCC, 2007). Precipitation patterns in particular will likely become more extreme with less frequent, but more intense, rainfall events and severe droughts (Trenberth et al., 2007). Moreover, tropical cyclones are expected to increase in strength and duration as they are fuelled by increasingly warmer sea surface temperatures (Emanuel, 2005). Recent numerical studies have emphasized the important role of vegetation influencing the climate system and hydrological cycle, as transpiration rates are reduced in response to increased CO_2 (Betts et al., 2007; Cao et al., 2010; Andrews et al., 2011). These studies, however, rely on semi-empirically determined plant responses, and the strength and duration of this plant CO_2-physiological forcing of the climate under decadal-scale CO_2 increase has not been properly quantified yet. As this biosphere-atmosphere interaction can lead to non-linear responses to climatic changes, a better understanding of these physiological feedbacks is essential for our assessments of future change and needs to be considered in addition to changes related to radiative forcing.

Particularly in low-lying and densely populated coastal areas in hurricane-prone regions like Florida (southeastern United States), changes in climate and sea level can have dramatic negative societal and economic consequences. The already increasing pressure on the freshwater availability for agricultural, natural and urban areas makes this area vulnerable to changes in the hydrological regime. Florida has a (sub)tropical climate with generally dry winters and extremely wet summers, characterized by frequent thunderstorms and tropical cyclones. Due to the permeable subsurface composed of sand and (dissolving) limestone, water has a relatively short residence time at the surface. Prior to large-scale human alterations of the landscape, Florida was predominantly vegetated with pine flatwoods and dry pine/oak forests (Davis, 1967). Extensive wetlands developed in areas where the groundwater table reaches the surface, like in the southern peninsula. Overall, minute differences in (ground)water depth, chemical composition of the water, or annual period of inundation (hydroperiod) have led to distinctly different ecosystems (Myers and Ewel, 1990). A better understanding of how these various hydrological conditions will alter under future changes in climate and sea level is of prime importance for maintaining and restoring natural areas, as well as for agricultural and urban planning.

While climate regimes over the recent decades are well-documented in observational and instrumental records, trends on longer timescales need to be deduced using proxy data. During most of the Holocene, the current warm period following the last ice age encompassing

the past 11.7 ka (= calibrated kilo year before present), conditions were comparable to today but far from stable. Long ice-core records suggest that global CO_2 was fairly constant (260-280 ppm) over the Holocene (e.g. Indermühle et al., 1999) (Fig. 1). However, major trends and perturbations in past climate and sea level have been deduced from various natural archives in the Gulf of Mexico and Caribbean Sea region. Regionally, relative sea level rose by tens of meters after the termination of the last glacial (Toscano and Macintyre, 2003; Törnqvist et al., 2004; Milliken et al., 2008). During the early to mid Holocene sea surface temperatures (SSTs) in the Gulf of Mexico were several degrees above present levels (Poore et al., 2003; Nürnberg et al., 2008). Also, the summer position of the 'Intertropical Convergence Zone' (ITCZ) precipitation belt was located further north than at present (Haug et al., 2001) as a consequence of orbitally forced increased summer insolation. The strong teleconnection of peninsular Florida to the El Niño-Southern Oscillation system causes anomalously high winter precipitation during El Niño phases (Cronin et al., 2002). This system has been found to intensify to its modern periodicities from the mid Holocene onwards (Rodbell et al., 1999; Moy et al., 2002).

Investigating how biota and environments adapted to these past changes allows for better prediction of future changes. So far, research has focused predominantly on biotic responses to climatic and sea level changes in the extensive south Florida wetlands and shallow Florida Bay, and in the elevated central Lake Wales Ridge. From peat sections in the southern Florida wetlands, decadal to multi-century scale environmental dynamics reflect wetter and drier conditions during the mid to late Holocene (Willard et al., 2001a; Donders et al., 2005a; Willard et al., 2006; Bernhardt and Willard, 2009; Bernhardt, 2011). On a multi-millennial scale, stadial-interstadial vegetation shifts were reconstructed from pollen in deep sinkhole lake deposits in central Florida, and are thought to be caused by large shifts in precipitation patterns (Watts, 1980; Grimm et al., 1993, 2006; Watts and Hansen, 1994). The spatial distribution and temporal resolution of the available records, however, do not allow for a comprehensive overview of climate vs sea level driven hydrological changes in Florida during the Holocene. This requires a more detailed investigation of sensitive environments at a larger geographical scale.

This research therefore focusses on ecosystems of 'transitional environments', for example estuaries and wetlands, which are highly sensitive to changes in local hydrology. Most biota, or organisms, living there have specific habitat requirements for waterdepth, hydroperiod, salinity, nutrient availability and water currents, which in turn are affected by climate and sea level changes. Some remains of organisms living in, or close to, these environments are well preserved under anoxic aquatic conditions, making peat and estuarine deposits valuable archives of biotic responses to past hydrological changes. The analyses of the organic-walled cysts of marine surface water dwelling dinoflagellates (dinocysts) and of the siliceous frustules of diatoms have proven to be a valuable tool to describe hydrological conditions in the aquatic realm (Marret and Zonneveld, 2003; Smol and Stoermer, 2010). As plants are directly dependent on freshwater availability and have species-specific preferences, vegetation-related proxies based on pollen and leaf cuticles, are particularly suitable for tracing past changes in

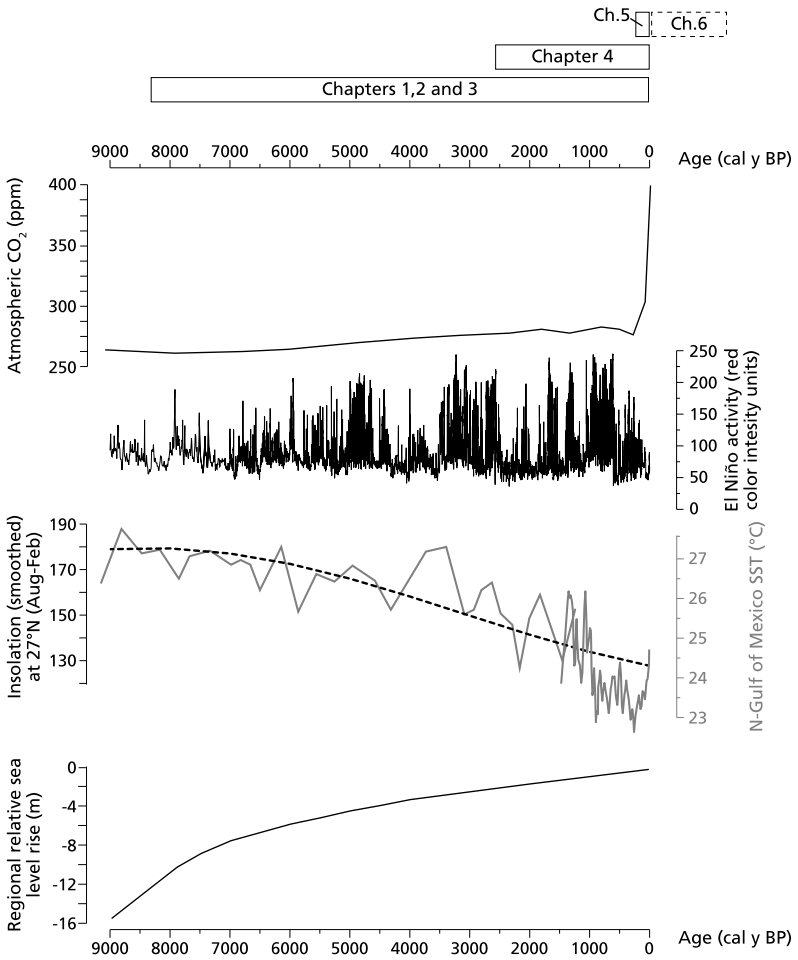

Figure 1. Global and regional forces and responses affecting Florida's climate and hydrology over the Holocene. From bottom to top: the Caribbean relative sea level rise (Toscano and Macintyre, 2003), sea surface temperatures (SSTs) in the northern Gulf of Mexico (Richey et al., 2007; Nürnberg et al., 2008), the difference in insolation at 27°N between the months August and February (dotted line; following Hodell et al., 1991), El Niño activity as reflected in Ecuador lake deposits (Moy et al., 2002) and the atmospheric CO_2 concentrations obtained from Greenland ice-cores (composite IPCC, 2007). At the top, the chapters of this thesis are indicated to give a temporal overview of the timeframes presented by the various studies.

the terrestrial water cycle (Willard et al., 2001b; Wagner-Cremer et al., 2010). Changes in the species assemblage of these organisms over depth of deposits can therefore reflect changing environmental conditions over time. In addition to leaf fragments preserved in peat, analysis of historical plant material of known age and habitat stored in herbaria provide insight into the potential transpiration rates of plants. Applying multiple proxies to describe past environmental change is key to a more robust reconstruction of hydrological variability.

In short, the general objective of this PhD research was to assess the background state of the hydrological regime during the Holocene in Florida, using palynological, micropaleontological and (paleo)botanical proxies. In this dissertation the following questions are addressed: how was the coastal and inland environment affected by the Holocene transgression? Is there a relation between Florida precipitation patterns and regional sea surface temperatures? Is there a pattern in Holocene regional tropical storm activity? What is the strenght and duration of the plant physiological response on climate and the hydrological cycle under rising CO_2?

Chapter 1 shows the environmental changes at Tampa Bay associated with sea level rise during the Holocene that were reconstructed through analyses of biomarkers, pollen, organic-walled dinoflagellate cysts and diatoms. Analyses on mid to late Holocene estuarine deposits show that the site flooded around 7.5 ka (calibrated kiloyears BP), progressively turning a fresh/brackish wet prairie into a shallow lagoonal environment. A shift in dinocyst and diatom assemblages from brackish to more marine taxa, increasing concentrations of marine biomarkers and a shift in the Diol Index indicate a gradually increasing salinity between 7.5 ka and the present. This study further refines other environmental reconstructions from the area (Cronin et al., 2007) by simultaneously investigating changes in the terrestrial and marine environment.

Despite the high environmental detail, the temporal resolution of the multi-proxy study from Tampa Bay is not sufficient to accurately infer possible climate changes during the mid to late Holocene. In Florida, the major transition from oak to pine dominated vegetation around 6.5 ka is interpreted as a large-scale transition from dry to wet conditions (e.g. Watts and Hansen, 1994). The apparent continuous wet conditions, however, seem inconsistent with reconstructions for the Gulf of Mexico and the Caribbean, which indicate a regional drying trend after ~4.5 ka. Additional information on precipitation variability in Florida is needed to better interpret the mid to late Holocene pine phase. In **Chapter 2** we build upon recently published detailed lithological and biomarker records from Charlotte Harbor (Van Soelen et al., 2012), to simultaneously study both regional vegetation changes and runoff patterns associated with precipitation. The substantial reduction of oak in the pollen record from ~7 ka concurs with increased runoff, as indicated by rising pollen accumulation rates and the presence of dinocyst *Lingulodinium machaerophorum*, which is considered indicative of high nutrient input and stratified water conditions. A strong reduction in the input of terrestrial material from ~4.5 ka suggests reduced precipitation, whereas increased *L. machaerophorum* from ~2.8 ka onwards again suggests higher runoff. Although the Charlotte Harbor runoff record is not conclusive about the timing and strenght of the processes controlling hydrological conditions on land, the pine vegetation development was likely the result of a complex interplay of sea level rise, precipitation and landscape dynamics over the mid to late Holocene.

In Tampa Bay and Charlotte Harbor, described in Chapters 1 and 2, distinct layers of coarse sediment (sand and shells fragments) occur in the generally fine-grained deposits. These are commonly interpreted as high energy conditions that resulted from peak runoff and storm surges, and thus possibly reflect past tropical storm occurrences. However, depositional conditions change over long timescales due to landscape dynamics and the relative sea

level rise, potentially causing the record of past storm occurrences to become incomplete. **Chapter 3** describes how this issue was overcome by complementing the lithological records with dinocyst records, which reflect hydrological changes (e.g. water column mixing) due to increased wind/wave energy, and hydrogen isotope ratios in terrestrial organic material, which reflect changes in the isotopic composition of rainwater. Besides clusters of coarse layers, increased abundances of marine dinocysts in an otherwise lagoonal environment are observed, and occur simultaneous with lighter hydrogen isotopes in terrestrial plant leaf waxes. The agreement of the palynological records at two separate sites shows that the observed changes were caused by forces acting on a large scale. Combined lithological, palynological and geochemical evidence indicates periods with increased tropical storm occurrences between ~6.4-5.5 ka, ~5.0-4.0 ka and ~3.2-1.9 ka, broadly consistent with other records in the Gulf of Mexico and Caribbean region. Millennial-scale shifts in the position of the Bermuda High are suggested to determine this regional pattern. This study shows that a more complete record of past storm occurrences can be obtained by analyzing multiple sensitive proxies at multiple sites.

The palynological records from inland lakes and the above-described estuaries reflect large-scale changes in vegetation cover and runoff patterns. However, they are less suited for tracking small scale hydrological variability. Palynological records from wetlands in southern Florida have shown that these environments are highly sensitive to minor changes in local hydrology associated with precipitation changes, but there is some disagreement among the records for the late Holocene. To establish regional hydrological patterns for this period more detailed information is needed from wetlands in the elevated Lake Wales Ridge which so far have not been thoroughly explored. In **Chapter 4** records of hydrological changes over the past ~2.5 ka are presented, inferred from pollen and diatom analyses on two peat cores from Highlands Hammock State Park, central Florida. The initiation of wetland conditions at ~2.5 ka indicates a first increase in humidity after which a general trend to drier conditions is observed that is likely related to natural wetland succession patterns. During the overall drying trend, the increasing presence of aquatic taxa indicates temporary wetter conditions between 1.3-1.0 ka. Both the initiation of the wetland and the intermittent wet phase seem forced by increased precipitation, which in turn is likely related to regionally higher sea surface temperatures and a temporary northward migration of the Intertropical Convergence Zone. The second wet phase and subsequent drier conditions over the last millennium, as indicated by shifts in both pollen and diatom assemblages, can be linked to the early Medieval Warm Period, and the later Medieval Warm Period and Little Ice Age, respectively. Distinct changes in both vegetation and diatom assemblages during the 20th century are the result of the construction of moats and dikes intended to protect the Highlands Hammock State Park from wildfires.

In the first 4 chapters, climatic variability was reconstructed based on the biotic response to hydrological changes. Land plants play a crucial role in regulating our planet's hydrological and energy balance by transpiring water through the stomatal pores on their leaf surfaces. A principle response of C3 plants to increasing concentrations of atmospheric CO_2 is to reduce transpirational water loss by decreasing stomatal conductance and simultaneously increasing

assimilation rates. Therefore, it is important to determine the adaptation of vegetation to the expected anthropogenic rise in CO_2. To date, the effects of decadal to centennial CO_2 perturbations on stomatal conductance are still largely unknown. In **Chapter 5,** it is shown that a 34 (± 12)% reduction in maximum stomatal conductance per 100 ppm CO_2 increase has occurred as a result of the adaptation in stomatal density and pore size at maximal stomatal opening of nine common plant species from Florida over the past 150 years. The species-specific maximum stomatal conductance values are determined by different evolutionary development. Although angiosperms and conifers use different adaptation strategies, the data show a coherent response in maximum stomatal conductance to CO_2 rise of the past century. The mechanisms of optimization of carbon gain to water loss described here could be used to better estimate this physiological forcing for the past and future CO_2.

Estimates of the strength and duration of this plant physiological CO_2 forcing of the studied species under continued CO_2 rise are given in **Chapter 6**. For this purpose, models are developed and validated that simulate structural stomatal adaptations based on diffusion of CO_2 and water vapor through stomata, photosynthesis, and optimization of carbon gain under the constraint of a plant physiological cost of water loss. The model adequately reproduces observed structural stomatal adaptations and predicts that adaptation will continue beyond double CO_2 until the limits of species-specific phenotypic plasticity is reached. Simulations predict that a doubling of present CO_2 will lead to a significant reduction of approximately 50% of the annual transpiration flux from the Florida subtropical vegetation. We conclude that plant adaptation to rising CO_2 is substrantially altering the freshwater cycle and climate and will continue to do so the forthcoming centuries.

N.B. The chapters of this thesis are or will be published as separate papers in scientific journals. As a consequence, some repetition of statements cannot be avoided.

Chapter 1

Late Holocene sea level rise in Tampa Bay: integrated reconstruction using biomarkers, pollen, organic-walled dinoflagellate cysts and diatoms

Abstract

A suite of organic geochemical, micropaleontological and palynological proxies was studied in sediments from southwest Florida, to determine environmental changes associated with Holocene sea level rise. Sediments were recovered from Hillsborough Bay, part of Tampa Bay, and studied using biomarkers, pollen, organic-walled dinoflagellate cysts and diatoms. Analyses show that the site flooded around 7.5 ka as a consequence of the Holocene transgression, progressively turning a fresh/brackish marl-marsh into a shallow, restricted marine environment. Immediately after the marine transgression started, limited water circulation and high amounts of runoff caused stratification of the water column. A shift in dinocysts and diatom assemblages to more marine species, increasing concentrations of marine biomarkers and a shift in the Diol Index indicate increasing salinity between 7.5 ka and the present, which is likely a consequence of progressing sea level rise. Reconstructed sea surface temperatures for the past 4 kyrs are between 25 and 26°C, and indicate stable temperatures during the late Holocene. A sharp increase in sedimentation rate in the top ~50 cm of the core is attributed to human impact. The results are in agreement with parallel studies from the area, but this study further refines the environmental reconstructions having the advantage of simultaneously investigating changes in the terrestrial and marine environment.

1. Introduction

Holocene sea level rise shaped the low-lying Gulf Coast of Florida into its present day appearance. Sea level studies for this region suggest a transgression over the past 10 kyrs, although there is a contrast between studies showing decelerating rates over the past 5000 years (Scholl and Stuiver, 1967; Törnqvist et al., 2004) and studies showing a mid or late Holocene sea level highstand (Goodbred et al., 1998; Blum et al., 2001; Törnqvist et al., 2004). Detailed studies of the impact of Holocene sea level rise can be used for improving our understanding of the environmental implications associated with the modern and forecasted sea level rise. Multi-proxy studies are a valuable tool for paleo-environmental reconstructions, especially when they combine marine and terrestrial environmental information.

Pollen provides a valuable proxy for environmental reconstructions because of its good preservation, abundant presence in most terrestrial and marine sediments and its sensitivity to changes in southwest Florida's hydrological cycle (Donders et al., 2005a,b; Willard et al., 2007). Pollen abundances reflect regional vegetation development and, in marine records, also record variations in runoff rates. Nearby coastal vegetation can further influence the signal (Donders et al., 2008). Facies changes as a result of sea level fluctuations can also affect the pollen signal by altering the depositional setting, as is evident in the lateglacial from the southwestern Florida Tampa Bay record (Willard et al., 2007).

Diatoms and dinoflagellates thrive in offshore waters and their remains (e.g. diatom frustules and organic-walled dinoflagellate cysts, or dinocysts) have been found in surface sediments of Florida shallow marine environments such as Rookery Bay (Cremer et al., 2007). Relative species distributions of these groups can be used to reconstruct amongst others: sea surface salinity, stratification and productivity (Laws, 1988; Marret and Zonneveld, 2003; Sangiorgi et al., 2006; Van der Meer et al., 2008).

Another valuable proxy for environmental reconstructions is biomarkers. These geochemical fossils are specific compounds, mostly lipids, which can be linked to their organic precursors and can preserve over long geological time scales (Killops and Killops, 2005). Biomarkers derive from plants and trees but also from micro-organisms like dinoflagellates, diatoms, coccolithophores, and are therefore ideally suited to link the terrestrial and marine environment. Terrestrial biomarkers can provide information on changes in hydrology like increased runoff. Marine biomarkers are often used for the reconstruction of variables such as sea surface temperature (Prahl and Wakeham, 1987), salinity (Versteegh et al., 1997) and productivity (Sachs and Anderson, 2005). Hence, combining biomarkers with terrestrial and marine microfossil records makes the environmental reconstructions more robust.

One of the largest estuaries in southwest Florida is Tampa Bay, which consists of interconnected bays and lagoons with shallow water depth. In 2004, a ~5 m continuous Holocene record was recovered from Hillsborough Bay, part of Tampa Bay (Cronin et al., 2007). A shift in sediment

and microfossil content around 7 ka was interpreted as a transition from a lacustrine to an estuarine environment, as a consequence of post-glacial sea level rise (Cronin et al., 2007). The rise in sea level is estimated to be about 7.5 – 8 m over the last ~7 kyrs at this site (Cronin et al., 2007). Here we build upon the initial study by Cronin et al. (2007) by applying a suite of organic geochemical and micropaleontological proxies to gain detailed environmental information from the terrestrial and the marine environment during Holocene sea level rise.

2. Material and methods

2.1 Material

Hillsborough Bay core TB-04-VC-77 (Fig. 1) was collected in summer 2004, by the U.S. Geological Survey in cooperation with Eckerd College and the University of South Florida, with a vibracorer deployed from the R/V Gilbert. The core comprises 511 cm of sediments collected at a water depth of ~4 m in a 6 m long by 7.6 cm wide aluminium barrel. Based on the down core changes in sediment colour, 10 samples were selected and freeze–dried (Fig. 1). These samples were split for the different analytical techniques, allowing direct comparison of proxies and results. Depths are relative to the core top and reported in cm below sea floor (cmbsf).

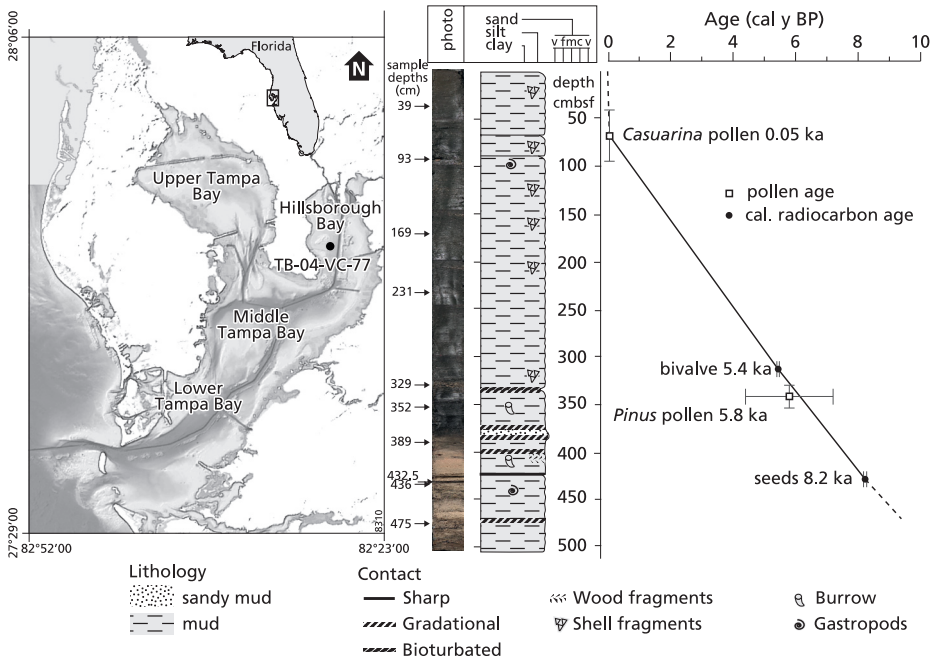

Fig. 1. On the left: map of Tampa Bay region and location of core TB-04-VC-77 (modified from Tyler et al., 2007). At the right: core photo and core log (modified from Cronin et al., 2007) and constructed age model.

2.2 Age model

The age model is constructed using two linearly interpolated radiocarbon dates (Cronin et al., 2007) and pollen biostratigraphical ages (Fig. 1). Radiocarbon ages are based on *Polygonum*-seeds (depth: 4.28 m, age: 8223 cal y BP ± 50 y), and *Mulinia* sp. shells (depth: 3.1 – 3.15m, age: 5441 cal y BP ± 40 y) and were calibrated using atmospheric and marine corrections (CALIB 5.0.2, http://calib. qub.ac.uk/calib/) (Cronin et al., 2007). *Casuarina* (Australian pine) has its first occurrence between samples 93 and 39 cmbsf. It is an exotic plant introduced to the Florida peninsula around 1900 AD (Alexander and Crook, 1974), corresponding with a pollen-age of ~50 y BP (i.e. before 1950). A strong expansion of *Pinus* between sample depths 352 and 329 cmbsf is dated between 7.2 and 4.4 ka based on regional correlation (Watts, 1969, 1971, 1975, 1980; Watts and Hansen, 1994). According to the age model, the sediments represent approximately the last ~10 kyr, presuming deposition rates of 0.04 cm/y to ~0.3 cm/y based on this core and previous studies (Brooks, 2011).

2.3 Biomarkers

Extracts were obtained from ca 1.5 – 6.5 g of freeze–dried and powdered sediments, using an ultrasonic homogenizer (Branson sonifier 250 Analog) and a solvent mixture of dichloromethane (DCM) and methanol (MeOH) (2:1 v/v). Samples were ultrasonically stirred 5 times for 3 min. Resulting extracts were combined and rotary-evaporated under near vacuum to remove solvents. Extracts were treated with activated copper to remove elemental sulfur. Traces of water were removed with sodium sulfate. Quantification of compounds was performed on gas chromatograms of total lipid fractions (TLFs). Extracts were treated with diazomethane to convert fatty acids into methyl esters and with N.O-Bis(trimethylsilyl) trifluoroacetamide (BSTFA) to convert alcohols into trimethylsilyl (TMS) ethers. Extracts were separated into three fractions of different polarity to enable identification of compounds with relative low concentrations. An aliquot of the total extracts (~80%) was separated over a column with activated aluminum oxide using solvent mixtures hexane:DCM (9:1 v/v), DCM and DCM:MeOH (1:1 v/v), resulting in, respectively, a fraction containing alkanes, alkenes and aromatics, a fraction containing aldehydes and ketones, and a fraction containing polar compounds.

Gas chromatography (GC) was performed using an HP Gas Chromatograph fitted with a CP-Sil 5CB fused silica capillary column (30m x 0.32 mm i.d.) and a flame ionization detector (FID). A flame photometric detector (FPD) was used to check for elemental and bound sulfur. Samples were injected on-column, with helium as carrier gas set at constant pressure (100 KPa). The oven was programmed starting at 70°C, heating by 20°C/min up to 130°C, by 4°C/min up to 320°C and then kept at this temperature for 20 min. Mass spectrometry (GCMS) was performed using a ThermoFinnigan Trace GCMS with the same type of column and oven program as used for the GC. Compounds were identified using retention times and mass spectra. Quantification of compounds was performed by peak area integration in FID chromatograms relative to a standard (squalane) which was co-injected with TLF.

Total organic carbon (TOC) content of sediment samples was determined with a FisonInstrumentNA1500NCS analyzer, on samples treated with HCl to remove inorganic carbon. The alkenone unsaturation index (UK'(37)) was calculated, based on the relative abundances of C37 alkenones with 2 or 3 double bonds (Prahl and Wakeham, 1987), which were present in the fraction containing aldehydes and ketones.

$$U^{K'}_{37} = [C37:2]/[C37:2+C37:3] \quad (1)$$

Sea surface temperatures were calculated using the global calibration of Müller et al., (1998).

$$U^{K'}_{37} = 0.033 \cdot T + 0.069 \quad (2)$$

A diol index (DI) was calculated based on relative abundances of C_{30}- and C_{32}- 1,15 diols (Versteegh et al., 1997), present in the TLF.

$$\text{Diol index} = 100 \cdot [C_{30}\text{1,15 diol}]/([C_{32}\text{1,15 diol}]+[C_{30}\text{1,15 diol}]) \quad (3)$$

2.4 Palynology

Sediments for palynological analysis were dried, weighed, and treated following standard methodology (Wood et al., 1996). Prior to processing *Lycopodium clavatum* tablets with known amount of spores were added to the samples in order to be able to calculate concentration values. Treatment included the removal of carbonates with hydrogen chloride (HCl) (30%), and silicates with hydrogen fluoride (HF) (40%). Coarse and fine material was removed from the samples using sieves with a 250 mm and 10 mm mesh, respectively. The residues were mixed with glycerine and mounted on glass slides for analysis using a Leitz light microscope (x400 magnification). Pollen was identified following Willard et al. (2004). Identification of dinoflagellate cysts (dinocysts) was based on Rochon et al. (1999), Marret and Zonneveld (2003), Fensome and Williams (2004), Cremer et al. (2007). The abundance of pollen and dinocysts is calculated relative to the total sum of pollen and dinocysts, respectively. Identified plant and tree taxa are grouped into 'marsh' and 'upland' vegetation according to their highest abundance in these vegetation types (Myers and Ewel, 1990; Willard et al., 2001b; Willard et al., 2006).

2.5 Diatoms

Diatom samples were treated with HCl and hydrogen peroxide (H_2O_2) to dissolve carbonate and organic matter. Diatom were settled on coverslips using sedimentation trays (Battarbee, 1973), and Naphrax® was used to mount the cover slips on slides. Identification is based on floras published by Hustedt (1930 – 1966), Hustedt, (1955), Witkowski et al. (2000), and Cremer et al. (2007). In general, up to 200 diatom valves were counted on each slide. Groups of polyhalobous and mesohalobous diatoms were made, based on the salinity tolerance of each species (Laws, 1988).

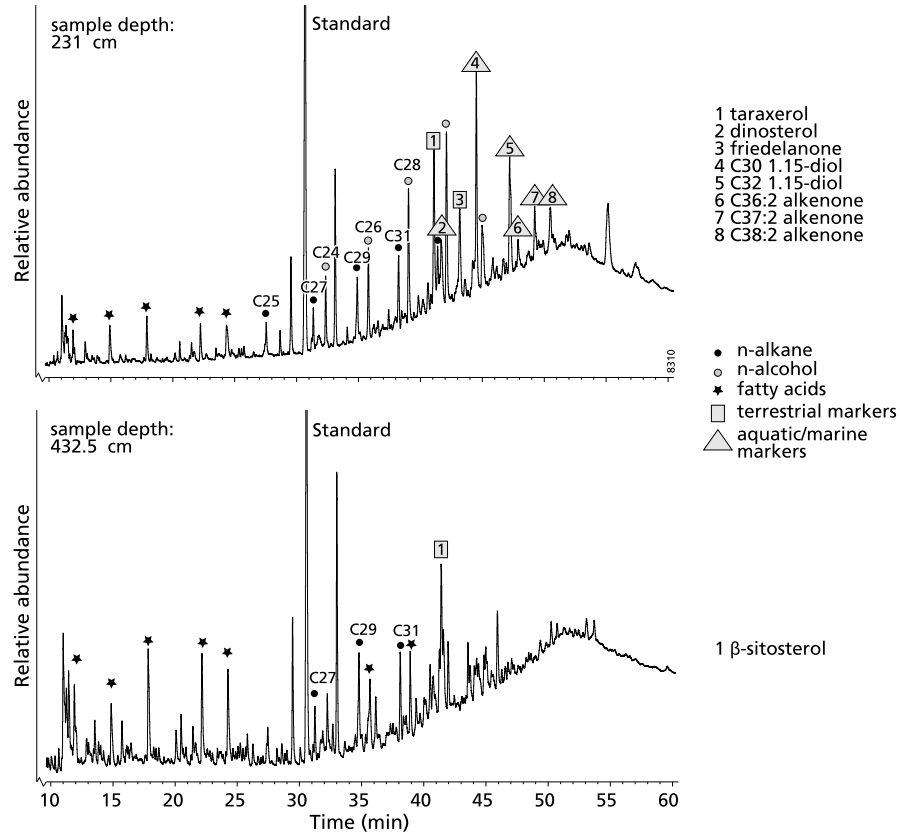

Fig. 2. Partial gas chromatograms (10 – 60 min) of total lipid fractions of samples 231 cmbsf (top) and 432.5 cmbsf (bottom).

3. Results

3.1 Biomarkers

Based on biomarker assemblages, the core can be divided into an upper section (above ~400 cmbsf) of which an example of a TLF GC trace is presented in Fig. 2A, and a lower section (below ~400 cmbsf) for which an example of a TLF GC trace is presented in Fig. 2B. Concentration profiles (in mg/g TOC) of most abundant biomarkers and biomarkers which can be related to specific environmental conditions are presented in Fig. 3.

The steroid β-sitosterol is most abundant in the lower section and concentrations vary between 8 and 14 mg/g TOC. Taraxerol is also present in this lower section albeit in low amounts (up to 2 mg/g TOC). Between 432.5 and 352 cmbsf there is a strong increase in concentrations of taraxerol, friedelanone, dinosterol and C_{30} 1,15- diol, all reaching maximum values at 352

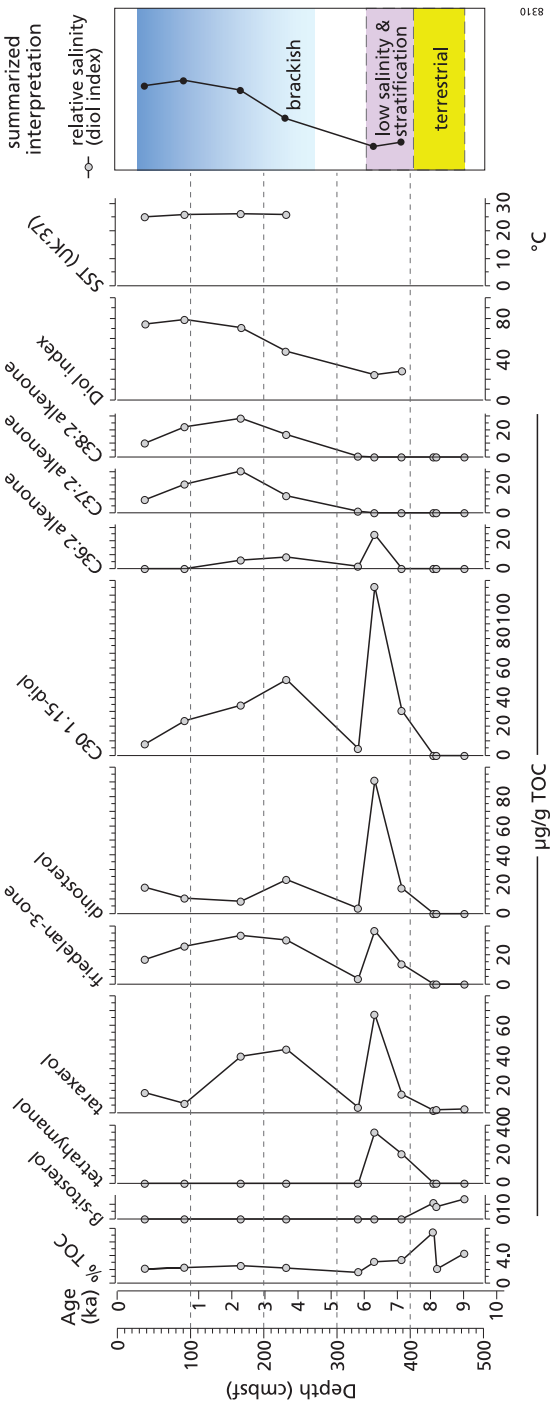

Fig. 3. Biomarker concentration profiles; concentration of biomarkers are presented in mg/g TOC. Percentage TOC is presented at the left, reconstructed SST in °C based on paleothermometer UK'(37), the Diol Index and summarized interpretations are presented at the right.

cmbsf. Above this depth level, concentrations of these biomarkers generally decrease. In the sample at 329 cmbsf concentrations are extremely low (between 3.5 and 5 mg/g TOC). The C_{36} alkenone has a similar concentration profile; however, it disappears from the record from 93 cmbsf upward. Long-chain C_{37} and C_{38} alkenones were absent in the lower part of the core and first recognized at a depth of ~329 cmbsf. Subsequently, concentrations first increase up to 169 cmbsf and then decrease again. Tetrahymanol was only present in samples 389 and 352 cmbsf. Calculation of UK'(37) resulted in values between 0.9 and 0.93, corresponding to temperatures between 25 and 26.2°C. The Diol Index is 28 at 389 cmbsf and 25 at 352 cmbsf, increases up to 48 at 231 cmbsf and in the upper part increases to >70, with a maximum of 97 at 93 cmbsf. At sample depth 329 cmbsf, concentrations of C_{30} and C_{32} 1,15-diol were too low to be quantified, and the Diol Index could not be calculated for this depth.

3.2 Pollen

In general, the samples were rich in pollen and a large diversity of plant and tree taxa could be distinguished. Based on the overall changes the record can be subdivided into two distinct zones: TB-I and TB-II (Fig. 4).

Pollen zone TB-I. Amaranthaceae – *Quercus* zone (475 – 340 cmbsf). This zone is characterized by a variety of herbaceous taxa, of which Amaranthaceae is dominant with values up to 80% at 432.5 cmbsf, after which it decreases to 23%. Simultaneous with maximum Amaranthaceae values, *Hydrocotyle* and Cyperaceae are most abundant, with maximum values of 14% for both. Following this, Poaceae (maximum of 7%), *Ambrosia* and Asteraceae Tubuliflorae and Asteraceae *Iva*-type (maximum of 4%) are most abundant. Of the trees, *Quercus* is dominant, comprising up to 42% in the top of this zone. Other woody taxa found are *Carya* and *Morella cerifera* (~3%), and *Ulmus, Fraxinus, Ostrya* and *Nyssa* (<1%), which are common in inland forests. With values up to 14%, *Pinus* is the second most abundant tree in this zone. *Taxodium* pollen does not exceed 3% of the assemblage. Mangrove taxa *Rhizophora* and *Avicennia* are present from 432.5 cmbsf up, albeit with values below 1%.

Pollen zone TB-II. Pinus zone (340 – 39 cmbsf). A distinct shift to mainly *Pinus* at ~340 cmbsf marks the transition to the next zone, comprising up to 83% of the total assemblage. *Quercus* shows a strong decrease compared to the previous zone, but remains co-dominant (7 – 25%). Other tree and shrub taxa that are found do not exceed 3%. *Liquidambar* occurs for the first time in this zone, albeit with values around 1%. The different herbaceous pollen types are practically absent in this zone (<2%), with the exception of Amaranthaceae comprising up to 7%. The bulk of the herbaceous taxa are generally found in marsh environments, whereas the identified woody taxa (with exception of mangrove species and swamp species like *Taxodium*) are most common in drier upland sites (Myers and Ewel, 1990; Willard et al., 2006). Shifts in the general abundance of the two groups are given in a summarizing diagram (Fig. 4), in which *Pinus* is given separately due to its expected remote origin. The total pollen concentration appears to be fairly constant throughout the core (~4 – $10{\cdot}10^4$ grains/g dry sediment), with exception of two samples. At depth 432.5 cmbsf concentrations are more than doubled,

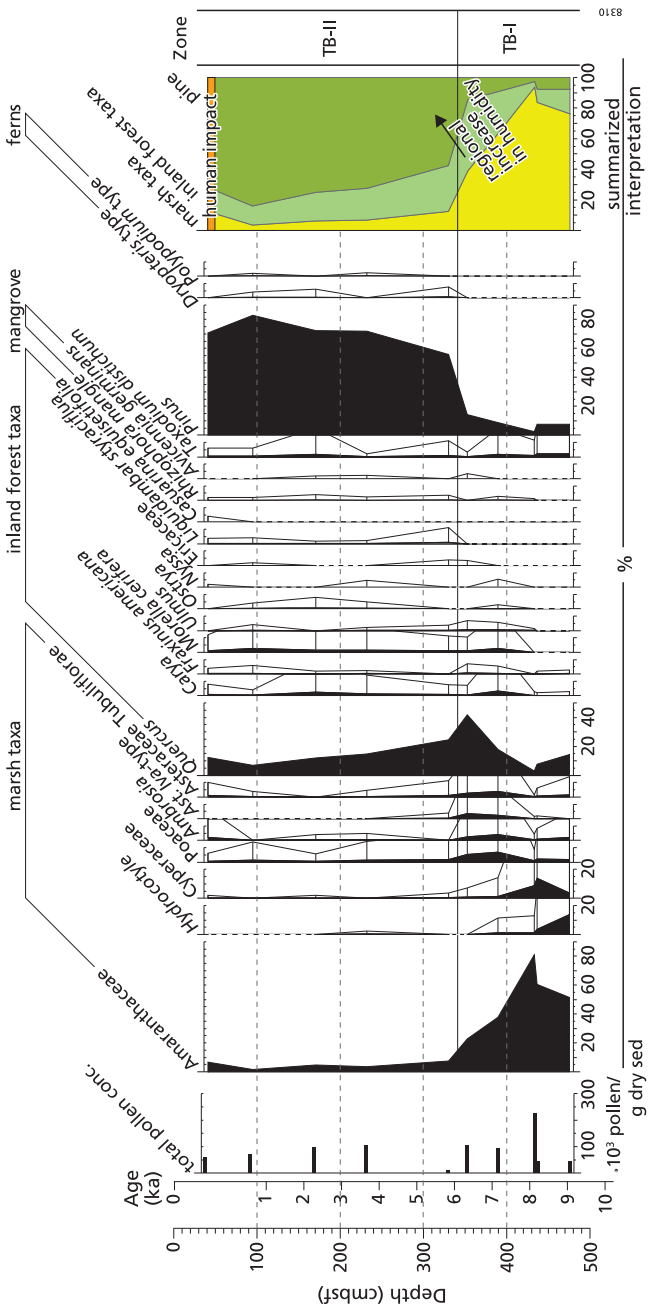

Fig. 4. Pollen percentage diagram; percentages are calculated relative to the total pollen sum. The depth bar areas in the diagram express a 10x exaggeration of the values for taxa with a low abundance. Total pollen concentrations in pollen per gram sediment. At the far right a composite diagram presents shifts in main vegetation communities and summarized interpretations.

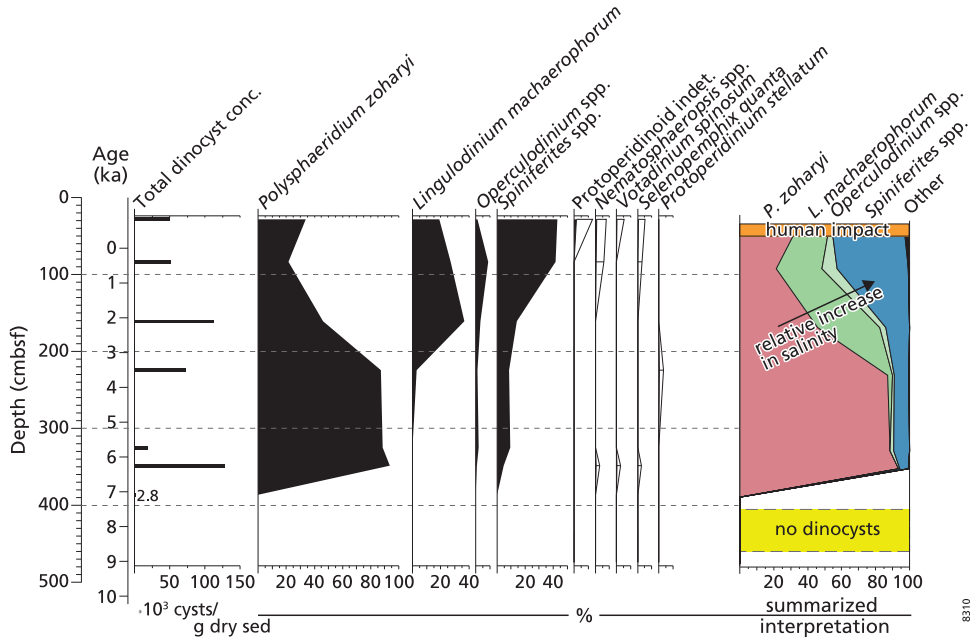

Fig. 5. Dinocysts percentage diagram; percentages are calculated relative to the total dinocyst sum. The depth bar areas in the diagram express a 10x exaggeration of the values for groups with a low abundance. Total dinoflagellate concentrations are presented in dinocysts per gram sediment. The summary column on the right hand side of the figure shows the major changes as inferred from the dinocysts.

mainly caused by the high abundance of Amaranthaceae pollen in this sample. A very low concentration (~1·10^4 grains/g dry sediment) is found at 329 cmbsf.

3.3 Dinoflagellate cysts

Relative abundances of the most frequently observed dinocysts are shown in Fig. 5. From the bottom of the sediment core up to 389 cmbsf no dinocysts are found. At 389 cmbsf cysts are rare, and their number is too low (11 cysts) to be considered for the reconstructions. Between 352 cmbsf and the core-top dinocysts are very abundant and their concentrations vary between ~4 and ~25·10^4 cysts/g dry sediment. The highest concentrations are found in the lower section, between 352 and 169 cmbsf, with exception of a minimum found at 329 cmbsf (~4·10^4 cysts/g dry sediment). *Polysphaeridium zoharyi, Lingulodinium machaerophorum* and *Spiniferites* spp. are the most represented species in the assemblages. *P. zoharyi* represents about 90% of the assemblages between 352 and 231 cmbsf. Above, the relative abundance drops and the minimum value is reached at 93 cmbsf. The upper part of the core shows again a slight increase. With the decrease of *P. zoharyi* between 231 and 169 cmbsf, relative abundances of *L. machaerophorum* and *Spiniferites* spp. increase. *L. machaerophorum* reaches its maximum

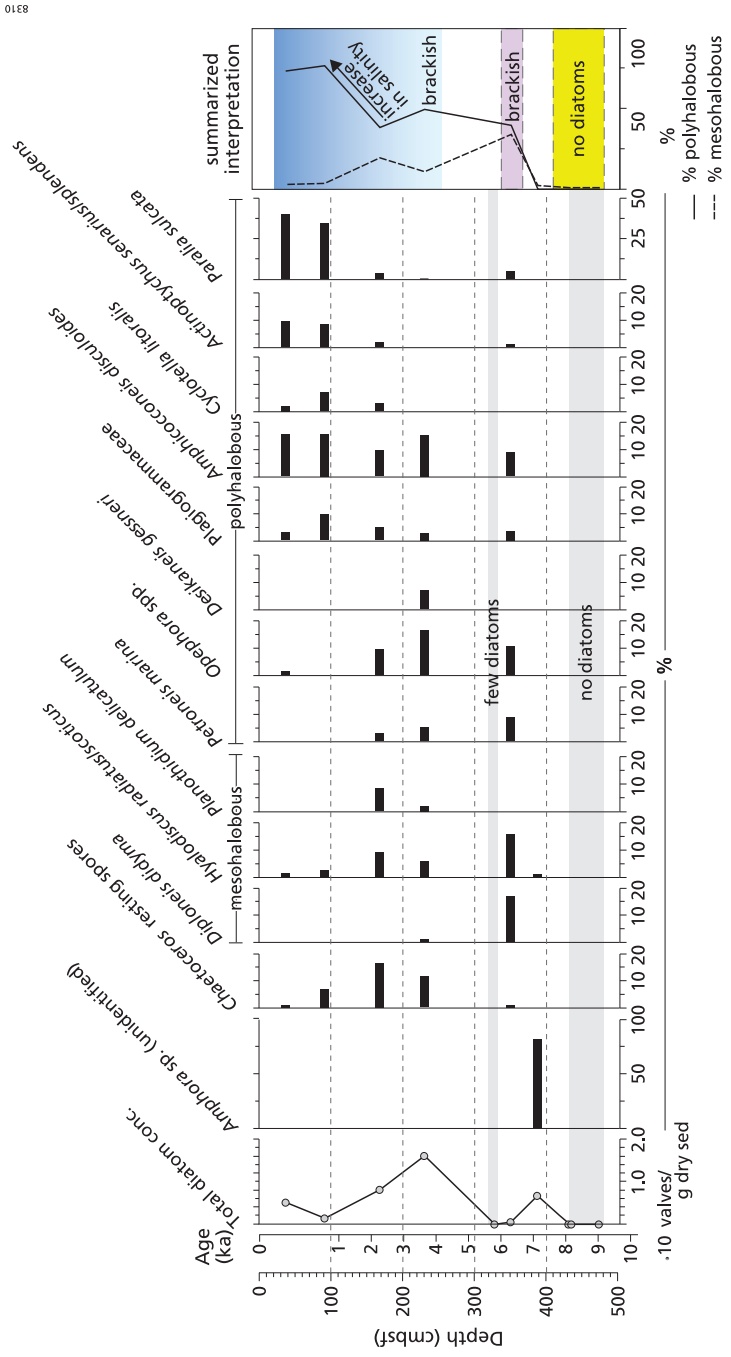

Fig. 6. Diatom percentage diagram; percentages are calculated relative to the total diatom sum. Total diatom concentrations are presented in valves $\cdot 10^6$ per gram sediment. The summary column on the right presents the ratio between polyhalobous and mesohalobous species and the interpretation.

of 37% at 169 cmbsf, and then slightly decreases in the upper part of the core. *Spiniferites* spp. increases up to values of about 40% in the upper part of the core. Other taxa found are rare and not persistently present in the core. Only *Operculodinium* spp. has been found throughout the core and shows a peak relative abundance of about 9% at 93 cmbsf.

3.4 Diatoms

Diatom preservation is generally moderate, and occasionally poor as valves are strongly corroded and sometimes only fragments are present. Diatoms are abundant from sample depth 389 cmbsf up, with exception of sample depth 329 cmbsf, which was barren. Diatoms with highest abundances are presented in Fig. 6. The diatom assemblage at 389 cmbsf consists of more than 80% of an *Amphora* species for which further identification was not possible (Fig. 6). It resembles the marine-brackish species *Amphora gacialis*, a species of which the ecology and distribution is not well known. Following the *Amphora*-spike, the diversity in diatoms becomes wider. Between 352 and 169 cmbsf, dominant species are *Diploneis didyma, Hyalodiscus radiatus* and *Hyalodiscus scoticus, Planothidium delicatulum, Petroneis marina, Opephora* spp. and *Desikaneis gessneri*. Between samples 169 and 39 cmbsf, *Plagiogrammaceae, Amphicocconeis deculoides, Cyclotella litroalis, Actinophtychus senarius, Actinoptychus splendens* and *Paralia sulcata* are dominant. Between 7 and ~2 ka, polyhalobous diatoms comprise about 50% of the total diatom assemblage. From ~2 ka onwards, polyhalobous species increase relative to mesohalobous species up to 80%.

4. Paleo-environmental reconstruction

4.1 Early-Holocene terrestrial environment

Vegetation in the early-Holocene (500 – 400 cmbsf, ~10 – 7.5 ka) was dominated by a variety of herbaceous taxa commonly found in fresh and brackish water marshes. β–Sitosterol is the dominant biomarker in this part of the core. It is a non-specific phytosterol generally found in vascular plants (Scheuer, 1973; Nes, 1974; Killops and Killops, 2005), and since its concentration profile is comparable to abundance profiles of *Hydrocotyle*, Cyperaceae and Amaranthaceae, here it seems mainly derived from herbs. The pinkish white to pale brown mud in this basal part of the record, dominated by non-marine ostracodes and molluscs, was interpreted by Cronin et al. (2007) as lacustrine. Considering these deposits and the found pollen assemblage the site can more specifically be indicated as a wet prairie or marl marsh (Willard et al., 2001b, 2006). The absence of diatoms in this section can possibly be the result of poor preservation of these fossils in this type of environment (Fig. 7).

The transition in marsh taxa between 9.5 and 6.5 ka, from *Hydrocotyle*/Amaranthaceae/Cyperaceae dominance to Poaceae/Asteraceae Tubuliflorae and Asteraceae *Iva*-type (likely *I. frutescens*), which is a common shrub in coastal saline wetlands, is indicative for increasing salinities at the site. This trend is confirmed by the first occurrence of mangrove vegetation (*Rhizophora mangle*) around 7.5 ka, which suggests a change from an inland to a more coastal

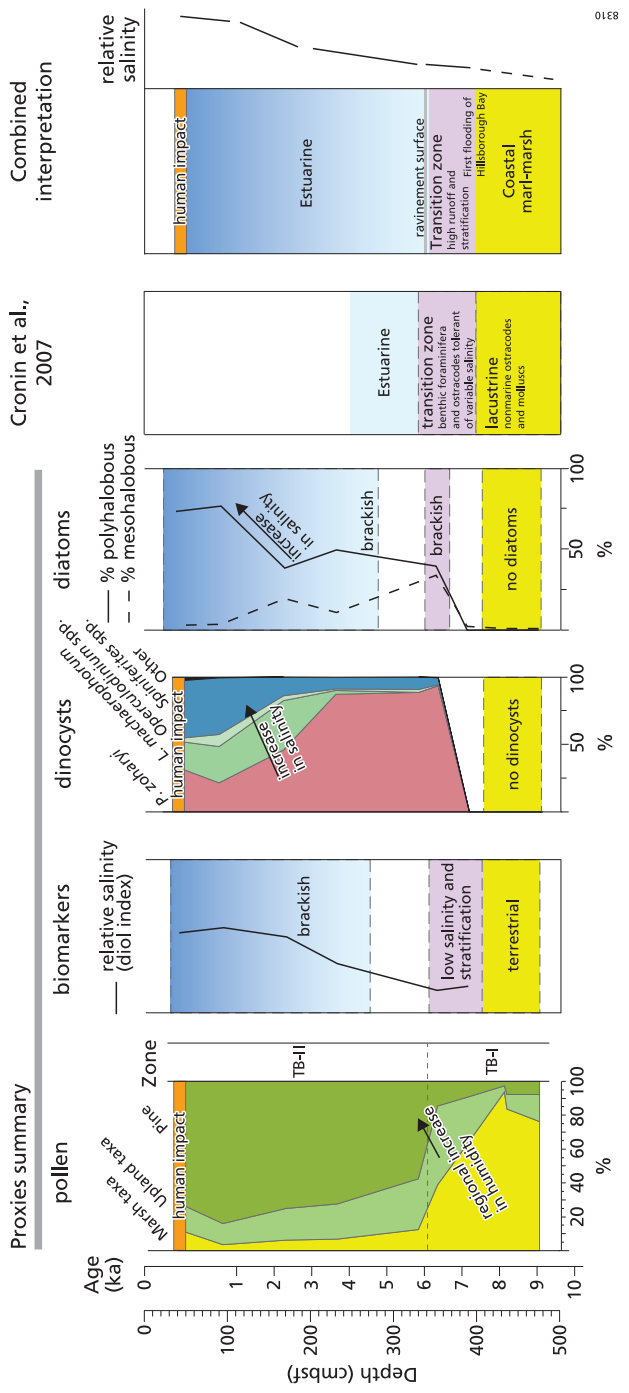

Fig. 7. The graphs show the summarized interpretation for each proxy. A summarized interpretation of the study by Cronin et al. (2007) is also presented. On the far right is the combined interpretation based on the multiple proxies and results by Cronin et al. (2007).

setting and further increasing salinities. *Rhizophora* pollen are small and they may be partly lost during sieving (Marret et al., 2001). This does not, however, necessarily affect the trend in the pollen curve (Versteegh et al., 2004). Absence of mangrove pollen before ~7.5 ka might indicate that the low levels of taraxerol that were detected in this part of the core originate from vascular plants other than mangroves (Versteegh et al., 2004, and references therein). The variety of upland tree pollen found in this period originate from long-distance transport, as this site was probably part of an extensive marsh with little or no upland vegetation in the area. The dominance of *Quercus* between 9.5 and 6.5 ka is in agreement with findings from inland lake records (Watts, 1969, 1971, 1975, 1980; Watts and Hansen, 1994) and was interpreted as indicative of relative aridity in Florida (Watts and Hansen, 1994).

4.2 Mid and late Holocene marine transgression

Hillsborough Bay initially flooded around 7.5 ka. Mid and late Holocene deposits (400 cmbsf – top, 7.5 ka – present) contain terrestrial as well as aquatic remains like diatoms, dinocysts and biomarkers such as dinosterol and alkenones. The period between 7.5 and 6 ka is characterized by relative high amounts of the biomarker tetrahymanol, which derives from ciliates and is indicative for water column stratification (Sinninghe Damsté et al., 1995). Between ~7 and 4 ka, up to 95% of the dinocyst assemblage is composed of *P. zoharyi*. This species is euryhaline, and can be found in warm and extremely stratified sea surface water environments (Marret and Zonneveld, 2003; Reichart et al., 2004; Sangiorgi et al., 2006). It can be particularly abundant in restricted marine environments like lagoons and bays and has been found abundantly in the estuarine surface sediments of Rookery Bay (Florida) (Cremer et al., 2007). Also C_{30} and C_{32} 1,15-diols are present in the sediments younger than 7.5 ka. These biomarkers most likely originate from eustigmatophytes, a group of eukaryotic algae (Volkman et al., 1992; Versteegh et al., 1997). The ratio between the two compounds, expressed in a Diol Index, is a function of salinity (Versteegh et al., 1997). Between 7.5 and 6 ka values for this index are about 25, typical for freshwater or restricted marine environments (Versteegh et al., 1997). Furthermore, long chain C36 alkenones (position of double bonds at ω15,20) have their highest concentrations around 6.5 ka. These alkenones, which so far have an unknown origin, were earlier reported in sediments from the Black Sea (Xu et al., 2001) and Japan Sea (Fujine et al., 2006), where they were associated with low salinity surface water conditions. These results fit well with the idea that Tampa Bay consisted at that time of a series of restricted lagoons, related to karst depressions (Locker et al., 2003), with limited water circulation.

Around 6 ka there is a strong decrease in biomarker, pollen, dinocyst and diatom concentrations. The sample was taken from a distinct layer (sample depth 329 cmbsf), characterized by high levels of shell fragments and sand, in contrast to the mostly clayey sediments above and below this level (Cronin et al., 2007). The high amounts of shell fragments indicate a high-energy depositional environment and thus probably poor preservation or dilution of the micro-remains. Sediment cores from the shelf of west-central Florida show, in the same time period, a similar sedimentary pattern of low energy deposits, interrupted by a sharp erosional contact and followed by a coarse, but fining upward, shell layer. Brooks et

al. (2003) interpreted the erosional contact as a ravinement surface and the shell layer as the initial shoreface deposition. Besides transgression, storms will have also affected sedimentation either by erosion due to storm surges or by increased runoff and consequent soil erosion. In Waccasassa Bay, north of Tampa Bay, storm driven surges were found to be an important mechanism for marsh surface accretion during the Holocene (Goodbred et al., 1998).

Increasing concentrations of friedelanone and disappearance of β–sitosterol around 7.5 ka suggest a change in vegetation cover and coincides with the terrestrial – marine transition already suggested by Cronin et al. (2007). Friedelanone, like β-sitosterol, originates from vascular plants (Scheuer, 1973; Nes, 1974; Killops and Killops, 2005). Possibly, β-sitosterol represents local herbaceous vegetation, which disappears when the environment becomes brackish. Marsh vegetation disappears almost completely from the pollen record simultaneous with the expansion of *Pinus*, between 6 and 5.5 ka. First occurrences of pollen of a number of plant and tree species like *Liquidambar* and ferns in this interval also indicate that the site became part of a more open area with a regional long-distance pollen input, rather than indicating changes in the local vegetation composition. Also friedelanone probably represents a more combined regional signal from the hinterland. The bisaccate *Pinus* pollen grains facilitate long-distance dispersal both by fluvial and aeolian transport, which might result in an over representation of this species. High levels of *Pinus* have been recovered for this period in sites throughout the peninsula (Watts, 1969, 1971, 1975, 1980; Watts and Hansen, 1994) and the expansion of pine forest is thought to be the result of warmer winters and increased precipitation (Watts, 1969; Grimm et al., 2006). These changes are however not clearly reflected in any of the other proxies, where it is possibly overwhelmed by the response to sea level rise.

Long-chain C_{37} – C_{38} alkenones present from ~4 ka and onwards, are biosynthesized exclusively by certain haptophyte algae, like *Emilinia huxleyi* and *Gephyrocapsa oceanica*. Reconstructed SST, based on the global core-top calibration of Müller et al. (1998) correspond well with current Tampa Bay spring temperatures of 24–26°C (nodc.noaa.gov), the period during which major groups of phytoplankton bloom in Florida bays and on the Florida shelf (Gilbes et al., 1996; Dixon et al., 2009). A transition to higher salinities towards the late Holocene is evident from a sharp increase in *L. machaerophorum* from 3 ka, followed by increases in *Spiniferites* spp. and polyhalobous diatoms. Also the Diol Index increases to about 80, which is typical for open marine conditions (Versteegh et al., 1997). *L. machaerophorum* has been recorded from brackish to fully marine environments, with salinity ranging between 16.9 and 36.7 psu, while the genus *Spiniferites* is usually found in waters with salinity higher than 22 psu (Marret and Zonneveld, 2003). Polyhalobous diatoms have an affinity for salinities higher than 30 psu, while mesohalobous diatoms thrive at salinities between 0.2 and 30 psu. Combined proxies thus indicate progressing Holocene sea level rise. A continuous marine submergence, with decelerating rates after 5 ka, was also proposed by Scholl et al. (1969).

The deepest occurrence of *Casuarina* between depth 93 – 39 cmbsf indicates a shift towards higher sedimentation rates in the upper part of the core. This could partly be the result of lower

compaction in the upper part of the sedimentary layer. However, the increase in sedimentation rate seems rather abrupt. Brooks (2011) reported a 10-fold increase in sedimentation rates in Tampa Bay over the past century, probably as a result of increased human activities in the areas surrounding Tampa Bay. The anthropogenic impact seems however, to have had little effect on the different proxies. A small decrease in pine might indicate a change in land use and in the marine realm a slight increase in some heterotrophic dinocysts (*Protoperidinioids, Votadinium spinosum, Selenopemphix quanta*) could indicate a higher nutrient input and higher productivity (Marret and Zonneveld, 2003).

5. Conclusions

Combined biomarker, pollen, dinocyst and diatom records clearly show the environmental evolution of Tampa Bay under the influence of rising Holocene sea level. Around 7.5 ka Tampa Bay is flooded and the pollen signal becomes representative of a larger catchment area. Between 7.5 ka and ~5 ka, the bay is characterized by low salinity surface waters and water column stratification. In this period the area is certainly more sensitive to storm and hurricane activity and the associated storm surges likely resulted in sedimentary hiatuses and/or storm deposits. Aquatic and marine proxies indicate increasing salinities from 7.5 ka to the present, which is likely the consequence of sea level rise following the last deglaciation. Around 6.5 ka, a change in vegetation from *Quercus* to *Pinus* indicate a regional change towards more humid conditions. Reconstructed SST for the past 4 kyrs are between 25 and 26°C and indicate stable temperatures during this period. A sharp increase in sedimentation rate in the top ~50 cm of the core is ascribed to human impact and coherent with other studies in the surroundings of Tampa Bay.

This environmental interpretation is in agreement with Cronin et al. (2007) who recognized a transition from lacustrine to estuarine conditions around 7.5 ka in the same sediment core. While the previous study established the presence of sea level rise at this site, this study provides a more detailed interpretation of the environment, like the transition from fresh to brackish/marine conditions. Proxies are in agreement with each other, which makes the environmental interpretation reliable. At the applied resolution, the marine signal is determined by the rising sea level. When higher resolution will be achieved changes in SST, humidity and salinity can provide information on past changes in the climate system and the effects in this area.

Chapter 2

Mid to late Holocene hydrological changes at Charlotte Harbor (Florida) inferred from dinoflagellate cysts and pollen

Abstract

In Florida, the major transition from oak (*Quercus*) to pine (*Pinus*) dominated vegetation, that took place around 6.5 ka (calibrated kilo years BP), is interpreted as a large-scale transition to more humid conditions. The apparent continuous humid conditions, however, seem inconsistent with reconstructions for the Gulf of Mexico and the Caribbean, which indicate regionally drier conditions after ~4.5 ka. Additional information on precipitation variability in Florida is needed to better interpret the mid to late Holocene pine phase. Terrestrial and marine sediments deposited in estuaries present an excellent archive to simultaneously study changes in relative sea level, climate and vegetation. Here, we build upon recently published detailed lithological and biomarker records from Charlotte Harbor covering the past ~8.2 ka (Van Soelen et al., 2012), using pollen and dinoflagellate cyst assemblages to simultaneously study regional vegetation changes and runoff patterns, associated with precipitation. The trend in dominant dinocyst taxa reflects an overall environmental change from lagoonal conditions to a more marine setting as the site was flooded by the rising sea. The substantial reduction of oak in the pollen record from ~7 ka concurs with increased runoff, as indicated by rising pollen accumulation rates and the presence of dinocyst *Lingulodinium machaerophorum*, which is considered indicative of high nutrient input and stratified water conditions. Afterwards, terrestrial input is strongly reduced, consistent with a trend to drier conditions in the Gulf of Mexico and the Caribbean. A second maximum in potential runoff-indicator *L. machaerophorum* after ~2.8 ka broadly concurs with known intensification of ENSO-tied winter precipitation. Although the Charlotte Harbor runoff record is not conclusive about the timing and strenght of the processes controlling hydrological conditions on land, the pine vegetation development was likely the result of a complex interplay of sea level rise, precipitation and landscape dynamics over the mid to late Holocene.

1. Introduction

Vegetation is highly dependent on water availability from precipitation and groundwater (Myers and Ewel, 1990). Therefore, the analysis of past changes in the vegetation composition is an effective tool for reconstructing past environmental and climatic changes in this region (Willard et al., 2001b). Long pollen-based vegetation histories have been described from deep lake deposits in central Florida (Watts, 1969, 1971, 1975; Watts et al., 1992; Grimm et al., 1993; Watts and Hansen, 1994). Major shifts between pine dominated and oak dominated vegetation over the past ~60 ka (calibrated kilo years BP) are observed throughout the peninsula. These Pleistocene millennial-scale pine phases are thought to reflect long-term warm and wet climatic conditions in Florida, occurring simultaneous with North Atlantic cold spells or Heinrich events (Grimm et al., 2006). This climatic pattern has been explained by reduced heat transport northward, and consequent persistent warming of the Gulf of Mexico and tropical Atlantic surface waters during the Pleistocene (Donders et al., 2011).

During the Holocene, pine becomes dominant again after ~6.5 ± 1 ka replacing oak- ragweed vegetation (Grimm et al., 1993; Watts and Hansen, 1994). This transition from generally dry to more humid vegetation occurs within a period characterized by regionally wetter conditions. Holocene precipitation maxima are recorded from Barbados speleothem isotopic signatures between 6 and 4 ka (Banner et al., 1996), higher lake levels, isotopic signatures of lake deposits and the expansion of wet vegetation on Haiti between 7.8 and 3.5 ka (Hodell et al., 1991; Higuera-Gundy et al., 1999), and high runoff into the Cariaco Basin between 10.5 and 4.5 ka (Haug et al., 2001). These changes have been related to a northern shift in the summer position of the Intertropical Convergence Zone (ITCZ) precipitation belt (Haug et al., 2001). This co-occurs with regionally warmer sea surface temperatures (Lea et al., 2003; Ziegler et al., 2008) during the Holocene Thermal Maximum (~10.5-5.4 ka). However, after ~4.5 ka these records indicate climatic drying and marine surface water cooling, whereas in Florida the pine vegetation remains present suggesting continuous summer wet conditions until present. Explanations for this apparent discrepancy include a decoupling of vegetation development and climatic changes and/or climatic conditions in Florida that differ from the Caribbean region.

Another factor potentially affecting hydrological conditions on land is the Holocene sea level rise. For the Gulf of Mexico and the Caribbean region several high-resolution relative sea level (RSL) curves have been constructed, based on basal peat and swash zone deposit chronologies in the northern Gulf of Mexico/Mississippi region (Törnqvist et al., 2004; Milliken et al., 2008), and intertidal mangrove peats and coral reefs in the eastern Caribbean (Toscano and Macintyre, 2003). These records show a highly consistent Holocene RSL for the region, with a fairly high transgression rate of 5.2 mm/y up to ~7 ka and a more gradual sea level increase afterwards to finally 0.9 mm/y (Toscano and Macintyre, 2003). Due to the broad Florida western shelf extending into the Gulf of Mexico, the coastline at the beginning of the Holocene was tens of kilometers westward. In areas with very low topography, like most of present

Florida, the reconstructed sea level rise of ~20 m over the past 10 ka is expected to have had far-reaching effects on the landscape and the vegetation.

A more comprehensive overview of past changes in the various processes affecting local hydrology is needed to put the Holocene vegetation development of the Florida peninsula into a regional perspective. Estuaries are excellent environments for recording both terrestrial and marine environmental changes, due to high accumulation rates of sediments rich in marine and terrestrial organic material. Pollen is transported into the estuary via wind and rivers from large distances, and therefore captures regional as well as local vegetation changes. Dinoflagellates have specific ecological requirements, and shifts in their cyst assemblages can therefore be applied to reconstruct past changes in runoff to the estuary.

A study on Holocene estuarine deposits from Tampa Bay (Florida) demonstrated that combined pollen, dinocyst, diatom, and terrestrial and marine biomarker analyses well describe the range of environmental changes associated with Holocene sea level rise (Chapter 1). The sample resolution of that study, however, is too low to differentiate between sea level and climate-induced environmental changes. Recently, a detailed lithological and organic geochemical study was performed on Holocene deposits of Charlotte Harbor, a large estuary located ~100 km south of Tampa Bay (Van Soelen et al., 2012). Results show the sensitivity of this site to hydrological changes due to sea level rise and runoff variability. To investigate the interdependencies between sea level, precipitation and seasonality in southwest Florida environments, we present high-resolution dinoflagellates cyst (dinocyst) and pollen records covering the past ~8.2 ka from Charlotte Harbor estuary.

2. Regional settings

The Charlotte Harbor estuary is located along the Gulf coast of the southwest Florida peninsula, in Charlotte and Lee counties. Three relatively large rivers discharge into the estuary; Myakka and Peace River in the north and Caloosahatchee River to the south. The embayment also encompasses several lagoons, the Gasparilla and Pine Island Sound and Matlacha Pass, which are secured behind a series of barrier islands (Fig. 1). The subsurface is composed of late Neogene/Quaternary siliclastic sediments on top of the Paleogene karstic limestone of the Florida Platform (Scott et al., 2001), which extends another ~250 km westward as a shelf into the Gulf of Mexico. The Charlotte Harbor area is likely formed by dissolution of the underlying limestone, which was exposed during periods of low sea levels (Evans and Hine, 1991). Afterwards, these sinkholes flooded by a rising sea level and deposition of estuarine sediments began.

The Florida peninsula generally has a humid subtropical to tropical climate, with summer temperatures ranging between 23-33˚C and with mild winters of ~12-25 ˚C. Most of the annual ~1300 mm precipitation falls between June and September, during numerous

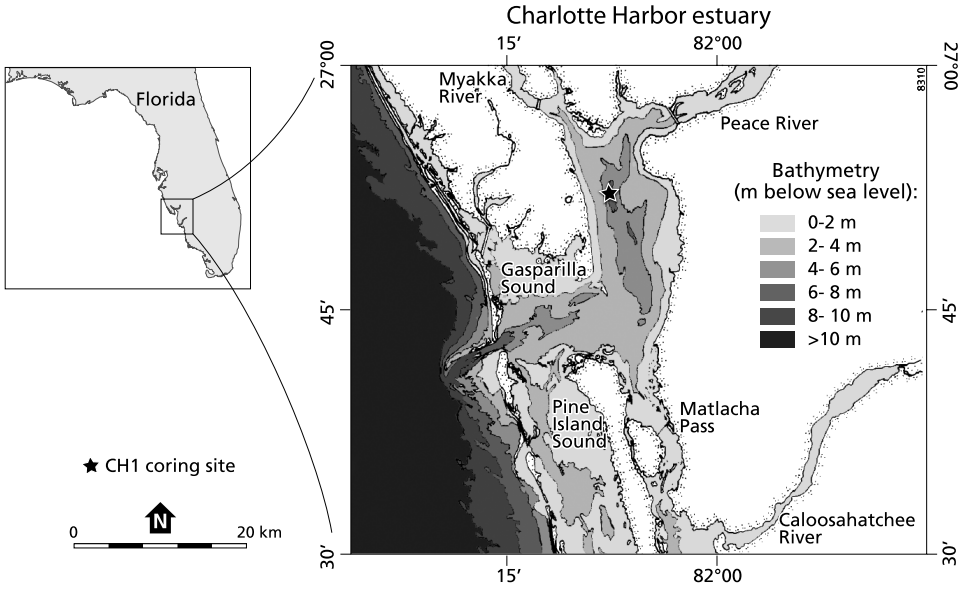

Figure 1. Left map: Florida with location of Charlotte Harbor: right map (modified after Evans et al., 1989) detail of the Charlotte Harbor estuary with position of rivers, bathymetry and the coring site indicated by a star.

thunderstorms (Port Charlotte weather station; www.weather.com). This weather pattern is strongly determined by the annual movement of the North Atlantic Subtropical- or Bermuda High (BH). In winter the centre is positioned over the Azores Islands, and a secondary high pressure area over southeastern US causes drier conditions in Florida. During summer the centre moves towards Bermuda, generally leading to wetter conditions in the southeastern US (Davis et al., 1997). On multi-decadal scale, enhanced summer precipitation over the Florida peninsula has been linked to warm phases of the Atlantic Multidecadal Oscillation (AMO) (Enfield et al., 2001). Winter precipitation variability is largely controlled by the modes of the Pacific El Niño- Southern Oscillation (ENSO), where the El Niño mode results in anomalously high winter precipitation (Schmidt et al., 2001; Cronin et al., 2002).

The seasonality of the precipitation is also reflected in the discharge of rivers on the peninsula, which peaks between July and October. Discharge is even higher during warm AMO phases (Kelly and Gore, 2008), and reaches a second peak in winter during strong El Niño events (Stoker, 1992). Salinity is inversely related to runoff, and consequently the lowest salinity is observed during summer and highest during winter (measured from 1982-1987; (Stoker, 1992). At the study site, surface salinity averages 14 and 29 psu in the wet and dry season, respectively, while constant salinity of 35 psu is measured in the coastal Gulf of Mexico (Miller et al., 1990). A direct link between El Niño related winter precipitation and reduced winter surface salinity is observed in Tampa Bay (Schmidt and Luther, 2002), north of Charlotte

Harbor. At times of high runoff and calm weather conditions the water becomes vertically stratified. Salinity differences between near surface and near bottom water can be as much as 20 psu (Stoker, 1992), which can result in temporary hypoxic or anoxic conditions at the bottom (Pierce et al., 2004). Otherwise, the estuarine water is vertically partially to well-mixed (McPherson et al., 1996).

The rivers' combined annual average discharge is about 190 m^3 per second, draining a watershed of ~11,000 km^2 including urban and agricultural areas (McPherson et al., 1996). Peace River drains areas of active phosphate mining, but is also naturally enriched in phosphorus as phosphate deposits are exposed in the riverbed of the upper drainage. Total phosphorus and total nitrogen are found to decrease in the estuarine water during the dry season, directly linking these nutrients to fluvial input (McPherson et al., 1996). Combined sediment supply via these rivers is relatively low with ~330,000 tons y^{-2} (Isphording et al., 1989). Due to the low slope gradient of the West Florida shelf, this part of the coast is generally characterized by low wave activity (30-50 cm) and tidal range (~1 m) of the mixed (diurnal and semi-diurnal) type (Hine et al., 1987).

Today the area surrounding the Harbor is largely urbanized, whereas further inland the catchment is mostly used for citrus plantations and cattle. Before these large-scale human alterations, the landscape was covered by evergreen conifer and mixed hardwood forests with patches of prairie (Davis, 1967), depending on the local hydrological conditions (Myers and Ewel, 1990).

3. Material and Methods

3.1 Core collection

Core CH-08-VC-01 (further referred to as CH1; coordinates 26°52,799' N; 082°07,612' W, water depth ~6 m) was collected in Spring 2008, using a vibracorer deployed from the R/V G.K. Gilbert. The coring site is located in a hypoxic basin within the Charlotte Harbor estuary (Fig. 1). This core has a total length of 549 cm and was cut in ~150 cm sections. Besides CH1, other sediment cores were taken directly south and in the Peace tidal river mouth more north of CH1 within the estuary (Van Soelen et al., 2012). Lithological comparison of these cores shows that the sedimentation at the sampled site does not deviate largely from the rest of the estuary, and that CH1 is representative for the area.

3.2 Lithology

The base of the core (549 to 425 cm) is mainly composed of quartz sand and clay (Fig. 2), indicated by elevated silica and heavy mineral components in the X-ray fluorescence (XRF) data (Van Soelen et al., 2012). Some razor clams (*Tagelus plebeius*) were observed at the top of this section in upright (so not redeposited) position, and these deposits are interpreted as estuarine sandbank or tidal flat (Van Soelen et al., 2012). On top of this sequence, organic

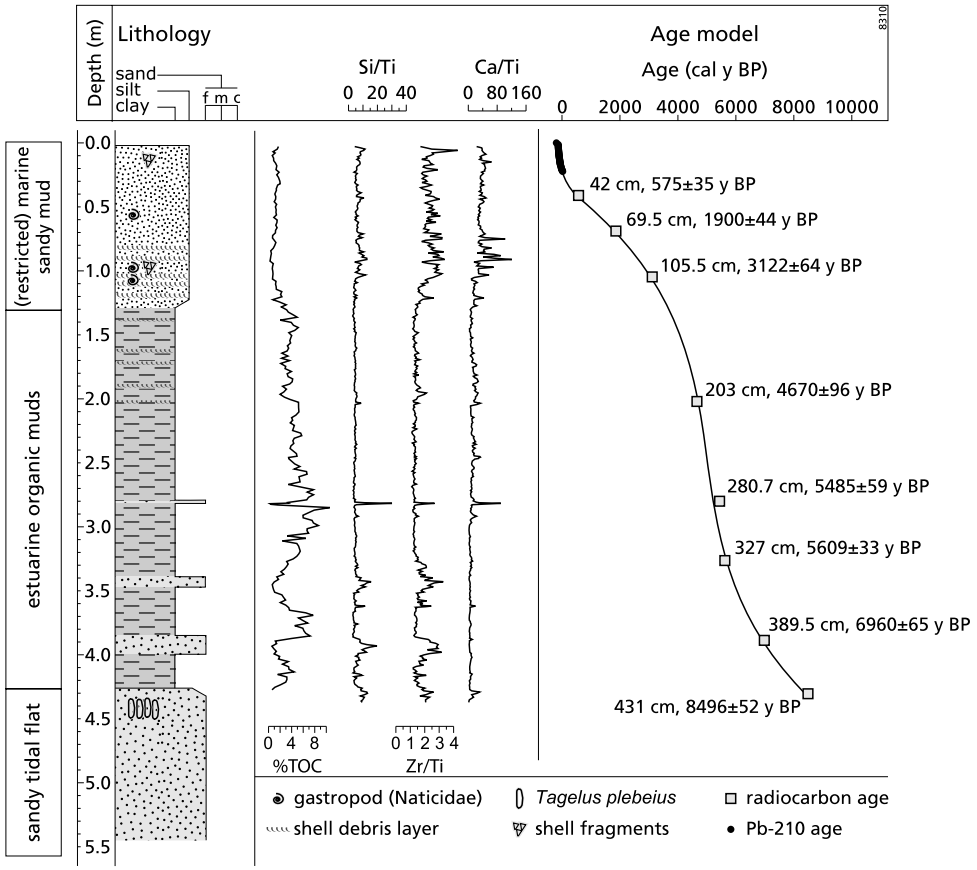

Figure 2. Core CH1 lithology and age model plotted against depth (modified after Van Soelen et al., 2012). The XRF counts for Ca (shell fragments), Si (quartz sand) and Zr (heavy minerals) are normalized to Ti. The age model is based on ^{210}Pb dates and 8 AMS radiocarbon dates, and is composed on two third order polynomial functions: 0-42 cm→ age (cal y BP)= 0.0082·depth (cm)^3 – 0.034·depth (cm)^2 + 2.13·depth (cm) – 60.00; R^2 = 0.99, and >42 cm → age (cal y BP) = 0.00037·depth (cm)^3 – 0.27·depth (cm)^2 + 74.22·depth (cm) – 2078.22; R^2 = 0.99 (Van Soelen et al., 2012).

rich clay is deposited (425 to 125 cm), disrupted between 400-280 cm by occasional distinct sand layers. Total organic carbon (TOC) values of these shallow estuarine deposits are high (~2-10%, excluding the sand layers), and are predominantly terrestrial derived (Van Soelen et al., 2012). Towards the top, TOC values gradually decrease, and above 125 cm the deposits change to silty sand, rich in shell debris layers. Other Charlotte Harbor XRF analyzed cores on a riverine to coastal transect indicate the high carbonate values increase towards the coast, and the shelly top reflects the transition to more marine deposits (Van Soelen et al., 2012).

3.3 Chronology

An age-depth model was constructed for the core section 0-425 cm, based on 8 AMS ^{14}C dates and ^{210}Pb short lived radio-isotope analyses on the top 42 cm sediments (Van Soelen et al., 2012). The selected shells (fragments) for radiocarbon dating were calibrated to years before present using Calib 6.0 (Stuiver et al., 2010) including the correction for the marine reservoir of ~400 y. The model indicates an age of ~8.2 ka for the start of the organic estuarine deposits. Sedimentation rate increases from 0.02 cm/y at the base to a maximum of 0.16 cm/y at ~5 ka, after which it decreases back to 0.02 cm/y in the top. Reduced compaction as well as human alterations of the landscape and hydrology are visible as sedimentation rates again increase to 0.74 cm/y in the past 100 years (Van Soelen et al., 2012).

3.4 Palynological processing

For the palynological analyses samples were taken from the top 425 cm, encompassing the estuarine organic clay deposits and overlying sandy silt deposits. Freeze-dried subsamples selected at 10-20 cm intervals (~0.3 to 1.4 gram) were treated with cold 10% hydrochloric acid (HCl) and cold 38% hydrofluoric acid (HF) in five alternate and subsequent steps to remove carbonates and silicates, respectively. Centrifuging (2000 rpm; 5 min) and decantation was carried out after each step. Prior to chemical treatment, tablets with a known amount of exotic spores (*Lycopodium clavatum*; 18,583 ± 4.1%) were added to the sample to be able to estimate the palynomorph concentrations in the samples. Samples were sieved over a 10 µm mesh to further remove clay particles, after which the residue was again centrifuged and decanted. The residue is mixed with glycerine water, and a homogenized fraction is mounted on glass slides for analysis using a Leitz light microscope (x400 magnification). Dinocysts and pollen grains were analyzed on the same slides; at least 200 dinocysts and 200 pollen (of which minimal 100 non-*Pinus* pollen) were counted per slide. Dinocyst identification follows Fensome and Williams (2004), Marret and Zonneveld (2003), Rochon et al. (1999) and Cremer et al., (2007). Identification of pollen largely follows Willard et al. (2004) and an in-house reference collection.

Relative abundances of both palynomorphs were based on the sum of all dinocysts and all pollen, individually. Palynomorph accumulation rates or fluxes (specimens/cm^2·y) were calculated by multiplying the concentrations (specimens/g) to mass accumulation rates (g/cm^2·y) determined from fixed volume samples. Zonation of the relative abundances diagrams is done based on visual inspection supported by cluster analysis provided by CONISS (Grimm, 1991-2001), using the total sum of squares on the non-transformed (Euclidian distance) data.

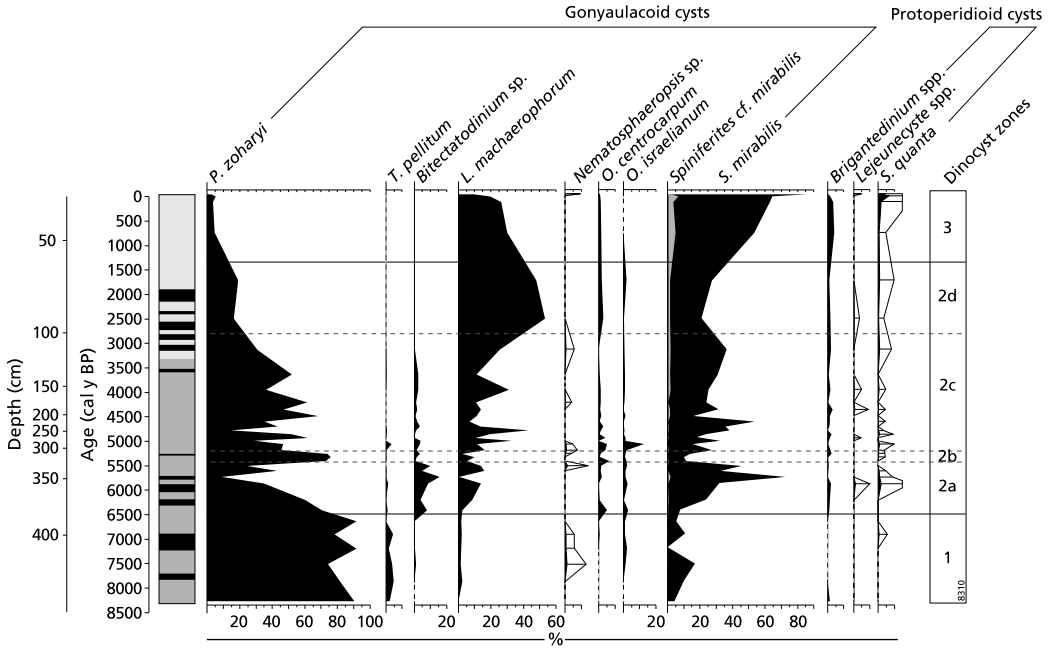

Figure 3. Diagram showing lithology (dark gray: organic mud, light gray: silt, black bars: sand/shell layers) and the relative abundance of selected dinocyst species (depth bars indicate 10x exaggeration). The relative abundance of *Spiniferites* cf. *mirabilis* (characterized by the antapical flange and apical nodule) is indicated within the relative abundance of the *Spiniferites mirabilis* (also including *S. hyperachantus*).

4. Results

4.1 Dinoflagellate cyst assemblages

A total of 21 species is identified in the CH1 sediments, of which relative abundances of the most common ones are plotted against age (Fig. 3). The assemblage is predominantly composed of the Gonyaulacoid species *Polysphaeridium zoharyi, Lingulodinium machaerophorum* and *Spiniferites* spp. (of which *S. mirabilis* s.l. is most commonly observed), in alternating relative abundances.

Dinocyst Zone 1 (425-360 cm; ~8.2-6.3 ka)

At the base of the core *P. zoharyi* dominates the assemblage with values of ~75-90% (zone 1). This (sub-) tropical species is associated with euryhaline mesotropic coastal waters, and such high relative abundances are commonly observed in the Gulf of Mexico region and Florida Bay, where they are associated with extreme salinity conditions (Wingard et al., 1995; Ishman et al., 1996; Edwards and Willard, 2001; Marret and Zonneveld, 2003; Cremer et al., 2007). Together with *P. zoharyi*, low relative abundance (up to 20%) of *Spiniferites* spp., mostly consisting of *S. mirabilis* s.l. (including *S. hyperachantus*) are found. *S. mirabilis* s.l. is a temperate to

tropical, coastal to marine species (Rochon et al., 1999). Also common in this lower section is *Tectatodinium pellitum* (~5%), a (sub-) tropical coastal species commonly found in the Florida Bay (Wingard et al., 1995; Ishman et al., 1996; Marret and Zonneveld, 2003).

Dinocyst Zone 2 (360-55 cm; ~6.3-1.2 ka)

After ~6.3 ka relative abundances of *P. zoharyi* are strongly reduced by a combined increase of *L. machaerophorum*, *Bitectatodium* sp. and *Spiniferites* spp.. In this zone, *P. zoharyi, L. machaerophorum* and *Spiniferites* spp. occur in alternating dominance. The abundance of *Spiniferites* spp. increases most considerably around 5.7 ka, with peak values of 50-75% (zone 2a). Within this genus *S. mirabilis* s.l. is most common taxon, but *S. bentorii* and *S. ramosus* s.l. are also occasionally observed (a temperate to tropical coastal and cosmopolitan species, respectively). In zone 2a a yet unknown morphotype of *Bitectatodinium* is present with values ranging between 5 and 15%. Generally, *Bitectatodinium* is considered a fully marine genus, of which the species *B. tepikiense* (cold/temperate) and *B. spongium* (subtropical/equatorial) have a much thicker cyst walls than the type observed here (Marret and Zonneveld, 2003). A major peak in *P. zoharyi* to 70% is observed at ~5.2 ka (zone 2b).

Lingulodinium machaerophorum abundance is variable, but peaks to 30-40% at ~4.8 and ~4.0 ka (zone 2c), and after ~2.8 ka this species becomes consistently dominant with ~50% abundance (zone 2d). This is a temperate to tropical coastal species of which high abundances are indicative for warm eutrophic conditions. The dinoflagellate *L. polyedrum* (motile stage of *L. machaerophorum* cyst) tends to bloom during periods of high nutrient availability and calm stratified waters (Marret and Zonneveld, 2003) and is common in lochs, bays and fjords at the end of the summer after high river discharge. *L. machaerophorum* highest relative abundances are found in upwelling regions or close to river mouths (Dale and Fjellså, 1994; Lewis and Hallett, 1997; Thorsen and Dale, 1997). *Operculodinium israelianum* (a temperate to tropical fully marine species) is consistently present in low abundances in both zones 1 and 2, but peaks to 13% at 5.1 ka.

Dinocyst Zone 3 (55-0 cm; ~1.2 ka to present)

After ~1.2 ka *Spiniferites* spp. dominates the assemblage with maximum relative abundances of 84% (zone 3). Overall, the processes of *Spiniferites* spp. were found to be poorly developed and short, potentially reflecting the presence of this species in the lower limit of its salinity range (Rochon et al., 2009). The Protoperidinioid cysts that were consistently present in minor percentages show a slight increase here, but never exceed 10% in total. Of these, the cosmopolitan *Brigantedinium* sp. and *Selenopemphix quanta* are the most common; both are associated with nutrient enriched waters (Rochon et al., 1999). High abundances of *S. quanta* were found in the Mississippi Sound, and showed a positive relation to water depth and well-mixed water conditions (Edwards and Willard, 2001). Interestingly, a cyst with characteristics of both *S. mirabilis* s.s. (antapical flange and intergonal processes) and *S. bentorii* (apical protuberance) is frequently observed (*Spiniferites* cf. *mirabilis*) and shows a trend similar to the Protoperidinioid cysts.

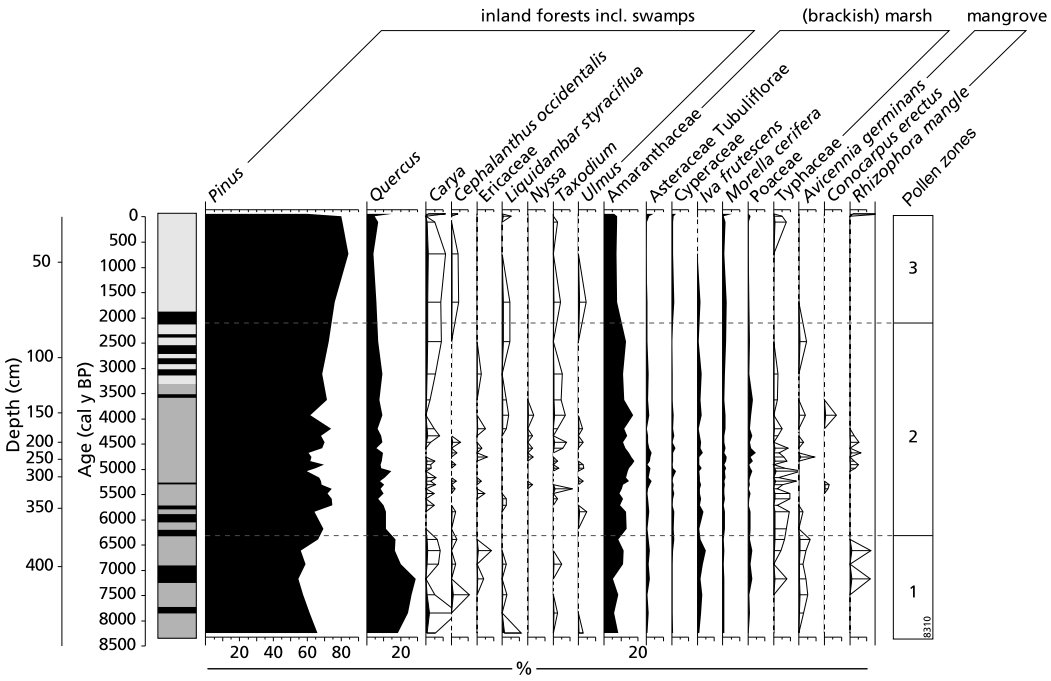

Figure 4. Pollen diagram showing lithology (dark gray: organic mud, light gray: silt, black bars: sand/shell layers) and the relative abundance of selected taxa (depth bars indicate 10x exaggeration). Indicated taxa are grouped according to their most common vegetation type (Myers and Ewel, 1990).

4.2 Pollen and spores assemblages

In the same samples as the dinocyst record, pollen and spores were analyzed and a total of 31 taxa were identified. The relative abundances of the most common inland trees, marsh/prairie herbs and shrubs, and mangrove species are plotted with age (Fig. 4). Overall, pollen of *Pinus* together with *Quercus* and Amaranthaceae dominate the entire assemblage. These species are commonly over-represented in such environments (Willard et al., 2007), due to their high pollen production and (wind) dispersal.

Pollen Zone 1 (425-360 cm; ~8.2-6.3 ka)

Although *Pinus* dominates the base of this zone with ~65%, the highest *Quercus* values of up to 30% are found here. Numerous species of *Quercus* are common in Florida environments, ranging from hydric hammocks to open/well drained scrubland (Myers and Ewel, 1990). This distinction between species cannot be made in the pollen samples. At the same time, Amaranthaceae (up to 12%) and other taxa like *Iva frutescens,* Asteraceae and Poaceae are consistently present (up to 5%). These are all commonly present in open landscapes, like wet prairies or (brackish) marshes (Willard et al., 2001b). Coastline fringing mangrove species

Avicennia and *Rhizophora* are most consistently present in this section, albeit in maximal 2% abundance in total.

Pollen Zone 2 (360-75 cm; ~6.3-2.1 ka)
After ~6.3 ka *Pinus* increases while *Quercus* is reduced and maintains a stable ~10% from this point on. These *Pinus* pollen likely derive from southern pine flatwoods, currently present on the well-drained upland areas in an almost monotypical canopy (Myers and Ewel, 1990). Although relative abundances of other inland trees are very low, an increase in diversity is observed; *Nyssa, Alnus, Taxodium* and *Ulmus* show a first/more consistent presence. These tree species are common in hydric hammocks and swamps, fringing the river channels (Myers and Ewel, 1990). The herb species that were already present show an increased abundance, of which most notably Amaranthaceae which increases to ~17%. The small tree *Morella cerifera*, common in hammocks as well as prairie landscapes, also shows a slight increase. Observed pollen of Poaceae and Cyperaceae could not be identified to the species level and distinction between salt and freshwater marshes is therefore not possible.

Pollen Zone 3 (75-0 cm; ~2.1 ka to present)
Pinus gradually increases further to maximal 80% after ~2.1 ka, whereas *Quercus* and the combined marsh species (particularly Amaranthaceae) are further reduced. The combined inland trees however double to a total of 3% between ~2.8-1.0 ka. The scarcely present mangrove pollen disappear in this zone.

4.3 Palynomorph accumulation rates

The accumulation rates of dinocysts and pollen (# palynomorphs per cm^2 per year) (Fig. 5) are comparable in magnitude. The total dinocyst accumulation rate ranges between 100 and 7000 cysts/cm^2·y with a single peak of 15,000 cysts, and the pollen accumulation rate ranges between 400 and 16,000 grains/cm^2·y. The trends in the palynomorph accumulation rates in CH1 over time are also highly similar: fluxes are relatively low from the core base (8.2 ka) up to ~6 ka, after which values increase and reach a peak between 5.5 and 4.5 ka, followed by a strong reduction. Remarkably, 4-fold increases in dinocyst flux occur at ~4.8 ka and ~3.6 ka although both peaks consist of one sample only. Distinct low values in the pollen accumulation rates mostly coincide with sand/shell layers.

Changes in palynomorph accumulation rates could be the result of differential preservation and/or variable productivity (dinocysts), change in terrestrial input (pollen), or dilution effects due to sandy deposits. The cysts of *P. zoharyi* and *L. machaerophorum* are found to be highly resistant to oxidation, whereas *Spiniferites* spp. and particularly Protoperidinioid cysts are more easily degraded (Zonneveld et al., 1997). There is no apparent relation between increased dinocyst accumulation rates and increases in one of the taxon, making (differential) preservation an unlikely process causing the variability in accumulation rates. Comparison of the general palynomorph accumulation rates to the total organic carbon in the sediment (% TOC) shows a comparable trend. The strong similarity with particularly the pollen curve

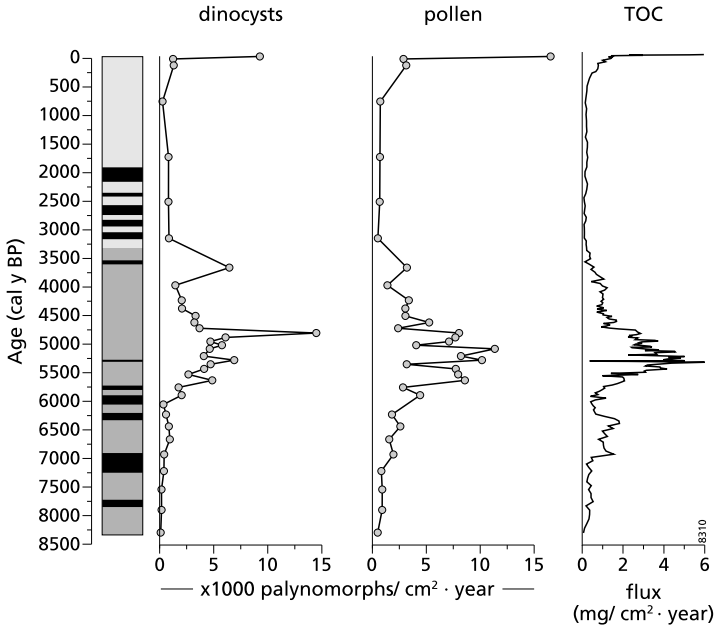

Figure 5. The lithology (dark gray: organic mud, light gray: silt, black bars: sand/shell layers) and total accumulation rates of pollen, dinocysts and TOC (Van Soelen et al., 2012).

supports the finding by Van Soelen et al. (2012) that the organic material is predominantly terrestrial-derived. Most likely, the increased pollen accumulation rates and TOC reflect periods of higher runoff. This would supply the estuary with terrestrial (organic) material as well as nutrients, which in turn potentially led to simultaneous increased primary productivity of dinoflagellates.

5. Discussion

5.1 Environmental development

The abrupt lithological transition at the base of the core (425 cm) from sandy tidal to organic rich clayey deposits indicates an environmental change towards permanently flooded conditions. The timing of the estuary flooding at ~8.2 ka is consistent with regional relative sea level curves (Toscano and Macintyre, 2003), and occurs simultaneous with a sea level jump recently inferred from Mississippi Delta records (Li et al., 2012). By subtracting this regional relative sea level rise from the sediment accumulation rates calculated for this core (based on the age model; Van Soelen et al., 2012) the variability in water depth over time can be estimated (Fig. 6A). This shows that the site was likely quickly flooded to reach a water depth of ~3 m between 8.2 and 6.5 ka. Assuming a bathymetry similar to that of today (Fig. 1), this implies that the basin in which the core was taken was only marginally connected to the coastal waters.

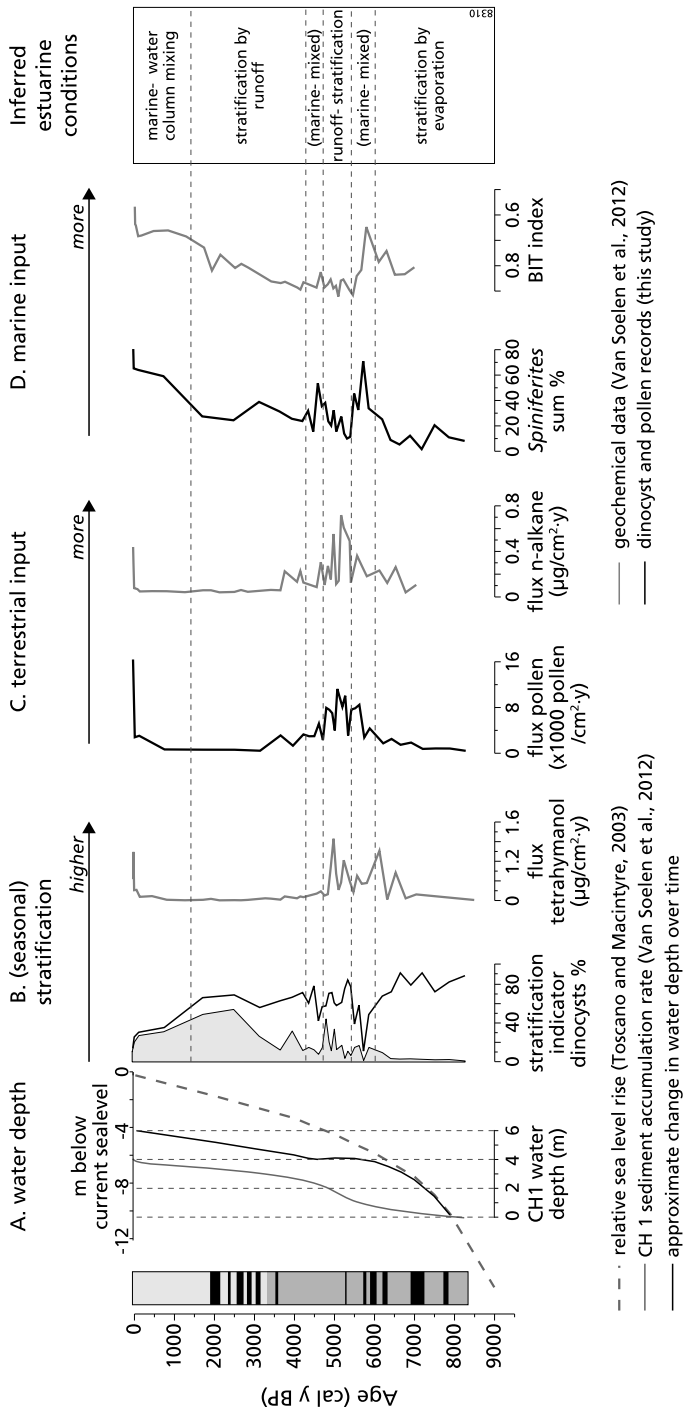

Figure 6. CH1 lithology (dark gray: organic mud, light gray: silt, black bars: sand/shell layers), A) water depth, and palynological and biomarker (Van Soelen et al., 2012) inferred changes in B) water stratification, C) terrestrial input inferred runoff, D) marine input. Stratification indicator species given by the sum (black continuous line) of *P. zoharyi* and *L. machaerophorum* (indicated by the gray shading). Note that the x-axis of the BIT index is reversed, and that some graphs indicate fluxes and other relative abundances. The (dashed) horizontal lines indicate transitions in the estuarine hydrological conditions.

In this restricted basin, the typical lagoonal dinocysts *P. zoharyi* and *T. pellitum* flourished. Similarly, almost monotypic occurrences of *P. zoharyi* are reported in surface samples of the Mississippi Sound in sheltered areas closest to the coast (Edwards and Willard, 2001). *P. zoharyi* generally indicates euryhaline and stratified water (Edwards and Andrle, 1992), a condition that can occur due to high evaporation relative to precipitation input. Although *Pinus* pollen dominate the assemblage throughout the core, the relatively high abundance of *Quercus* until ~7.0 ka is in agreement to pollen records from lake deposits across central Florida. At the onset of the Holocene, oak in association with upland herbs dominated a region from Florida to the southern Appalachians, which is interpreted to indicate generally dry conditions (Watts, 1980; Grimm et al., 1993). Such dry conditions as a consequence of relatively low precipitation is consistent with the interpretation of an estuary where evaporation and stratification prevailed (Fig. 6B).

Several changes point to wetter conditions, beginning with the increase of southern pine after ~6.5 ±1 ka (Watts and Hansen, 1994). In Charlotte Harbor, the increasing presence of *L. machaerophorum* after ~6.3 ka reflects a gradual change towards a runoff-dominated basin with high (seasonal) stratification and nutrient input (Fig. 6B). Moreover, a simultaneous increase in terrestrial input is reflected by higher accumulation rates of pollen. A sharp increase in the accumulation rate of *n*-alkanes, which originate from leaf waxes of higher plants and are fluvially transported into the estuary (Fig. 6C) is also observed (Van Soelen et al., 2012). These independent lines of evidence point to increased runoff, likely caused by a climatic shift towards increased or seasonally intensified precipitation. This is broadly consistent with Holocene wetter conditions inferred from the various circum-Caribbean sites (Hodell et al., 1991; Banner et al., 1996; Higuera-Gundy et al., 1999; Haug et al., 2001). Increased precipitation between 9.4-5.2 ka has also been inferred from fluvial development in Georgia (Leigh and Feeney, 1995), indicating increased mid Holocene wetness also occurred outside the Caribbean.

Before and after the peak in runoff, short-lived maximum *Spiniferites* spp. and minimum BIT (branched isoprenoid index) values suggest ingression of marine water between ~6.0-5.5 ka (and to lesser extent ~4.8-4.5 ka) (Fig. 6D). At this time, water depth likely changes very little due to increasing sediment accumulation rates and a reducing rate of sea level rise. Physical mechanisms that would lead to temporary more marine conditions in the restricted lagoon like tsunamis or temporary deepening of the estuary inlet are considered unlikely. These changes therefore seem to be climatically induced. Although the terrestrial input is reduced during these phases compared to the peak at 5.0 ka, it is still higher than in periods directly before and after the marine peaks. Therefore, more marine conditions due to strongly reduced runoff is also considered unlikely. The possibility of increased wave/wind induced water mixing due to temporary increased tropical storm occurrences in this region is extensively investigated in Chapter 3.

The reduction in terrestrial input after 4.5 ka occurs within the same lithological unit, and can therefore be considered an actual reflection of reduced runoff, although the presence of *L. machaerophorum* still indicates seasonal stratification and high nutrient input. Particularly between ~2.8 and 1.4 ka this runoff indicating dinocyst dominates the assemblage. A parallel increase in the occurrence of pollen of upland tree species, common in hammocks fringing river channels (e.g. *Alnus, Liquidambar* and *Ulmus*), and likely transported into the estuary via rivers, support high runoff. Apart from the slight increased input from inland hammocks and the reduction of oak vegetation inland, the vegetation record of Charlotte Harbor likely largely reflects local environmental changes. Many of the observed pollen could not be identified to the species level, and the plant families are common in various landscapes (Myers and Ewel, 1990; Willard et al., 2001b; Willard et al., 2004). Herbs dominate coastal (salt) marshes and are the closest abundant source to explain the expansion of herbaceous species between ~6.3-2.1 ka as the rising sea level slowly flooded the region. As the transgression continued, the increasing distance of the shoreline is reflected in the decreasing presence of pollen from shore vegetation.

A notable increase in the length of the processes and the spines of the dinocysts *L. machaerophorum* and *Spiniferites* spp., respectively, is observed after ~2 ka. A direct positive relationship between process length and salinity/temperature has been observed for *L. machaerophorum* (Hallet, 1999; Mertens et al., 2009). The increasing relative abundance of marine dinocysts *Spiniferites* spp. and Protoperidinioid species clearly reflects the establishment of marine conditions similar to present-day. This finding is supported by a shift in diatom assemblages after ~3.5 ka from typical epipsammic/epiphytic brackish-marine species to planktonic marine species, analyzed on the same core (E. Nodine, pers. comm.). The present-day measured salinity at the site of 14-29 psu (Miller et al., 1990) is still in the lower range of the *Spiniferites* spp. preference (Marret and Zonneveld, 2003), and this overall low salinity may also explain the occurrence of abnormal morphotypes like our *Spiniferites* cf. *mirabilis*.

5.2 Potential hydrological forcing factors

Clearly the environmental development of the Charlotte Harbor from a shallow lagoonal site to more marine conditions is determined by the Holocene transgression, similar to that of Tampa Bay (Chapter 1). Superimposed on this trend, shifts in the terrestrial input, primary productivity and water column stratification within the estuary point to changes in runoff (Fig. 7). The continuously low terrestrial input after ~3.5 ka is related to a distinct lithological transition characterized by a trend to increased marine components (Fig. 6), and could therefore be considered a result of the Holocene transgression. Several local mechanisms can explain the inferred reduced runoff to the estuary. Overall wetter conditions on land allow soils and peat deposits to develop, which is observed on large scale throughout southeastern US after ~6 ka (Gleason and Stone, 1994; Gaiser et al., 2001; Winkler et al., 2001). Recent numerical research has shown that the inferred precipitation throughout the Holocene is always high enough for peat development (Dekker et al., in review). They conclude that that

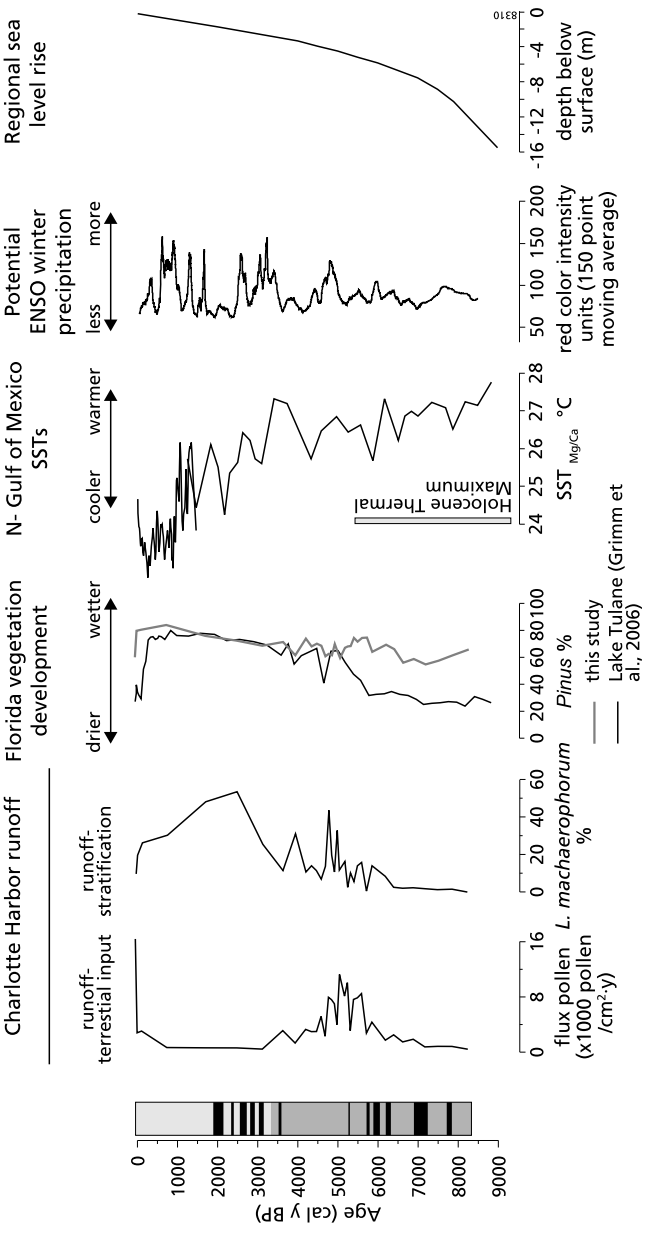

Figure 7. CH1 terrestrial input and water column stratification inferred runoff, Florida main vegetation changes reflected by pine abundance in Charlotte Harbor and Lake Tulane (Grimm et al., 2006), compared to Holocene SSTs in the Gulf of Mexico (Ziegler et al., 2008), past El Niño activity and potentially related winter precipitation in Florida (Moy et al., 2002), the regional relative sea level curve (Toscano and Macintyre, 2003).

the mid Holocene peat initiation in the Everglades is likely related to the reduced hydrological gradient following the transgression. Likely throughout the peninsula wetlands developed in lower lying areas, and such a development could have increased the water holding capacity of the landscape sufficiently to reduce actual runoff.

The significant change in vegetation cover may have also affected the rainfall-runoff relationship of the watershed (Hernandez et al., 2000). Vegetation has the ability to alter the hydrological cycle, through e.g. the uptake and transpiration of soil water (Gedney et al., 2006). Important physiological factors determining potential transpiration and thus hydrological control include the plant response to atmospheric CO_2 concentrations (Chapter 5, Chapter 6) and the vegetation density (Piao et al., 2007). The mid Holocene transition from an open oak forest/scrub to denser pine forests potentially resulted in regionally higher transpiration rates, and consequently reduced or buffered excess soil water. Such a physiological forcing could also be responsible for the observed reduction in runoff after 5.0 ka, masking precipitation variability. However, both an increase in water retaining capacity of the land and increased (evapo)transpiration are expected to remain high after the soil and vegetation development, not explaining the inferred second runoff increase after ~2.8 ka.

Assuming that the observed runoff variability is ultimately controlled by precipitation, a comparison to known precipitation trends is needed. During the mid Holocene summer convective precipitation in the Gulf of Mexico and Caribbean region was likely higher than present, as a result of regional high SSTs related to the Holocene Thermal Maximum (e.g. Ziegler et al., 2008) (Fig. 7), and a more northward summer position of the ITCZ (Haug et al., 2001). However, as the SSTs were gradually lowered and the summer ITCZ moved south, convective summer precipitation was likely regionally reduced (Hodell et al., 1991; Poore et al., 2003). Unlike the Caribbean region, Florida has a strong teleconnection to the El Niño-Southern Oscillation (Ropelewski and Halpert, 1987). El Niño phases lead to anomalously high winter precipitation and consequent winter runoff (Schmidt et al., 2001; Cronin et al., 2002). The intensification of the ENSO after ~3.5 ka is suggested to have led to increasing wetness in southern Florida (Donders et al., 2005a). A distinct increase of dinocyst *L. machaerophorum* is observed during the short peak in El Niño activity at ~5.0 ka, and again after ~2.8 ka, consistent with more frequent El Niño occurrences. Such a yearly double peak in runoff, with high nutrient input and water stratified for longer period of the year, possibly favors this species. Therefore, the high relative abundance of *L. machaerophorum* may reflect runoff-controlled conditions in the estuary forced by persistent El Niño events. The link between ENSO winter runoff and *L. machaerophorum,* however, requires further investigation.

Besides climatically forced wet conditions on land, the Holocene transgression should be considered an important driver of environmental change. The Pleistocene pine phases occurred at a time when the sea level was ~75-125 meters lower than today (Shackleton, 1987), and a climatic cause for pine expansion is evident. Around ~6 ka the sea level was only ~5-8 meters below current level, and gradually continued to rise (Toscano and Macintyre, 2003)

(Fig. 7). The shift from oak to pine domination was, hence, likely a combined effect of raised groundwater level and increased precipitation. Although the Charlotte Harbor estuarine records are not conclusive to explain the strength and the timing of the various forcing factors, this study illustrates that mid to late Holocene hydrological conditions on land are likely more dynamic than the continuous pine dominance in the pollen records suggests. The seasonally dry fire-sensitive pine flatwoods and permeable Florida soil did stop the development into a closed forest in upland areas, even though total annual precipitation might have been higher in the mid Holocene optimum in comparison with today.

6. Conclusions

Detailed analyses of pollen and dinoflagellate cyst assemblages in Charlotte Harbor estuarine deposits clearly reflect mid to late Holocene local and regional changes in hydrology. The overall environmental development of the estuary is controlled by the Holocene transgression. The site gradually flooded at ~8.2 ka, changing from lagoonal to progressively more marine conditions. Superimposed on this trend, millennial scale shifts in the local hydrological conditions are observed. Increased runoff between ~6.5-4.5 ka is inferred from distinctly higher pollen and dinocyst accumulation rates, pointing to high terrestrial input and dinocyst primary productivity. The subsequent reduction in runoff suggests lower total annual precipitation rates, combined with increased water retention in the developing peatland. This is consistent with a regional drying trend and surface water temperature decrease after the Holocene Thermal Maximum. Increased runoff between ~2.8-1.2 ka, inferred from the increasing presence of the dinocyst *Lingulodinium machaerophorum*, which thrives in high nutrient and run-off induced stratification, is tentatively related to the intensification of the ENSO leading to increased winter precipitation in Florida. Overall, the observed hydrological changes of the Charlotte Harbor estuary are an expression of the complex interaction between mid to late Holocene climatic changes, landscape dynamics and the Holocene transgression.

Chapter 3

Mid to late Holocene tropical storm occurrences in Florida: regional evidences from estuarine deposits

Abstract

The increased hurricane activity at the start of the century has led to a debate about a potential forcing by global warming. To better understand (natural) centennial to millennial scale variability in Atlantic tropical storm frequency, long, continuous and highly resolved records are needed. A commonly used method to detect tropical storms involves the grain size analyses to identify overwash layers in coastal deposits, which in turn reflect storm surges. Increased precipitation and wind/wave energy associated with tropical storms also affect shallow marine environments and the isotopic composition of precipitation. To record these changes, we apply a multi-proxy approach to estuarine deposits from the Florida Gulf coast, combining lithology, organic-walled dinoflagellate cyst assemblages and hydrogen isotope ratios (δD) analyses on long-chain n-alkanes from leaf waxes. Clustered layers of coarse material are observed, as well as abrupt shifts in the *Spiniferites* spp. (marine dinocysts) and δD, measured in homogenous fine deposits. The reproduction of the palynological evidence at two separate sites critically shows changes are caused by a large-scale forcing. The concurrent increase of marine dinocysts in an otherwise lagoonal environment, and lighter hydrogen isotopes in leaf waxes, point to increased wind/wave energy and isotopically more depleted precipitation. Based on the combined palynological, geochemical and lithological evidences we propose regional increased tropical storm occurrences between ~6.4-5.5 ka, ~5.0-4.0 ka and ~3.2-1.9 ka. This is broadly consistent with records from the Gulf of Mexico and Caribbean region. Millennial scale shifts in the position of the Bermuda High are proposed to have determined tropical storm variability in Florida over the mid to late Holocene. This study shows that a more robust record of past storm occurrences can be obtained by analyzing multiple sensitive proxies at multiple sites.

1. Introduction

The apparent increase in Atlantic tropical storm activity over the past decades has triggered a debate whether there is an intensification, and if so wheter it is related to on-going global warming and higher sea surface temperatures (SSTs) (e.g. Emanuel, 2005; Landsea, 2005). Although processes controlling inter-annual to multi-decadal changes in the storm activity and its regional expression are still poorly understood, a complex interplay of large-scale weather determining systems and SSTs in the tropical Atlantic basin have been proposed (Elsner et al., 2000; Goldenberg et al., 2001; Mann et al., 2009). The instrumental and historical records of tropical storms are however too short to capture variability on centennial to millennial scale. To understand the full natural range of storm activity, long continuous records are needed on a high spatial resolution for the areas affected by tropical storms.

An effective method to reconstruct past tropical storm variability is the lithological analysis of overwash deposits caused by storm surges. Deposition and thickness of characteristic sand/shell layers depends on the distance of the sampled site to the coast and the strength of tropical storm (Woodruff et al., 2008). The completeness of lithological storm surge records, however, depends on the spatial distribution of landfall localities as well as the temporal dynamics of the coastline. The most detailed records are so far obtained from back-barrier lake and lagoonal environments, where the impact of storm surges is believed to be most pronounced (Liu and Fearn, 1993, 2000; Donnelly and Woodruff, 2007; McCloskey and Keller, 2009; Malaizé et al., 2011). These highly storm-sensitive areas, however, are subject to alterations associated with long-term landscape dynamics, barrier island migration and gradually changing sea level (Otvos, 1970; Morris et al., 2002). Consequently, evidence for high-energy events with a characteristic signature as storm-surges may not be reflected as such at an individual site that is gradually changing through time.

Tropical storms are often associated with extreme precipitation (Franklin et al., 2006). Just like storm-surge related sand/shell layers originating from the open marine waters, river floods can also deposit high energy sediment layers in the basin (Koltermann and Gorelick, 1992). However, the reflection of high-energy conditions likely decreases with increasing distance from the coarse sediment sources. This is supported by recent storm-generated sedimentary facies from the Sarasota Bay estuary (Florida), characterized by runoff-induced terrigenous mud and free of sand/shell layers (Davis et al., 1989). Under these conditions an alternative approach is required to detect high-energy conditions associated with tropical storms.

Increased wave activity, storm surges and peak runoff directly affect the hydrological conditions of shallow coastal environments, like estuaries, through vigorous water column mixing or stratification, and high terrestrial organic material and fresh water input (Paerl et al., 2001; Ming et al., 2007). Aquatic organisms like dinoflagellates are highly sensitive to changes in environmental parameters like salinity and water column stratification and shifts in their cyst (resting stage) assemblages can be used to detect hydrological changes

(Marret and Zonneveld, 2003). Moreover, tropical storm precipitation is characterized by a distinct depletion in deuterium isotopes (δD) as compared to normal low latitude summer thunderstorms, due to the removal of heavy isotopes (fractionation) (Gedzelman and Lawrence, 1990; Lawrence et al., 2002). It has been shown that δD in long-chain *n*-alkanes deriving from leaf waxes record the isotopic composition of precipitation (Sachse et al., 2004; Sachse et al., 2006). Leaf waxes are transported to coastal sediments via runoff and wind, and therefore provide a potential archive for past isotopic composition of precipitation on land. Complementing the lithology-based tropical storm reconstruction with proxies such as dinocyst counts and hydrogen isotope ratios, indicative for changes in estuarine water column stratification and on-land precipitation, is expected to lead to a more complete record of long term tropical storm variability.

This multi-proxy approach has been applied to the Tampa Bay and Charlotte Harbor estuaries on the Florida Gulf of Mexico coast (Fig. 1). Due to its central position in the Atlantic mean storm track, Florida is frequently hit by tropical storms. Both estuaries are positioned behind peninsulas and the inlets are currently separated from the Gulf of Mexico by a series of barrier islands. Considerable environmental changes in both estuaries result from the gradual sea level rise throughout the Holocene (Chapter 1 and 2; Van Soelen et al., 2012). It has been shown that local flooding of the sites started at ~8.2 ka (Charlotte Harbor) and at ~7.5 ka (Tampa Bay). As

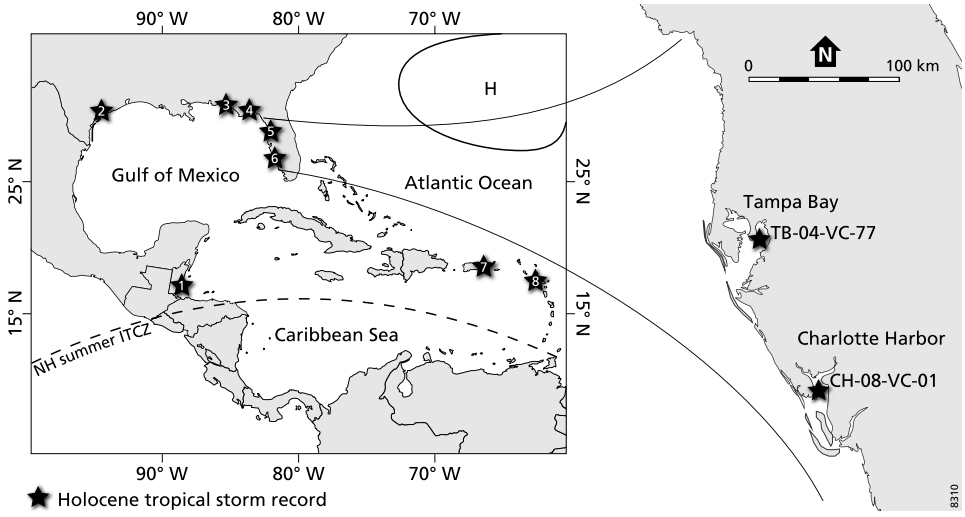

Figure 1. Left map: Gulf of Mexico and Caribbean Sea region with generalized position of the summer ITCZ and Bermuda High (H), and including sites that are discussed in this study. Tropical storm records are 1) Belize, (McCloskey and Keller, 2009); 2) Texas USA, (Troiani et al., 2011); 3) Alabama USA, (Liu and Fearn, 2000); 4) N Florida USA, (Lane et al., 2011); 5) Tampa Bay, Florida USA (this study); 6) Charlotte Harbor, Florida USA (this study); Puerto Rico, (Donnelly and Woodruff, 2007) and 8) St. Martin, (Malaizé et al., 2011). Right map shows the Florida Gulf coastline with Tampa Bay and Charlotte Harbor in more detail.

a consequence of the Holocene transgression, the initial lagoonal environment progressively became more open marine. Superimposed on the long-term development, sub-millennial scale changes in lithology as well as hydrological conditions were observed in the Charlotte Harbor and Tampa Bay records (Chapter 1 and 2; Van Soelen et al., 2012), indicating the site is also sensitive to short-term, potentially climatically forced, changes.

Currently, this part of the coast is characterized by a low wave activity (30-50cm) and tidal range (~1m) of the mixed (diurnal and semi-diurnal) type (Hine et al., 1987), due to the low slope gradient of the West Florida shelf. River discharge from the hinterland into the estuaries is highest during summer thunderstorms and tropical cyclones, but can reach a second peak in winter when El Niño-related winter precipitation is received (Stoker, 1992; Schmidt and Luther, 2002). We expect that in these relatively sheltered settings abnormal wave energy and/or long term peak precipitation will lead to a distinct alteration of hydrological conditions.

Here we present a multi-proxy study to investigate changes linked to storm activity in Charlotte Harbor and Tampa Bay sediment cores, focusing on the mid to late Holocene. In this novel approach we combine X-ray fluorescence analyses, dinoflagellate cyst analysis and hydrogen isotopic ratios of *n*-alkanes. A complete set of analyses is performed on the Charlotte Harbor core to verify sub-millennial scale variability in storm surge frequency, excessive precipitation, and associated mixing conditions. The replication of the dinocyst records on the two sites tests the spatial scale of the observed changes. The multi proxy approach provides a continuous record of Holocene storm frequencies independent of the long-term development of the Florida estuarine settings.

2. Material and Methods

2.1 Core description and chronology

Charlotte Harbor

In Charlotte Harbor a 549 cm long core CH-08-VC-01 (hereafter CH1; coordinates 26°52,799' N; 082°07,612' W; water depth ~6m) was retrieved in 2008, using a vibracorer deployed from the R/V Gilbert (Van Soelen et al., 2012). The core was taken from a hypoxic basin within the estuary, which is several meters deeper than the rest of the estuary (Evans et al., 1989). The lithology of core CH1 consists of a sandy base, which changes to estuarine organic clay above ~425 cm (~8.2 ka), and to sandy silt above 125 cm (~3.2 ka) (Van Soelen et al., 2012) (Fig. 2). Detailed X-ray fluorescence (XRF) scanning performed on core CH1 shows a number of predominantly sandy layers between 400 and 280 cm, and predominantly shell layers between 125 and 80 cm. Core chronology is based on 8 accelerated mass spectrometry (AMS) radiocarbon dated bivalves and gastropods, and additional ^{210}Pb measurements on the top 42 cm (Van Soelen et al., 2012). Radiocarbon ages were calibrated to years before present using Calib 6.0 (Stuiver et al., 2010), using the marine calibration curve with a 400-year correction.

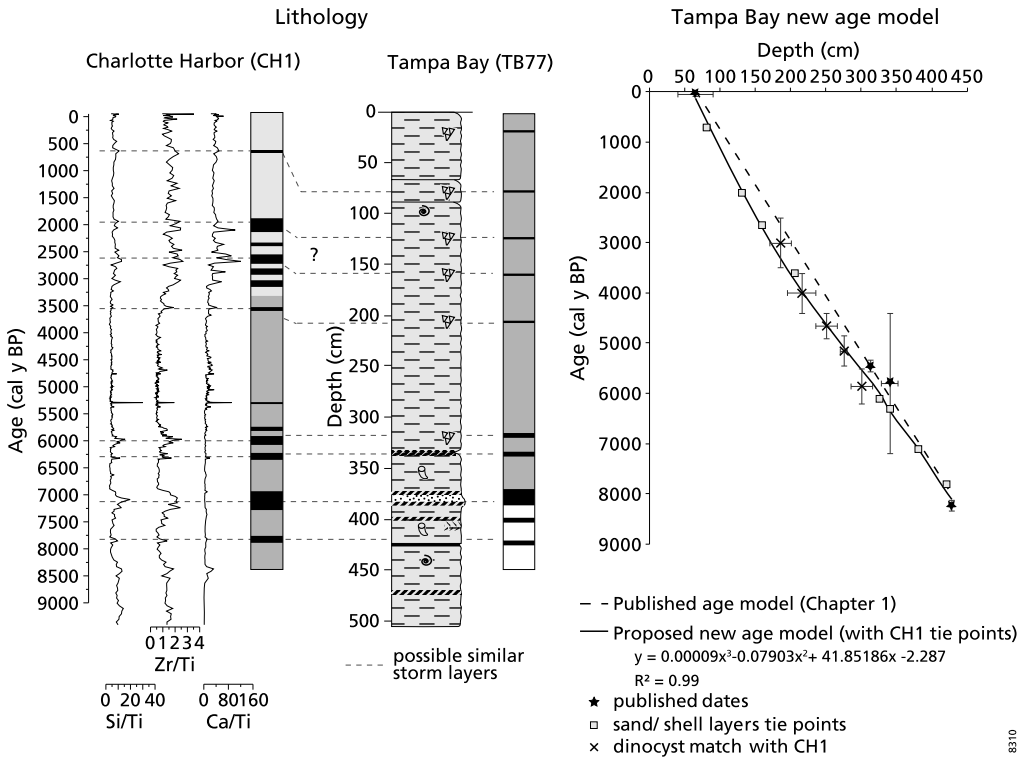

Figure 2. Left: Lithological descriptions of core CH1 (Charlotte Harbor) against age (cal y BP) and of core TB77 (Tampa Bay) against depth. High resolution XRF data for CH1 indicates shifts in quartz sand (Si), heavy minerals (Zr) and shells (Ca), normalized against Ti. Lithological columns are based on XRF data and previously published lithological description of TB77 (dark gray: estuarine organic mud, light gray: sandy silt, white: lacustrine mud, black bands: high energy deposits). Correlation of the observed high energy (storm) deposits is used as additional age-depth points for the new TB77 age model (right). Error bars indicate the age and depth uncertainty. For the dinocyst records errorbars indicate the mid-point between distinct assemblage changes, in age (CH1) and depth (TB77).

The age model indicates increased sedimentation rates from 0.02 cm/y around 8.5 ka to 0.16 cm/y around 5 ka, a subsequent reduction to 0.02 cm/y until the 20th century where it again increases to 0.74 cm/y.

Tampa Bay

From Hillsborough Bay, an inland lobe of the Tampa Bay estuary, a 511 cm long core TB-04-VC-77 core (hereafter TB77; coordinates 27°52' N; 82°27' W; water depth ~4 m) was retrieved in 2004, using a vibracorer deployed from the R/V Gilbert (Chapter 1). The bathymetry of this embayment indicates very little variation in water depth (average of 4 m), and does not exceed

6 m within the entire estuary (Brooks and Doyle, 1998). The lithology of TB77 changes from lacustrine pinkish mud to estuarine organic (sandy) mud above 375 cm (Cronin et al., 2007). Distinct layers of sand and shell fragments are present between 381 and 336 cm and above 210 cm (Fig. 2). The age determination is based on 2 AMS radiocarbon dates on *Polygonum* seeds (428 cm) and shells (315 cm) (Cronin et al., 2007), supported by pollen biostratigraphy (Chapter 1). The radiocarbon ages are calibrated using Calib 6.0 (Stuiver et al., 2010), where the atmospheric and marine calibration (with 400 year correction) curves are used on the seeds and shells, respectively. A linear model indicates sediment accumulation rates changing from 0.04 cm/y for the section between ~8.2 ka and 1900 AD to 0.6 cm/y for the 20th century.

Core correlation and adjusted age model for Tampa Bay

The low-resolution age determination of TB77 hampers an accurate temporal comparison of changes between the sites. In both cores, the observed sand or shell layers differ distinctly from the fine grained background sediment and are interpreted as high-energy or storm deposits (Van Soelen et al., 2012). Based on the assumption that these layers are simultaneously deposited, we apply the CH1 age determination of these layers to core TB77 (Fig. 2). Although various options are possible, correlation of the layers is done so that the resulting age determinations do not deviate too much from the original linear model. Based on these additional age-depth points, a new age model is determined. Age-depth points of distinct shifts in the dinoflagellate cyst assemblages of both cores are also plotted (see Fig. 2). These provide an independent support for the tuned age model, which is applied to TB77 onwards. Based on this model, the site flooded after ~6.9 ka which is still consistent with the regional relative sea level rise (Toscano and Macintyre, 2003). Sedimentation rates now show a similar pattern to CH1, with a distinct increase from 0.04 cm/y to 0.055 cm/y around 5 ka, and subsequent decrease to 0.04 cm/y, up to the 20th century.

2.2 Palynological analysis

Palynological samples were produced following standard procedures of the Laboratory of Palaeobotany and Palynology (Wood et al., 1996). For both TB77 and CH1 samples of ~1 gram freeze-dried material was used. In CH1 the 1 cm-thick samples represent an average of 10-50 year, and the TB77 samples approximately 18-25 year (based on the new age model). Prior to chemical processing, one tablet with a known amount of exotic spores (*Lycopodium clavatum*; 18,583 ± 4.1%) is added to each sample to allow quantitative analysis. Samples were treated with cold 10% hydrochloric acid (HCl) and cold 38% hydrofluoric acid (HF) in five alternate and subsequent steps to remove carbonates and silicates, respectively. Centrifuging (2000 rpm; 5 min) and decantation was carried out after each step. To remove clay-sized particles, the samples were sieved over a 10 µm mesh, after which the residue is again centrifuged (2500 rpm; 5 min) and decanted. The residue is mixed with glycerine water, and a homogenized fraction is mounted on glass slides for analysis. Counting was performed using a Leitz microscope (x400 magnification). At least 200 specimens were counted for each sample, and the identification of dinocysts follows Marret and Zonneveld (2003), Fensome and Williams (2004), Cremer et al. (2007). Relative abundances of the dinocysts assemblages are based on the total dinocyst sum.

2.3 Hydrogen isotope ratios of long chain *n*-alkanes

Samples from core CH1, that were analyzed earlier for biomarker content (Van Soelen et al., 2012), were selected for hydrogen isotope analyses of long chain *n*-alkanes. In the upper 130 cm of the core concentrations were too low to allow δD analyses. The 1 cm-thick samples represent an average of 10-20 y. Long chain *n*-alkanes were isolated from the hydrocarbon fractions using urea-adduction. Equal amounts (~200 µl) of hexane, acetone and urea dissolved in methanol (saturated) were added. Solvents were then evaporated under a nitrogen flow and remaining urea crystals were washed with hexane, resulting in a non-adduct fraction. Urea crystals were subsequently dissolved in approximately 500 µl of ultra-pure water and methanol. The solution was washed with hexane, resulting in the adduct fraction containing the straight chain, saturated alkanes. Purity was checked using a gas chromatograph (GC) fitted with a CP-Sil 5CB fused silica capillary column (30 m, 0.32 mm i.d.) and a flame ionization detector (FID). The oven temperature increased from 70 °C up to 130 °C by heating with 20 °C/min and then up to 320 °C by heating with 4 °C/min and then kept at this temperature for 20 min. Stable hydrogen isotope ratios of long chain *n*-alkanes were measured on a GC-IRMS (Delta^{plus}XP) using the same method and program as for the GC, but using a constant flow instead of constant pressure. Hydrogen isotope ratios (δD) were normalized to the VSMOW scale using a standard mixture of *n*-alkanes and squalane, which were calibrated against stable isotope reference materials (Schimmelmann, Biogeochemical Laboratories, Indiana University). The amount of material was insufficient for duplicate measurements.

3. Results and discussion

3.1 Florida estuarine records

The distinct high energy deposits of sand and shells embedded in finer grain size sediments are interpreted as simultaneously deposited storm layers. Particularly in CH1, these appear to be clustered. XRF scans on CH1 show that the older ones between ~7.8-5.9 ka are typically more rich in quartz sand (Si), and the younger ones between ~3.6-1.9 ka are richer in shell fragments (Ca) (Fig. 2) (Van Soelen et al., 2012). Before and after these two clusters, deposits are generally more homogenous and distinct sand/shell layers are fewer and/or thinner. XRF scans of cores taken along a riverine to coastal transect in Charlotte Harbor (Van Soelen et al., 2012) demonstrate that the quartz sand is largely supplied by fluvial input from the hinterland, whereas shell fragments have a marine origin. Although the lithological description of TB77 is not as detailed as CH1, layers of shell fragments are also generally observed in the top. This is consistent with a generalized spatial model of estuarine deposits: coarse grained terrestrial deposits close to the tidal river, fine homogenous mud in the center of the estuary and again coarse marine deposits closest to the coast (Dalrymple et al., 1992). The transition from riverine components at the base to marine components in the top of core CH1 reflects a temporal succession of these facies within the basin during the Holocene transgression. This also intrinsically implies that runoff or wave related high energy events in mid estuary depositional conditions (between ~5.9-3.6 ka) may not be reflected by either sand or shell deposits, respectively.

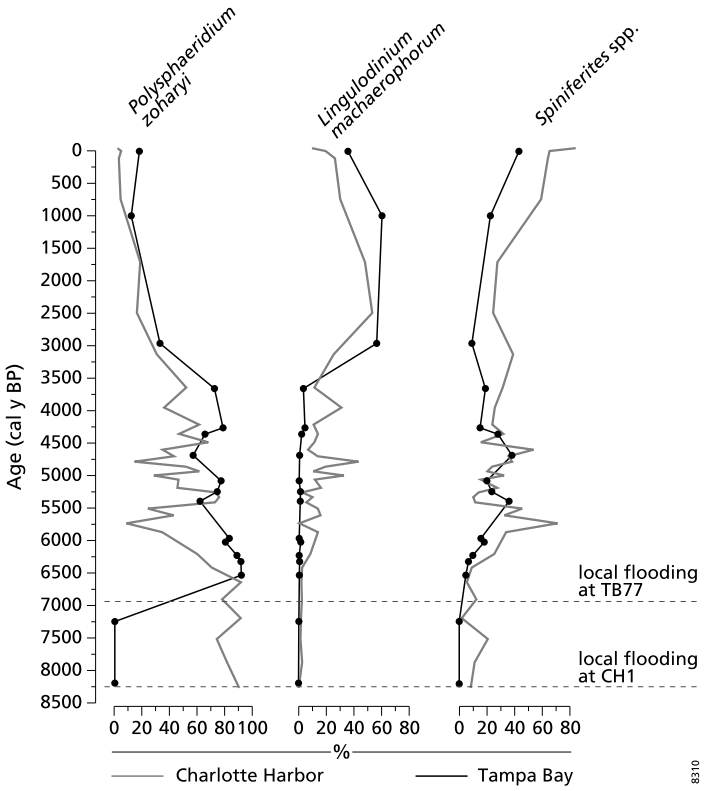

Figure 3. Diagrams showing relative abundances of main dinocyst species plotted against age, and the time of flooding at TB77 and CH1. More extensive dinocyst diagrams are presented in Chapters 1 and 2. Note: TB77 data is plotted against age using the adjusted age model.

The dinocyst assemblages of CH1 and TB77 are highly comparable, and both are dominated by the species *Polysphaeridium zoharyi*, *Lingulodinium machaerophorum* and *Spiniferites* spp. (Fig. 3) (Chapter 1 and 2). *P. zoharyi* overall dominates (to ~90%) both records up to ~3.5 ka. Afterwards, a co-dominance of *L. machaerophorum* (to maximal 50% in CH and 60% in TB) and *Spiniferites* spp. (to maximal 80% in CH1 and 40% in TB77) occurs, with *Spiniferites* spp. becoming more abundant after ~1.5 ka. Superimposed on this overall trend, distinct increases in *Spiniferites* spp. to 40-70% are observed in both cores between ~6.3 and 4.2 ka, in a section otherwise dominated by *P. zoharyi*. In the Gulf of Mexico, *P. zoharyi* commonly dominates shallow sheltered sites characterized by limited water circulation and high evaporation (Wall et al., 1977; Edwards and Willard, 2001; Cremer et al., 2007). *Spiniferites* spp. (mostly *S. mirabilis* s.l.) on the other hand, is common in coastal to open marine waters and has been found abundant in areas with low interseasonal SST variations and good water column mixing and/or where upwelling occurs (Marret and Zonneveld, 2003). Interestingly, the processes of

Spiniferites spp. are often found short and poorly developed, a morphological feature that has been related to low salinity conditions (Rochon et al., 2009). The observed peaks of *Spiniferites* spp. may point to more vigorous water mixing and/or ingression of marine water into an otherwise stratified lagoonal basin. The *Spiniferites* spp. shifts in both cores are summarized by merging the normalized relative abundances of each core (z-score = sample % minus average %, divided by standard deviation %) (Fig. 4). Despite the lower sample resolution achieved in TB77, the compatibility of the Tampa Bay and Charlotte Harbor dinocyst records critically shows that the observed shifts are reflecting a regionally occurring change.

Hydrogen isotope ratios (δD) of C_{27} *n*-alkanes measured on the mid Holocene section of CH1 range between -125 and -160 ‰ (vs. VSMOW), and show excursions towards more depleted values at 5.5 ka and between 4.9-4.1 ka (Fig. 4). A significant positive correlation between C27 and other less abundant *n*-alkanes like C25 and C29 (R^2 =0.6 and 0.7, respectively) suggests that these shifts are robust (unpublished data, E. van Soelen). To date, annual δD values of precipitation in southwest Florida vary between -11 to -31‰ (Bowen et al., 2005; Bowen, 2008; Price et al., 2008), whereas δD in tropical storms and cyclone–tied precipitation is generally more depleted, and can be as low as -200‰ (Lawrence et al.2002; Price et al., 2008). An offset in hydrogen isotope ratios in leaf waxes compared to precipitation results from evapotranspiration and biosynthetic fractionation (Sachse et al., 2004, 2006). Although the level of fractionation is highly species specific, no large-scale changes in the tree composition, from which the leaf waxes most likely derive, are observed in pollen assemblages during this time to explain the shifts observed in our record (Grimm et al., 1993; Watts and Hansen, 1994; Chapter 2). Therefore, the reduced values are most likely linked to isotopically lighter precipitation. One sample in the top of the core dated to 2002 AD ± 1.5 y has a depleted δD of -150 ‰, and may correspond to one of the most hurricane-active decades in recent history. Considering the extent of the observed 30‰ shifts in δD occurring over decades to centuries, these periods represent a strong and persistent increase in heavily depleted precipitation.

From the above it is clear that over the past ~8.2 ka gradual as well as highly dynamic changes occurred in depositional and hydrological conditions of both estuaries, and in the isotopic composition of water taken up by vegetation on land. The distinct shifts in the dinocyst and δD records only partly overlap with the clusters of sand/shell layers. As the concentration of organic matter is very low in the coarse-grained layers, changes in the dinocysts and isotopic composition of *n*-alkanes could not be measured in these layers specifically. Potential leads and lags between the dinocyst and δD records can moreover not be determined due to a different sample resolution, but the observed shifts occur broadly between 6.0-5.5 ka and 5.0-4.0 ka.

Temporary more marine conditions, as indicated by the increases in the abundance of *Spiniferites* spp., can theoretically be explained by a rise in the relative sea level. Mid Holocene sea level highstands in the Gulf of Mexico have been proposed, based on dated elevated beach ridges on the Texas and Alabama coast (Morton et al., 2000; Blum et al., 2001). The occurrence of these highstands, however, has been heavily debated (e.g. Törnqvist et al., 2004; Donnelly

and Giosan, 2008) as it contradicts Holocene records that show a continuous gradual relative sea level rise in the Gulf of Mexico (Törnqvist et al., 2004; Milliken et al., 2008). An alternative explanation for the elevated beach ridges is provided by Donnelly and Giosan (2008), who hypothesize that a mid Holocene higher 'constructional' wave swell associated with increased tropical storm activity may have shaped these coastal features. Strong winds and waves can also explain the ingression of marine water and/or ventilation of the water column in both estuaries. The concurrent increase in average precipitation rates, as observed in CH1, can best be explained by an overall increase in tropical storm activity, even though there is no direct lithological evidence. Based on the combined lithological, palynological, and isotopic evidence we propose that tropical storm activity in Florida increased broadly between ~6.4-5.5 ka, between ~5.0-4.0 ka and between ~3.2-1.9 ka.

3.2 Comparison to regional tropical storm records

Evidence supporting our findings is provided by multiple sites in the Gulf of Mexico and Caribbean Sea region (see Fig. 1), although few records cover the mid Holocene period. A continuous grain size analysis on lagoonal deposits of Puerto Rico shows a highly similar pattern in storm activity as our Florida sites, with overwash deposits clustered between ~5.5-4.0 ka and between ~2.5-1.0 ka (Fig. 4) (Donnelly and Woodruff, 2007). Clustered layers of coarse overwash deposits also are observed in coastal peats of Belize between ~5.4-4.5 ka and between ~3.4-2.6 ka (McCloskey and Keller, 2009). Grain size analyses focusing on aeolian input in Texas estuarine deposits indicate that the windiest conditions occurred between ~5.2-4.1 ka (Troiani et al., 2011). Late Holocene coastal records show increased overwash deposits between ~3.6-1.0 ka on the Alabama coast (Liu and Fearn, 1993, 2000), between ~2.8-2.3 ka on the north Florida Gulf coast (Lane et al., 2011), and between ~3.7-2.5 ka on the Caribbean St. Martin island (Malaizé et al., 2011). The timing of the inferred storm phases varies between the records, obscuring a possible regional trend. Latitudinal shifts of the general storm track within the Gulf of Mexico – Caribbean region have been proposed as an explanation for the variable timing (McCloskey and Knowles, 2009; Malaizé et al., 2011). An additional critical factor is the low resolution age-determination of a number of records, leading to offsets in timing. The well-dated (CH1) multiple proxy records from the Florida estuaries possibly provides a more robust reflection of mid to late Holocene tropical storm variability for the Gulf of Mexico–Caribbean region.

3.3 Potential forcing mechanisms

Historical Atlantic tropical storm variability has been related to a variety of factors. Higher SSTs in the main development region, broadly covering the tropical Atlantic Ocean, leads to increased tropical storm formation or intensification (Wang et al., 2006). During the early to mid Holocene, high SSTs are observed in the Gulf of Mexico and Caribbean Sea (Lea et al., 2003; Poore et al., 2003; Nürnberg et al., 2008), reflecting a maximal expansion of the Atlantic Warm Pool during the Holocene Thermal Maximum. The ITCZ had a more northward position during summer (Haug et al., 2001), and the Gulf of Mexico–Caribbean region experienced wet conditions due to strong convective precipitation (Hodell et al., 1991). Such

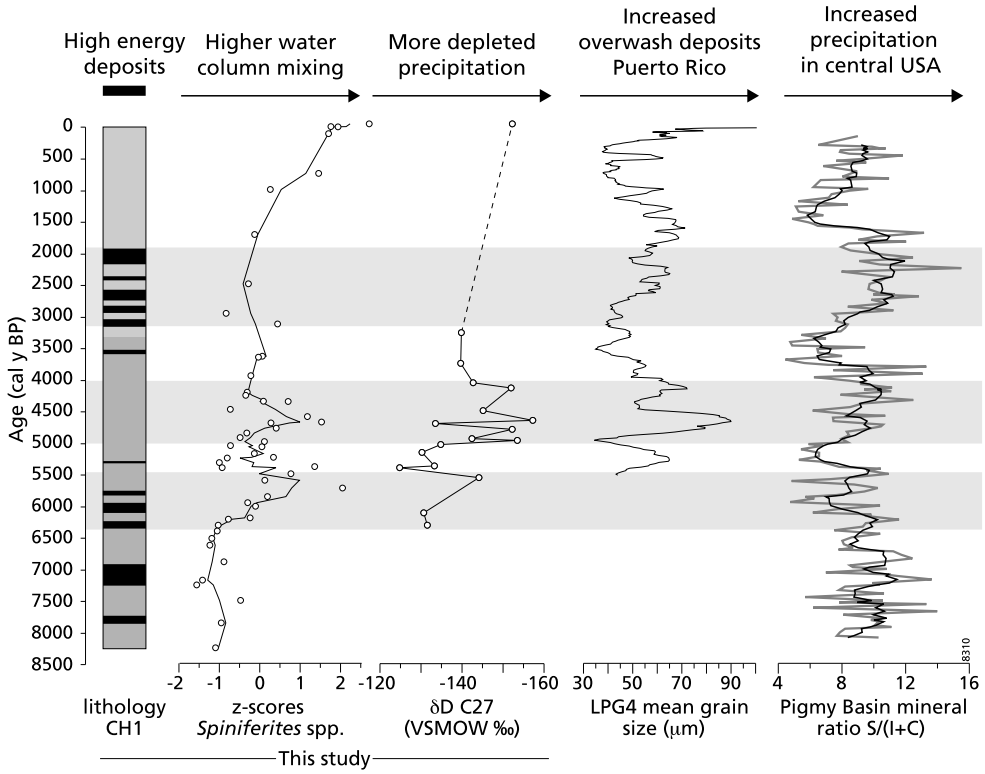

Figure 4. Overview of results, including lithology (dark gray: organic mud, light gray: sandy silt, black bands: sand/shell layers), combined CH1 and TB77 z-scores of *Spiniferites* spp. and 3point moving average (black line), δD measured on C27 *n*-alkanes from leaf waxes in core CH1, mean grain size data on Puerto Rico lagoonal deposits (5 point moving average) (Donnelly and Woodruff, 2007), and the inland mineral ratio recorded in the Pigmy Basin, Gulf of Mexico (Montero-Serrano et al., 2010). Horizontal bars indicate proposed phases of increased storm occurrences in the CH1 and TB77 records.

elevated SSTs would have fuelled tropical storm activity during the early to mid Holocene. After ~4.5 ka a cooling trend in regional SSTs is observed, related to the gradually reduced northern hemisphere insolation (e.g. Ziegler et al., 2008). This millennial-scale trend does not explain the observed sub-millennial variability in storm deposits throughout the Gulf of Mexico and Caribbean region, suggesting interference of processes pacing on shorter time scales.

Donnelly and Woodruff (2007) relate mid to late Holocene increased tropical storm activity in Puerto Rico to periods of an enhanced African monsoon and reduced El Niño activity (Moy et al., 2002). The increased vertical wind shear during El Niño events hinders tropical storms to form, whereas La Niña event are found to enhance their development (Gray, 1984). Besides

the potential storm intensification under high SSTs and reduced El Niño, historical records indicate that the general storm track zone is determined by modes of the North Atlantic Oscillation (NAO) and the summer position of the Bermuda High (BH) (Walsh and Reading, 1991; Elsner et al., 2000). A weak, southwestward extending BH during a negative NAO generally leads storms into the Gulf and Caribbean region, whereas they recurve northward to the US east coast during a strong eastward positioned BH and positive NAO (Elsner et al., 2000). Sub-millennial scale changes in such NAO-like conditions may be an additional factor determining the tropical storm occurrences expressed in the Florida records.

Under a long term dominant control of the BH, increased tropical storm activity in the Gulf of Mexico–Caribbean region would coincide with tranquil conditions along the East Coast. Storm activity records from the northeastern coastal States are contradictory, and usually do not extend further back than the past 2 millennia. Some of the available long records indeed show a pattern opposite to that of the Gulf of Mexico–Caribbean sites, with high storm activity in the past 1.0 ka and calmer conditions before (Scott et al., 2003; Boldt et al., 2010), whereas others are comparable to the Gulf of Mexico–Caribbean records (Scileppi and Donnelly, 2007). This relation however, cannot be sufficiently confirmed or denied as the temporal overlap with eastern USA coastal storm records is too short. However, tropical storms are an integral component of the atmospheric system, and precipitation patterns which are not directly linked to tropical storms can serve as a substitute for reflecting past BH variability.

Away from the coastal regions, a dominant role of the BH has been proposed in the distribution of precipitation over the North American continent (Knox, 2000; Forman et al., 1995). The precipitation belt over the continent is modulated by a complex interaction between the summer position of the Jet Stream, BH and ITCZ (Knox, 2000). Moist air transport from the Gulf of Mexico into the central USA is particularly enhanced by a more southwestward position of the BH (Forman et al., 1995). Detailed lithological analyses on deposits from the Pigmy Basin (Gulf of Mexico) reveal alternating mineral compositions, which are directly linked to precipitation variability in the central and eastern USA source areas within the Mississippi catchment (Sionneau et al., 2008; Montero-Serrano et al., 2010) (Fig. 4). Indeed, the late Holocene cluster of shell debris layers in CH1 (Van Soelen et al., 2012) coincides with an increase in precipitation in central USA (Montero-Serrano et al., 2010). Moreover, comparison of our dinocyst and δD shifts during the mid Holocene, as well as the tropical storm record from Puerto Rico (Donnelly and Woodruff, 2007), to the ratio of specific inland minerals shows a highly consistent pattern. There is no strong (opposite) teleconnection for either central or eastern USA to the El Niño-Southern Oscillation (Ropelewski and Halpert, 1986) that can explain the highly similar precipitation-tropical storm pattern. Therefore, these results strongly suggest a dominant role of the Bermuda High besides the ENSO in controlling sub-millennial scale tropical storm activity in the Gulf of Mexico–Caribbean region during the mid to late Holocene.

4. Concluding remarks

Evidence for increased tropical storm occurrences between ~6.4-5.5 ka, ~5.0-4.0 ka and ~3.2-1.9 ka is inferred from combined XRF, dinoflagellate and δD records from Tampa Bay and Charlotte Harbor, Florida. Because long-term landscape dynamics and the Holocene transgression have altered deposition in the coastal environments, high energy conditions are not reflected in the same fashion throughout multiple millennia. We have shown that the use of proxies reflecting estuarine hydrological changes associated with tropical storms, like dinocysts, and changes in the isotopic composition of precipitation, like δD in leaf waxes, are a valuable addition to the traditional lithological approach. In particular the reproduction of the dinocyst records at two separate locations confirms the forcing by a large-scale mechanism.

Our results from the Florida estuaries are broadly consistent with records throughout the Gulf of Mexico and Caribbean, and are an important contribution to the better understanding of spatial and temporal Holocene tropical storm variability. The mid and late Holocene variability expressed in the Florida records is potentially related to the position and strength of the Bermuda High, which may have determined the general storm track into the Gulf of Mexico-Caribbean region. Long, high-resolution archives from the northeastern US coast are needed to confirm the proposed sub-millennial scale alternation of storm tracks forced by the Bermuda High.

170 x 240 mm

Chapter 4

Late Holocene wetland development in Highlands Hammock State Park (central Florida) inferred from pollen and diatom assemblages

Abstract

Available proxy records from across the Florida peninsula sometimes give an inconsistent view on hydrological changes during the late Holocene. At low elevation sites a rising groundwater table related to the Holocene transgression may have overprinted precipitation-related hydrological variability. Wetlands in the elevated central ridge of Florida are possibly more sensitive records of precipitation variability. Here we present records of hydrological changes over the past ~2.5 ka (calibrated kiloyears BP), inferred from pollen and diatom analyses on two peat cores from Highlands Hammock State Park, central Florida. The initiation of the wetland at ~2.5 ka indicates a first increase in humidity. The subsequent vegetation development towards increasingly dry conditions is likely related to natural succession and basin infilling, although continuous long hydroperiods are indicated by the diatom assemblage. A distinct expansion of aquatic taxa between ~1.3-1.0 ka indicates a climatic shift to wetter conditions. The wetland initiation and aquatic expansion are possibly caused by increased precipitation, related to regionally higher sea surface temperatures and a temporary northward migration of the Intertropical Convergence Zone. The wet phase and subsequent strong drying over the last millennium, as indicated by shifts in both pollen and diatom assemblages, can be linked to the early Medieval Warm Period and Little Ice Age, respectively. Distinct changes in both vegetation and diatoms during the 20th century are the result of moats and dike construction intended to protect the Highlands Hammock State Park from wildfires.

1. Introduction

Major long-term hydrological changes have been reported in pollen records from central Florida lake deposits, where prominently the alteration between oak-ragweed and pine dominated vegetation reflects drier and wetter periods over the past 60 ka (calibrated kiloyears BP) (Grimm et al., 1993; Watts and Hansen, 1994; Grimm et al., 2006). During the Holocene, regional vegetation again shifted from dry oak to wetter pine dominance across the peninsula around 6.5 ± 1 ka (Watts and Hansen, 1994). Recent work on Florida estuarine deposits shows that this vegetation change co-occurs with an increase in runoff, suggesting increased precipitation in combination with sea level rise as important driver (Van Soelen et al., 2012; Chapter 2). An ongoing change to wetter conditions is indicated by increased *Taxodium* abundance after ~2.7 ka (Watts and Hansen, 1994). Although the central Florida lake pollen records demonstrate the pronounced precipitation linked vegetation dynamics on the longer time-scales, no detailed evidence for sub-millennial scale changes in precipitation after the major mid Holocene vegetation transition are available from this source.

Palynological evidence for mid to late Holocene sub-millennial scale hydrological variability, however, is available from wetland environments in south Florida (Willard et al., 2001a; Donders et al., 2005a). High-resolution pollen analysis of peaty substrates from the Everglades area reveal wet conditions between ~3.8-3.0 ka and a subsequent drying, as reflected by the transition from long hydroperiod slough vegetation to moderate hydroperiod saw grasses (Willard et al., 2001a). From multiple records throughout the area, two dry intervals are deduced around 1.0 ka and 0.4 ka, indicated by increasing presence of drought indicator plant species and wetland development (Willard et al., 2001a; Willard et al., 2006; Bernhardt and Willard, 2009). Conversely, a stepwise increase in wetland development, as observed in a pollen record from southwest Florida, an intensified fresh water flow over the past 5 ka is suggested to be precipitation-driven (Donders et al., 2005a). At this location, late Holocene century-scale dynamics are less clear due to the establishment of a closed *Taxodium* dominated swamp vegetation.

Additional evidence for precipitation-linked hydrological changes are available from speleothem growth rate analysis (Van Beynen et al., 2007, 2008), and stable isotopes on otoliths and shell from coastal archaeological mounts (Wang et al., 2011) and on ostracod assemblages in lake deposits (Alvarez Zarikian et al., 2005). In particular the latter study provides a full Holocene record, but the strong influence of other (ground- and sea water) sources also strongly affect the isotopic composition at this site, potentially masking precipitation related changes. Overall, the large variety in environments studied and proxies used, as well as dating uncertainties and sampling resolution, so far hamper the construction of a reasoned regional pattern of hydrological conditions for Florida during the late Holocene. Moreover, the low elevation of a number of sites might induce an overprint of the record by the Holocene relative sea level (RSL) rise, which affected the groundwater table. The lack of consistency between the

Florida records may thus relate to a whole range of causes originating from site specific, local hydrological conditions, and the general dry/wet sensitivity of the studied environments.

Wetland areas in the elevated central part of Florida are hardly explored so far, and are expected to be largely dependent on precipitation, or precipitation induced seepage from the aquifers. The plant associations in wetlands are directly related to surface water depth and ponding duration (hydroperiod) (Kushlan, 1990; Willard et al., 2001b; Givnish et al., 2008; Bernhardt and Willard, 2009). Sub-century to decadal scale dry or wet periods directly lead to compositional reorganization of the wetland flora, traceable in the pollen record. Besides pollen-based vegetation reconstructions, the analysis of diatoms (siliceous algae) has proven to be a highly useful tool for determining aquatic environmental change (Gaiser et al., 1998, 2001, 2004). Due to their short reproductive cycle and sensitivity to environmental conditions as water depth, acidity, and hydroperiod (Battarbee et al., 1986; Smol and Stoermer, 2010), changes in their assemblages can be applied for reconstructing local hydrological changes in freshwater environments.

Here we present sub-centennial scale resolution pollen and diatom records from two peat sections from Highlands Hammock State Park in central Florida. A substantial and continuous peat layer within the park developed over the past ~2.5 ka. As the basin from which the peat sections were recovered is largely rainwater fed, vegetation and diatoms likely responded to past precipitation. Studying records from two closely spaced sites may lead to a more robust documentation of local hydrological conditions. The study of peat sections will add substantial information on short-term precipitation dynamics contributing to a more comprehensive overview of hydrological changes in Florida. Once the local precipitation-induced variability is determined, the records can be placed into a broader spatial and temporal context by comparison with additional Gulf of Mexico and Caribbean records of late Holocene climatic signals.

2. Regional setting

2.1 Geomorphology

Highlands Hammock State Park (HHSP) is located along the western edge of the Lake Wales Ridge in Highlands County, central Florida (Fig. 1A). This area is characterized by a series of north-south-oriented relict shorelines and dunes formed during Pleistocene sea level highstands of the Yarmouth and Sangamon interglacials. These sandy deposits overlay a karstic Eocene to Miocene limestone bedrock (Scott et al., 2001). The HHSP is located in a basin between two of these sandy beach ridges, resulting in an elevation range within the park of ~45 to 24 m above sea level (m asl). Clay deposits present in the subsurface of the basin hamper water percolation, and allow for the formation of peat in the lowest and wettest sections of the area. A peaty top layer has formed within the basin surrounding a limestone 'bump' present in the center of the park (Fig. 1B). Below the continuous organic top layer the deposits first

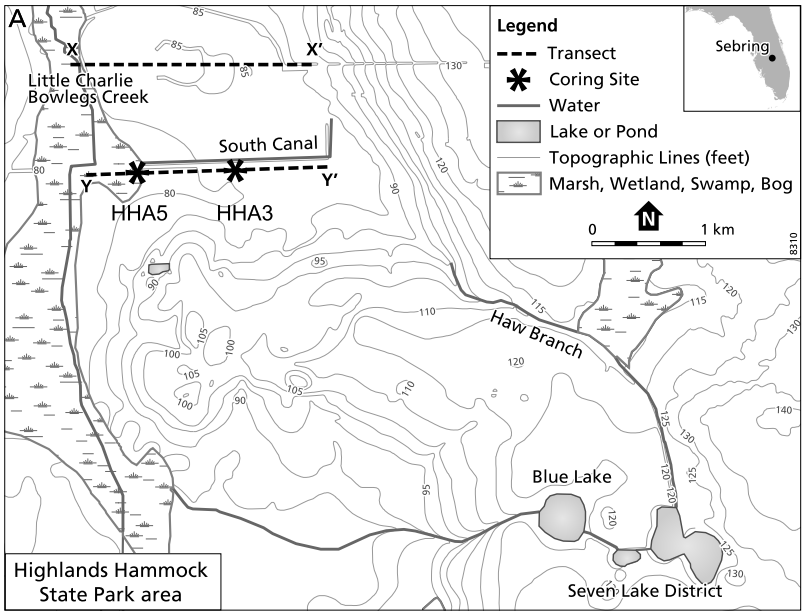

Figure 1. A) Map of the Highlands Hammock State Park and surrounding area, with topographic lines (in feet above sea level). The two coring transects are indicated by dotted lines, and locations of the sampled sites are indicated by asterisks.

become more clayey and then more sandy, up to a depth of ~230 cm where a sudden transition to a compacted black horizon, likely a paleosol, is present (Fig. 1C).

Central Florida has a subtropical climate with day temperatures ranging between 23-33°C. The mean annual precipitation measured at the closed meteorological station is 1325 mm, of which most is received between June and September, during summer storms (Sebring weather station; weather.com). This weather pattern is strongly determined by the annual movement of the North Atlantic Subtropical- or Bermuda High (BH). On multi-decadal scale, enhanced summer precipitation over the Florida peninsula has been linked to warm phases of the Atlantic Multidecadal Oscillation (AMO) (Enfield et al., 2001), whereas anomalously high winter precipitation is related to the El Niño mode of the Pacific El Niño-Southern Oscillation (Cronin et al., 2002). Rain water percolates through the sandy ridges and seeps out at the slopes and base of low lying sites like HHSP, resulting in two minor creeks named Haw Branch and Tiger Branch that enter the park from the eastern beach ridge. Of these two, Haw Branch is a seasonal creek discharging precipitation surplus from the Seven Lake district, and dissipates to sheetflow as soon as it enters the basin. The main drainage through the park is Little Charlie Bowlegs Creek with a south to north discharge of the park, into which Haw– and Tiger Branch merge. Water depth and discharge of this system is subject to highly seasonal fluctuations.

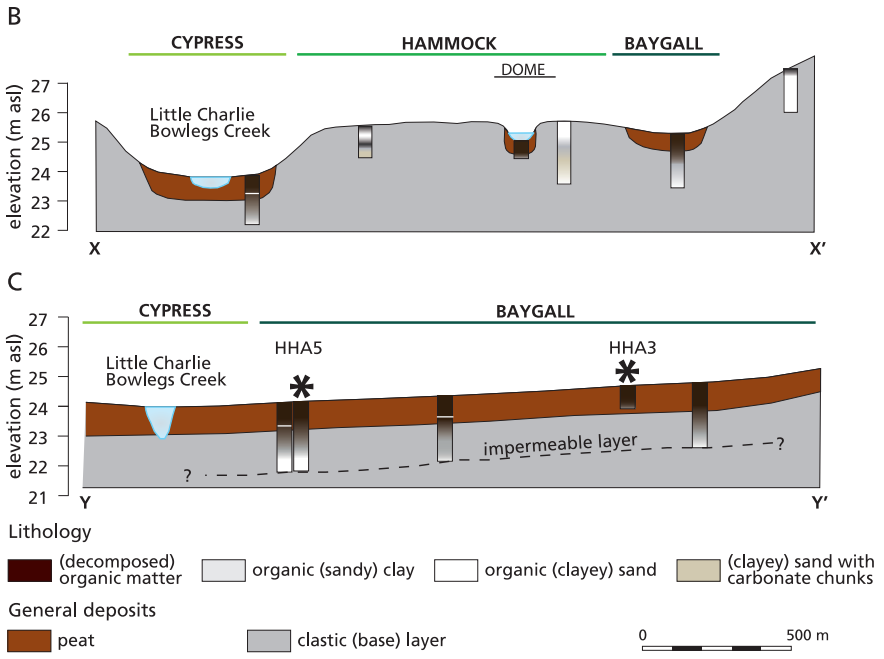

Figure 1. B) Cross-section of transect X-X' with main vegetation types. C) Cross-section of transect Y-Y' with main vegetation types and sampled sites (asterisks).

2.2 Present-day vegetation

The distribution of the natural communities reflects the local topography, which determines local hydrological conditions (FDEP, 2007). On the elevated well-drained sandy ridges east and west of the park pine flatwoods are present, characterized by longleaf pine (*Pinus palustris*) and slash pine (*P. elliottii*), accompanied by live oak (*Quercus virginiana*), with a palmetto (*Serenoa repens*) and wiregrass (*Aristida stricta*) ground cover. The central feature of the park is the hydric hammock located on the limestone hill, dominated by a variety of hardwood species like live oak, sweet gum (*Liquidambar styraciflua*), pignut hickory (*Carya glabra*), together with cabbage palm (*Sabal palmetto*) and a dense understory of various shrubs, ferns and epiphytes. Within the hammock a number of 'domes' are present due to karstic solution features, where pop ash (*Fraxinus caroliniana*) and swamp tupelo *(Nyssa sylvatica*) are common. Surrounding the central hammock, following the sheetflow drainage, baygall swamp with mostly sweetbay (*Magnolia virginiana*), loblolly bay (*Gordonia lasianthus*), and red maple (*Acer rubrum*) is present, with a common understory of wax myrtle (*Morella cerifera*), dahoon (*Ilex cassine*) and a variety of ericaceous species and vines. The lower section of the main drainage is wettest and is dominated by swamp cypress (*Taxodium distichum*), but accompanied by laurel oak (*Quercus laurifolia*) and red maple. At present, the area surrounding the park is mainly occupied by citrus plantations and urban areas.

3. Material and methods

3.1 Core collection

Prior to collecting the cores in April 2008, test corings were done in an east-west transect along the park road south of the hydric hammock through the baygall swamp (Figs. 1B and 1C). Two sample cores were collected along transect Y-Y': HHA3 27°27'47.45" N, 81°32'21.48" W) of 79 cm in length was taken with a manual peat corer, and HHA5 (27°27'47.40" N, 81°33'03.35" W) of 231 cm in length with a vibracorer. The distance between the two cores is approximately 1100 m. Site HHA3 is situated at an elevation of ~24.5 m asl with dominant *Acer rubrum* vegetation, whereas HHA5 is located closer to Little Charlie Bowlegs Creek at an elevation of ~24 m asl and dominant *Magnolia virginiana* vegetation. At both sites the water table was 10-20 cm below the surface at the time of coring.

3.2 Sub-sampling and analyses

Loss-on-ignition (LOI) was measured following Heiri et al. (2001), for core HHA3 on a resolution of 1 cm and for core HHA5 every 2.5 cm. Organic remains including charcoal, seeds, and insect remains from the top sections of both peat cores and bulk material for the deeper core sections was used for accelerated mass spectrometry (AMS) radiocarbon dating at Beta Analytics (Miami, USA) and Poznan Radiocarbon Laboratory (Poznan, Poland) (Table 1). The total of 16 AMS ^{14}C dates are calibrated to calendar year before present (0 y BP = 1950 AD), using the bomb-pulse method for the core top samples (Levin and Kromer, 2004) and IntCal09 (Stuiver et al., 2010) for the other samples. Calibrated calendar years before present will be referred to as ka (kilo annum before present) in the following.

Subsamples of ~0.1-0.3 g freeze-dried sediment were used for pollen analysis. Standard procedures by (Fægri et al., 1989) were followed, including HCl (30%), KOH (10%), HF (40%) and acetolysis treatments, to remove carbonates, organic matter, and silicates. Prior to chemical treatment *Lycopodium clavatum* tablets with a known amount of spores were included to allow quantitative analysis. Samples were sieved over a 250 µm and 10 µm mesh to further remove remaining organic detritus and clay-sized particles. The 250-10 µm fraction residues were mixed with glycerine water and mounted on microscopic slides for analysis using a Leitz light microscope (x400 magnification). At least 300 pollen were counted for each slide, of which at least 200 pollen of non-arboreal species. Identification of the pollen was largely based on Willard et al. (2004) and the unpublished reference collection of the Utrecht University.

For diatom analysis subsamples of ~0.5-1 g of freeze-dried sediment were subsequently treated with H_2O_2 (1.5 hours at 100 °C), HCl, and HNO_3 (2 hours at 120 °C) solutions to remove organic matter and carbonates. After seven cycles of decanting and refilling with demineralized water to attain a neutral pH, a known fraction of each sample was allowed to settle onto coverslips in evaporation trays (Battarbee, 1973) before being permanently fixed on slides using the high refraction mountant Naphrax®. On each slide at least 400 diatom valves were counted using a Leica DM2500 microscope, equipped with an oil immersion lens

HHA3	Depth (cm)	Material	Lab ID	Conventional ^{14}C age	Cal.age (year BP)
	1-2	Leaf fragments	Poz-32696	105.92 ± 0.34 pMC	-55.86 ± 1.01 *
	6-7	Leaf fragments, chitin, seed	Poz-32771	106.94 ± 0.36 pMC	-53.93 ± 1.14 *
	12-13	Leaf fragments, chitin, seeds	Poz-32695	100.6 ± 0.35 pMC	-1.31 ± 0.36 *
	22-23	Charcoal	Poz-35343	230 ± 30 year BP	291 ± 24 ^
	31-33	Leaf fragments, chitin, seeds	Poz-32697	550 ± 40 year BP	539 ± 27 ^
	47-48	Charcoal	Beta-254241	1360 ± 40 year BP	1288.5 ± 55.5 ^
	60-61	Bulk sediment	Poz-35344	1645 ± 30 year BP	1551 ± 66 ^
	64-65	Leaf fragment, charcoal	Poz-32699	104.41 ± 0.36 pMC	-56.84 ± 1.01 ^ X
	74-76	Plant material	Beta-254242	810± 40 year BP	731.5 ± 58.5 ^ X
	78-79	Bulk sediment	Poz-35345	2460 ± 30 year BP	2489.5 ± 62.5 ^
HHA5					
	10-11	Leaf fragments, seeds	Poz-32700	107.7 ± 0.35 pMC	-52.495 ± 1.01 *
	19-20	Leaf fragments, charcoal	Poz-35336	103.55 ± 0.34 pMC	-2.575 ± 1.1 *
	29-30	Charcoal, chitin, seeds	Poz-35337	970 ± 30 BP	835 ± 39^
	40-41	Bulk organics	Poz-32701	680 ± 30 BP	657 ± 24 ^
	55-56	Bulk sediment	Poz-35338	1555 ± 30 BP	1453 ± 72.5 ^
	67-68	Bulk sediment	Poz-35339	4375 ± 35 BP	4922.5 ± 64.5 ^
	80-81	Bulk sediment	Poz-35340	4470 ± 35 BP	5220 ± 69 ^

Table 1. Radiocarbon dates HHA3 and HHA5. Conventional radiocarbon dates were given in years before present (year BP) or percentage modern carbon (pMC). All dates were calibrated into calendar years before present (ka; 0 ka refers to 1950 AD) using the following radiocarbon calibration datasets: Levin ^{14}C (Levin and Kromer 2004; indicated by *) and IntCal09 (Stuiver et al., 2010; indicated by ^). Means and uncertainties were calculated from the lowest and highest dates at the 2σ probability distribution. Samples in HHA3 with X are considered outliers.

and differential interference contrast at a magnification of x945. Diatom identification for most species followed Patrick and Reimer (1966), Camburn and Charles (2000), Gaiser and Johansen (2000), Siver et al. (2005).

3.3 Data analysis

Zonation of the pollen (PAZ: pollen assemblage zone) and diatom (DAZ: diatom assemblage zone) diagrams is based visual inspection supported by CONISS output on the non-transformed (Euclidean distance) percentage data. Due to the 20th century human alteration of the landscape, no surface samples could be taken that could serve as reliable modern analogues of past wetland plant associations. In the Everglades National Park extensive surface sampling has been performed in a large variety of wetland types, covering a large range of hydrological

conditions (Willard et al., 2001b, 2006; Bernhardt and Willard, 2009). To be able to apply this information for the reconstruction of environmental changes in HHSP, pollen relative abundances are based on a pollen sum including all observed vascular plants (so excluding *Sphagnum*), as is the standard procedure in the Everglades studies. This will inevitably include pollen transported into the basin from elsewhere, not reflecting the local hydrological variability. To prevent masking of hydrological trends by this 'background' pollen rain, relative abundance changes are supported by pollen concentrations (pollen/g dried sediment).

Based on the diatom records, changes in hydroperiod or ponding duration were reconstructed for both sites, using a weighted-averaging regression model on taxon-specific hydroperiod optima in comparable South Carolina wetlands in South Carolina and Georgia (Gaiser et al., 1998). For this approach only species with a relative abundance of >3% in at least one sample were used. Following Gaiser et al., (1998), the hydroperiods are indicated by numbers 1-5, indicating ponding duration of <50% (< 6 months), 50-75% (6-9 months), 75-83% (9-10 months), 83-98% (10-almost 12 months) of the year and annual inundation, respectively.

4. Results

4.1 Lithostratigraphy and chronology

Core HHA5 shows that on top of the compacted soil layer at a depth of 231 cm, deposits are predominantly sandy but gradually become more clayey from ~120 cm upwards (see Fig. 1C). Despite the blackish color of these clastic deposits, LOI values of <5% indicate organic matter is practically absent in this core section. From 55 cm upwards in HHA5 and 79 cm upwards in HHA3 lithological changes are comparable. The deposits change to dark brown clay and become more organic, with LOI values gradually increasing from 20% to 80% (Fig. 2). Decomposition of these organic deposits becomes less towards the top, but only the top ~20 cm is rich in recognizable plant remains. The LOI at 950°C results in values around 1% throughout core HHA3, reflecting the error range of the method (Heiri et al., 2001), and indicating that there is no considerable carbonate present in the organic deposits. The cores reflect lithological changes that are found throughout this section of the swamp (see Fig. 1C). Because the clastic deposits are barren in pollen below the organic top 70 cm of HHA5, they are not considered in this study.

Based on eight AMS ^{14}C dates (Table 1) an age-depth model is constructed for core HHA3 (Fig. 2), using the open source R code package CLAM (Blaauw, 2010). Two other AMS ^{14}C dates (Poz-32699 and Beta-254242) are identified as outliers, due to their distinctly younger ages at these depths, possibly due to a coring artifact. Deposition rates change from ~0.03 cm/year at the base (20-79 cm), to ~0.1 cm/year (10-20 cm), to ~0.33 cm/year in the top (0-10 cm). The gradually increasing decomposition and compaction of organic matter is reflected in the exponential change in sedimentation rate from the top down. The constructed age model suggests a basal age for core HHA3 of 2511 ± 177 y.

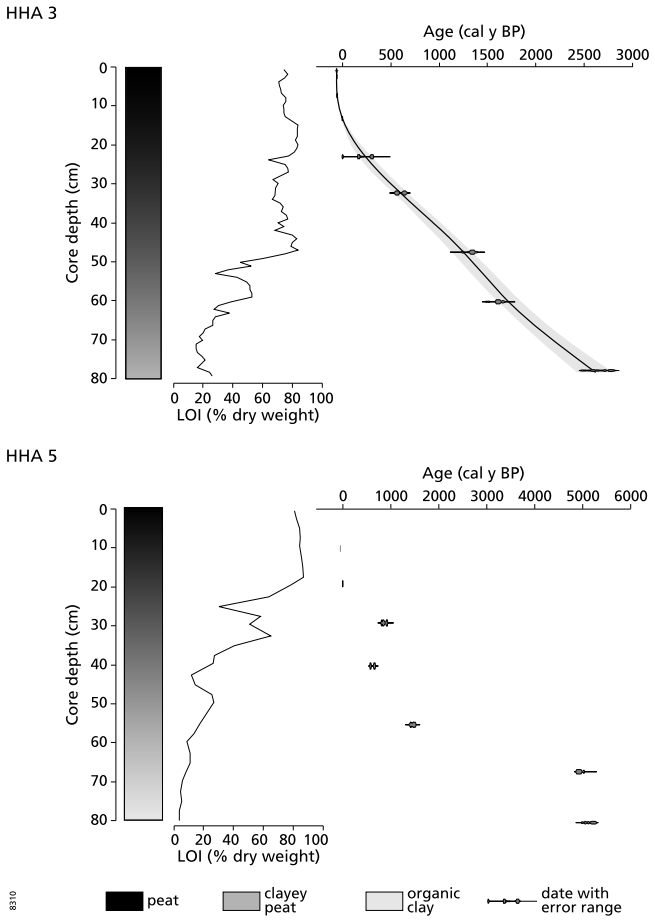

Figure 2. Lithology, loss on ignition and available calibrated radiocarbon dates for cores HHA3 (top) and HHA5 (bottom). An age model (black line) and associated error range (gray band) is constructed for HHA3.

Constructing a reliable age model for HHA5, based on the seven AMS ^{14}C dates available for this core (Table 1), is controversial. Besides an age reversal between the dates at 29.5 cm and 40.5 cm, the dates at depths 67.5 cm and 80.5 cm show an unlikely strong aging as compared to the dates above this depth (Fig. 2). The core lithology does not show any distinct bioturbation or indications for hiatuses. So unlike with HHA3, outliers could not be securely identified. The available dates thus lead to various options for age models. In this setting it can be assumed that changes in the absolute background pollen rain are similar at the two sites. Additionally, a distinct vegetation change after 16 cm likely reflects the 1930s human interference of the landscape. We therefore correlate core HHA5 to core HHA3 by wiggle matching these main shifts in the pollen concentration data, assuming that the changes occurred simultaneously at the two sites. Further details on the strategy are provided in section 'pollen concentrations and core comparison'.

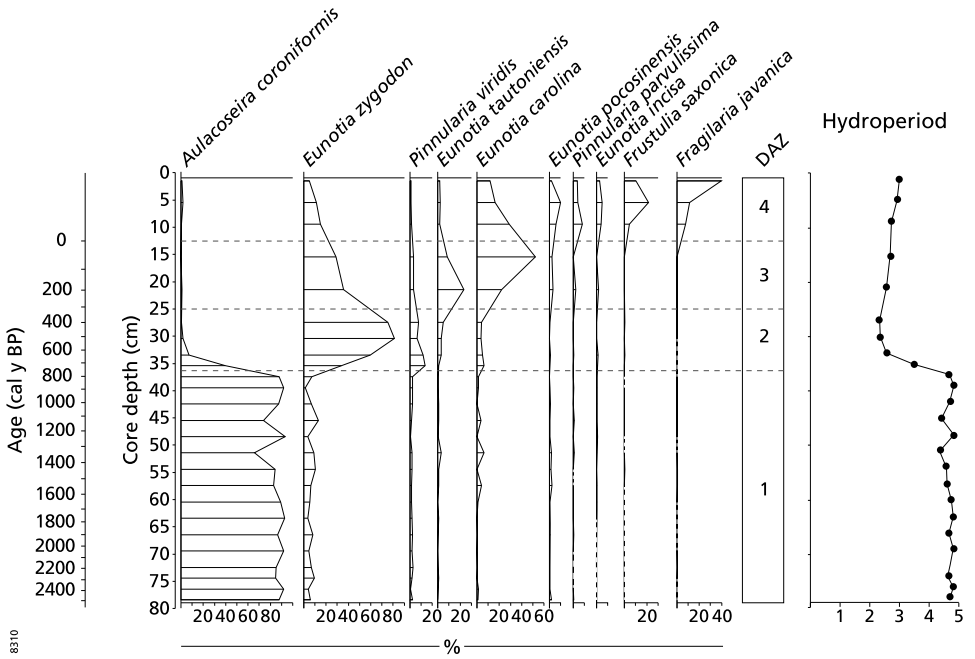

Figure 3. HHA3 diagram showing the most abundant diatom species plotted against depth, with addition of the age scale on the second y-axis, and calculated hydroperiods (see section Material and Methods, data analysis).

4.2 Diatom relative abundances

Diatom valves are moderately to well preserved in all studied samples. The species composition in both cores is similar, encompassing a total of 45 taxa representing 16 different genera. Other well-preserved and frequently observed siliceous microfossil remains include phytoliths, sponge spicules, and chrysophyte statospores. A detailed description of siliceous microfossil assemblages in core HHA3 was published by Pearce et al. (2011).

Diatoms HHA3

The CONISS subdivides the diatom record into four zones, which are consistent with those described in Pearce et al. (2011) (Fig. 3). At the core base the tychoplanktonic species *Aulacoseira coroniformis* is the dominant diatom species (>80%) (DAZ1, diatom assemblage zone). Epiphytic species such as *Eunotia zygodon* and *Eunotia carolina* are also present in this zone. A transition to an *Eunotia zygodon* (50-80%) dominated zone, accompanied by *Pinularia viridis* (to 14%), is observed in DAZ2. In DAZ3 *E. tautoniensis* (up to 22%) and *E. carolina* (up to 55%) were most frequently observed. Finally, in the top sediment layer the *Eunotia* species are accompanied by a number of tychoplanktonic species such as *Fragilaria javanica* (up to 40%), species of the genus *Frustulia* spp. (up to 20%), and *Pinnularia parvulissima* (up

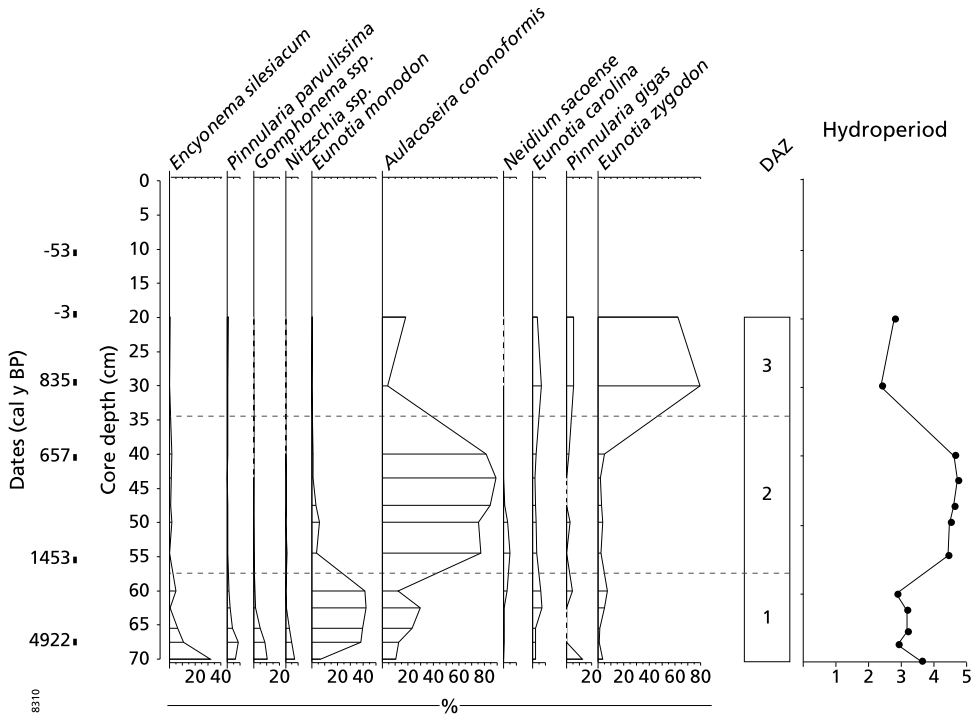

Figure 4. HHA5 diagram showing the most abundant diatom species plotted against depth with available calibrated radiocarbon dates, and calculated hydroperiods (see section Material and Methods, data analysis).

to ~10%) (DAZ4). Based on the observed changes of the diatom assemblages the hydroperiod was calculated, and the species agreement with the training set is 58-100% (Gaiser et al., 1998). The hydroperiod is continuously high during the period represented by DAZ1 with a value of ~4.7, and lower in periods represented by DAZ2-4 with a value around ~2.6.

Diatoms HHA5

This diatom record is divided into three zones (Fig. 4). The basal part of core HHA5 is generally dominated by epiphytic species of the genus *Eunotia* (mostly *E. monodon* with 40%), together with *Gomphonema* spp. and *Nitschia* spp. (each up to 10%). *Encyonema silesiacum* is remarkably abundant (30%) in the lowermost sample of this zone (DAZ 1). The tychoplanktonic species *Aulacoseira coroniformis* is present in DAZ1 with ~30%. Its abundance increases up to >80% in DAZ2. In DAZ3 the high abundance of *A. coroniformis* decreases, and is replaced by *Eunotia zygodon* (80%) which is accompanied by *E. carolina* and *Pinnularia gigas* (both ~5%). The diatom-inferred hydroperiod (species agreement with the training set is 50-75%, Gaiser et al., 1998) indicates a shift from the relatively low value of ~2.9 in DAZ1 to a high of ~4.5 in DAZ2, after which it again decreases to ~2.5 in DAZ3.

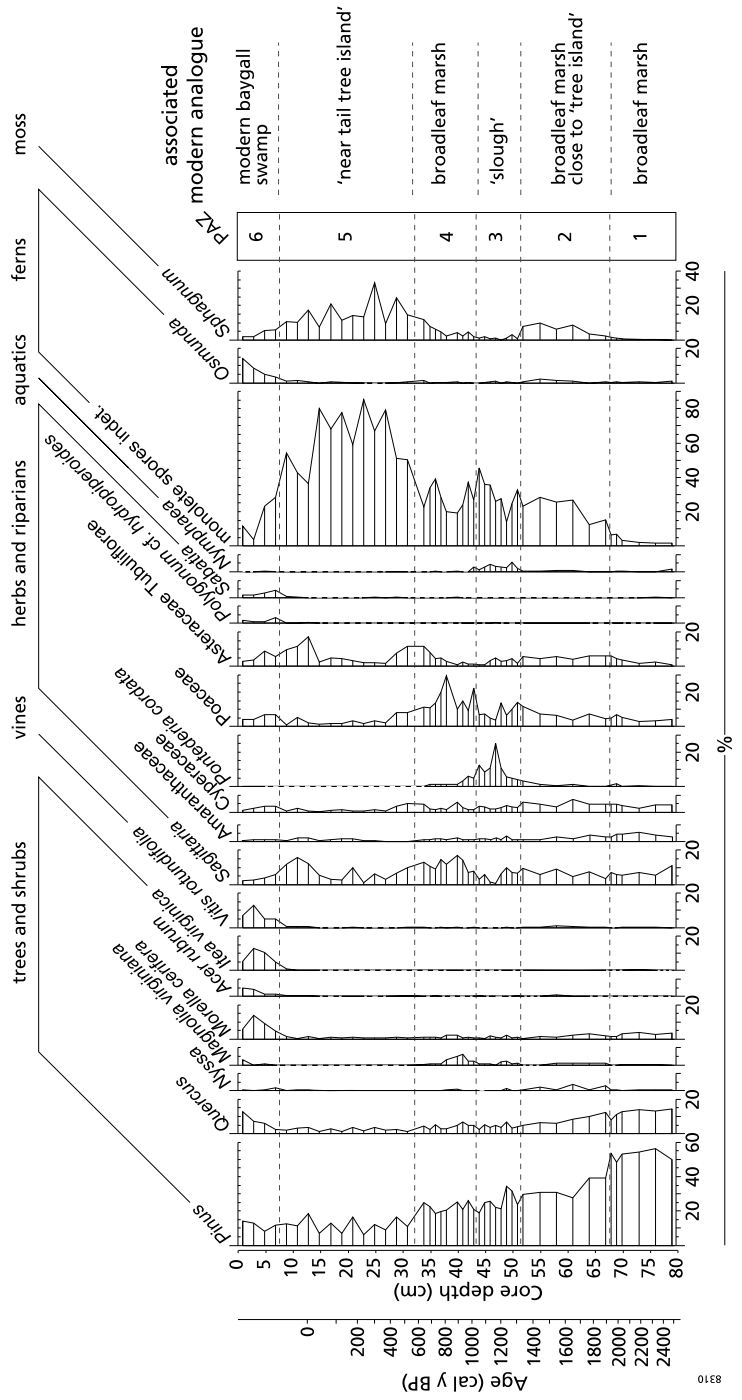

Figure 5. HHA3 diagram showing the most abundant pollen species plotted against depth, with addition of the age scale on the second y-axis, and interpreted modern analogue vegetation.

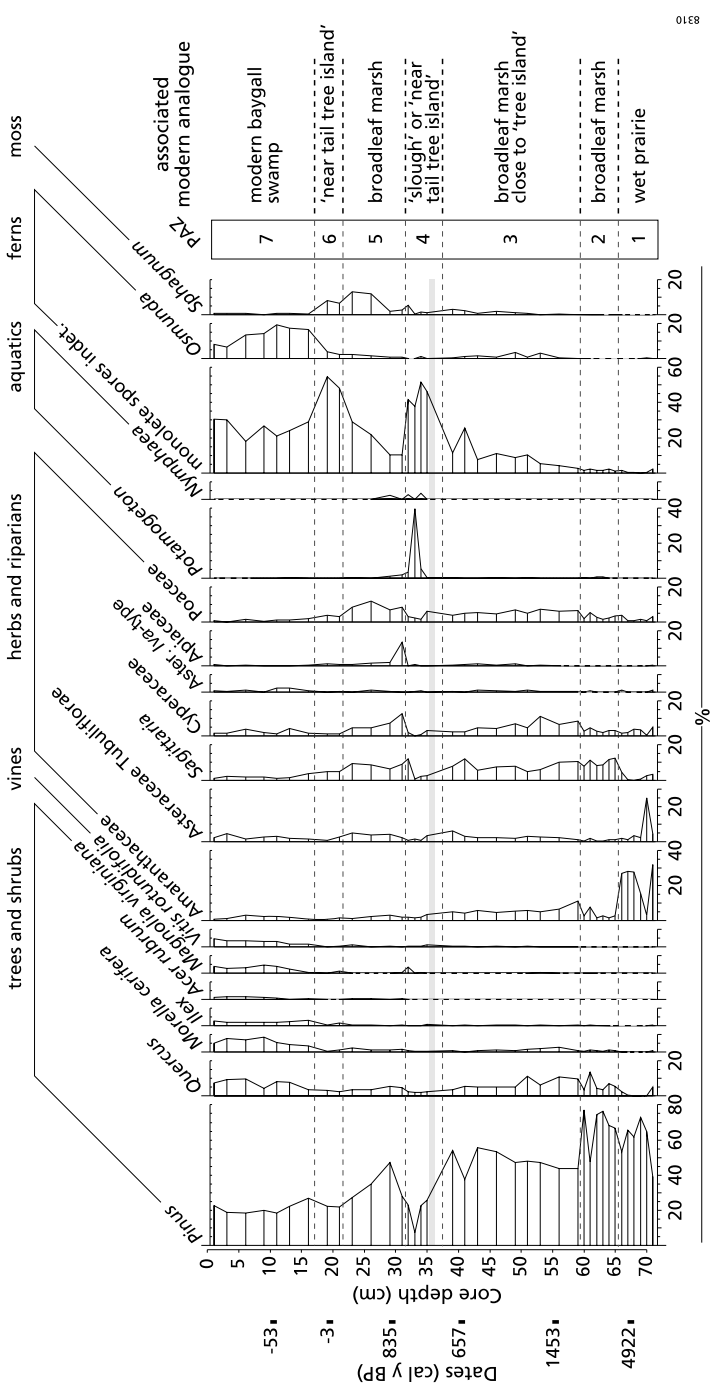

Figure 6. HHA5 diagram showing the most abundant pollen species plotted against depth, with addition of available calibrated radiocarbon dates, and interpreted modern analogue vegetation. Gray bar at 36 cm indicates a barren sample.

4.3 Pollen relative abundances

The pollen/spore assemblages in both cores as well as major shifts through time are highly comparable, including 42 taxa of which 22 are non-arboreal. In HHA5 from ~70 cm up, and throughout HHA3, pollen are found well preserved and abundant. Changes in the dominant species over depth are described, and calibrated radiocarbon dates are given along the y-axes.

Pollen HHA3

The record is subdivided into six pollen assemblage zones (PAZ) (Fig. 5). Pollen of the trees *Pinus* and *Quercus* dominate the base with 55% and 15%, respectively. Of the herbaceous species *Sagittaria* is most common with 5-10% and Asteraceae, Poaceae, and Cyperaceae are consistently present with <5% (PAZ1). Monolete spores of unidentified fern species expand to 28% in PAZ2, together with *Sphagnum* spores up to 10%, while *Pinus* and *Quercus* are gradually reduced. *Sagittaria*, Poaceae, Cyperaceae, and Asteraceae remain present with 5-10% each. A distinct increase in *Pontederia* (to 25%) and *Nymphaea* (to 5%) is then observed (PAZ3). Afterwards, *Sagittaria* and Poaceae (to 17% and 28%), and later Asteraceae and *Sphagnum* (to 11%), again expand together with a notable presence of *Magnolia* to 6% (PAZ4). Monolete spores then become dominant with values of 50-85%, together with *Sphagnum* to 33%, and Asteraceae to 12% at the beginning and end of PAZ5. A distinctly different assemblage and higher diversity is observed for the top (PAZ6), where monolete spores and *Sphagnum* are reduced in favor of the trees and shrubs *Morella*, *Acer*, *Itea,* of *Vitis* and *Osmunda* with values of 10-20%.

Pollen HHA5

This pollen record is subdivided in seven PAZ (Fig. 6). At the base, pollen of *Pinus* dominate with 70%, together with high values of Amaranthaceae and Asteraceae up to 30% (PAZ1). Afterwards, *Pinus* remains high but the herbs are replaced by *Sagittaria* (up to 13%) as well as Poaceae and Cyperaceae to 5% (PAZ2). Amaranthaceae, Cyperaceae, and Poaceae were consistently present in the background but increase to 5-10%, whereas *Pinus* is abruptly reduced in PAZ3. *Morella* as well as ferns and moss increase in this zone, of which monolete spores up to 25% towards the end. This trend continues into PAZ 4, where monolete spores peak to 50% together with the aquatic *Potamogeton* (single sample of 40%), and a minor but consistent presence of *Nymphaea* (1%). An assemblage similar to PAZ3 then re-establishes, but with a higher presence of *Sphagnum* to 13% (PAZ5). Monolete spores again expand, and become dominant (up to 55%) in PAZ6. In the top, the assemblage changes distinctly with increasing values of *Magnolia*, *Quercus*, *Morella*, *Vitis* (2-10%) and *Osmunda* (up to 20%).

4.4 Pollen concentrations and core comparison

For both cores, the pollen concentrations are calculated and the taxa are grouped according to the species ecological groups and hydrological preference (Table 2). The resulting diagrams are plotted together with the total pollen concentrations, the LOI and the diatom inferred hydroperiod (Fig. 7). HHA3 is plotted against age, whereas HHA5 is plotted against depth together with the calibrated radiocarbon dates. The top PAZ of both cores which is

Table 2. Grouping of pollen according to eco-hydrological preference

Groups	Common taxa
Aquatic	*Nymphaea, Utricularia, Potamogeton*
Riparian	*Sagittaria*, *Pontederia,* Typhaceae, Apiaceae
Wetland trees	*Alnus*, *Fraxinus, Magnolia*, *Nyssa*, *Acer*
Herbs	Asteraceae, Amaranthaceae, Poaceae, Cyperaceae
Ferns and moss	Monolete spores, *Sphagnum, Osmunda*
Upland trees	*Pinus*, *Quercus*, *Carya, Liquidambar*

characterized by the distinct change in the pollen assemblage is excluded here, because the exponential increase in sedimentation rate of core HHA3 cannot be fitted to the linear depth axis of HHA5. The results for both cores are combined based on the onset of the 20th century vegetation and trends in the background pollen rain of the upland trees (mostly *Pinus*), supported by the radiocarbon date at 29.5 cm. Although the age scale of HHA3 should only be considered an approximation for the changes in HHA5, a highly comparable trend can be observed for the LOI, the diatom inferred hydroperiod, and the concentration curves. This suggests that the changes observed in HHA3 are representative of the environmental development for the larger part of the basin.

The total pollen concentrations range between $1.5{\cdot}10^5$ and $3.7{\cdot}10^6$ for HHA3, with a distinct increase after ~1.1 ka. Total concentrations of HHA5 range between $4.3{\cdot}10^4$ and $2.0{\cdot}10^6$, and show an increase after 35 cm. Pollen of upland trees are present with the highest concentrations and show a pattern with up to 10-fold higher values between ~2.5-1.9 ka in HHA3 (65-53 cm in HHA5) and between ~1.1-0.3 (32-19 cm in HHA5). These shifts are simultaneous with increases/decreases in the other groups, and the observed pattern more likely reflects overall increased preservation, rather than phases of increased pine pollen production. In the other groups a clear trend is apparent: at the base herbs are present in HHA5, after which successively increases in aquatics, riparians, wetland trees, herbs, ferns and moss are observed up to ~1.3 ka (and 34 cm in HHA5). After this point, a highly similar succession is again present in both cores albeit with much higher concentrations. Interesting to note is that the LOI values do not reflect the (total) concentration curves, but rather show a distinct increase together with the second expansion of aquatic species in both cores. Despite the lower concentrations in the bottom half of the core, the apparent double successional cycle of the vegetation groups (except the upland trees) highly resembles the results presented by the relative abundances.

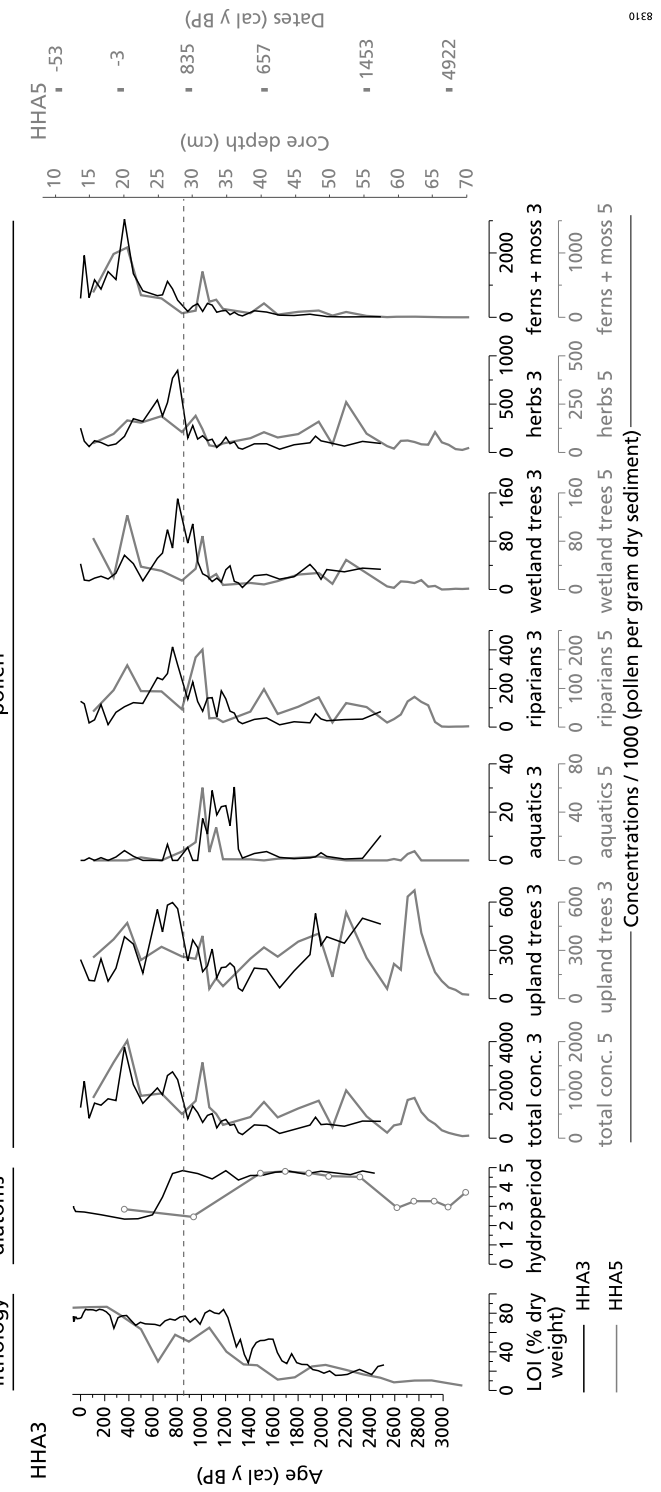

Figure 7. Overview of HHA3 and HHA5: loss on ignition, diatom inferred hydroperiod, total pollen concentrations in the sediment, and summed concentrations of plant subgroups based on growth types and hydrological preferences (see Table 2). Note: the x-axes for HHA3 (denoted by a 3) may differ from those of HHA5 (denoted by a 5).

5. Discussion

5.1 Wetland development

The pollen and diatom analyses on both HHSP cores reflect distinct changes over at least the past ~2.5 ka. Deposits below the studied organic top layer are characterized by low organic matter content (LOI <5%) and are almost barren in pollen. This likely reflects overall dry conditions, in which organic material of potentially present vegetation is not preserved. At the base of HHA5 the first observed pollen, albeit in low concentrations include high values of herb species Amaranthaceae and Asteraceae with common Poaceae and Cyperaceae. The high herb abundance suggests the presence of a (wet) prairie (Fig. 5), a vegetation type characterized by low pollen concentrations and high oxidation (Willard et al., 2001b). The transition to wetter conditions is indicated by the expansion of marsh species *Sagittaria*, in a pollen assemblage that corresponds to broadleaf marshes (Willard et al., 2001b).

The transition from a short to a moderate hydroperiod marsh type (Kushlan, 1990) is not directly concurrent with changes in the diatom assemblages. The diatom-inferred hydroperiod in HHA5 of around 3 corresponds to inundated conditions for 9-10 months of the year, which is suitable for a broadleaf marsh but higher than expected for the wet prairie (Kushlan, 1990; Givnish et al., 2008). Surface samples from the Everglades show distinctly different pollen assemblages for the various wetland types present over short distances (Willard et al., 2001b, 2006; Bernhardt and Willard, 2009). However, diatoms in isolated basins likely give an even more local signal as the assemblage composition is largely dependent on *in situ* habitat conditions. A possible expansion for the observed changes in HHA5 therefore could be that vegetation changed close to, but not directly at the site. Critical in this assumption is that some surface elevation variability is present within the basin, allowing for non-linear responses between the proxies to hydrological changes. Alternatively, diatoms and wetland plants have a different sensitivity to hydrological changes. Despite the initial discrepancy between the pollen and diatom signal observed in the basal part of HHA5, at ~2.5 ka a broadleaf marsh is present with close to annual inundation.

A gradual change in the pollen assemblages of both HHA3 and HHA5 towards an increasing presence of wetland tree species, Asteraceae, and ferns is observed. This is consistent with the modern analogue of broadleaf marshes 'close to tree islands' (Willard et al., 2001b). Tree islands are characteristic features of the Everglades Ridge and Slough area, with their elongate shape parallel to the sheetflow overflowing from lake Okeechobee. As they are elevated slightly above the surrounding marshes and sloughs, the hydroperiod is gradually reduced uphill towards the 'head' of the tree island, leading to a series of specific plant associations (Willard et al., 2006). High abundances of in particular fern spores are considered characteristic for the presence of tree islands in the marsh landscape (Willard et al., 2001b, 2006). Although it is unlikely that actual tree islands were also present in the HHSP, the pollen assemblages can serve as a good analogue for shorter hydroperiod conditions. *Sphagnum* does not occur in the Everglades, but is commonly observed in the upper edge of basin marsh wetlands (Kushlan, 1990). Therefore,

the gradual expansion of ferns, *Sphagnum* and wetland trees in combination with broadleaf marsh likely reflects a gradual drying trend.

The diatom assemblages, however, indicate continuous long hydroperiod conditions, in which *Aulacoseira coroniformis* dominated. This particular tychoplantonic species has a thickly silicified valve and requires some water turbulence to stay in the productive zone of the water column (Pearce et al., 2010). The dominance of *A. coroniformis* is therefore thought to reflect a continuous inflow from the Haw Branch (Pearce et al., 2011). Again, it is possible that the pollen reflect a vegetation development close to, but not directly at, the sampling site which remained a pond for the entire period.

The apparent drying trend in the vegetation is interrupted by a distinct expansion of aquatic plants between ~1.3- 1.0 ka in HHA3. In combination with high values for *Pinus*, ferns, and herbs this assemblage is analogous to Everglades sloughs (Willard et al., 2001b; Bernhardt, 2011). Such open water sites typically capture the extra-local or regional pollen like *Pinus* and monolete spores (Willard et al., 2006), as the local aquatic species generally produce very few pollen and the site is not as densely vegetated as most other vegetation types. After ~1.0 ka, a second drying trend is apparent as the pollen change to assemblages typical for broadleaf marsh (high *Sagittaria*) with more elevated areas nearby (gradually increasing ferns and Asteraceae) (Willard et al., 2001b). The dominance of monolete spores after ~0.6 ka in HHA3 is characteristic for the short hydroperiod tails of tree islands in the Everglades (Willard et al., 2006). The ongoing drying trend is also reflected by an abrupt shift in the diatom inferred hydroperiod from a value around 4.8 to 2.5 in both cores, indicated by the replacement of *A. coroniformis* by *Eunotia* spp. However, this change in diatom species composition possibly reflects local habitat changes rather than an abrupt climatic change. A hydroperiod of 2.5 implies that the site was inundated at least 9 months of year, which is within the range measured for tree island tails (Givnish et al., 2008).

The distinct change in the pollen assemblages in the top of both cores likely indicates the start of human alterations to the landscape. Initially, *Sagittaria* and Asteraceae expand again after 1950 AD (in HHA3) indicating wetter conditions. This is supported by a distinctly different and more diverse diatom assemblage, which has been linked to a slightly greater water depth (Pearce et al., 2011). The pollen assemblage in the top of both cores is highly comparable and reflects the baygall swamp forest that is now present. Aerial photographs of the region from the early 20th century show that an open park landscape instead of dense swamp surrounded the hydric hammock at that time. In the 1930s and 1940s the natural drainage was altered through the construction of dikes and canals by the Civilian Conservation Corps (CCC) to protect the park's hydric hammock from wildfires. Just north of our cored sites an elevated road was built, which blocked the water flow and potentially led to increased wetness at these locations. With the exclusion of wild fires tree seedlings were able to mature, and the marsh was likely gradually replaced by swamp forest through natural succession.

5.2 Climatic implications

With exception of the observed changes during the 20th century, which are directly related to anthropogenic interference, the vegetation and diatom development likely reflect natural changes in the environment. Overall, the local development from the initial long hydroperiods in a marsh setting to drier vegetation associations and shorter hydroperiod reflect a natural wetland succession pattern, caused by gradual infilling of the basin. Superimposed on this general trend, however, a distinct increase in the presence of aquatic plants between ~1.3-1.0 suggests a shift to temporary wetter conditions. An environmental response to drier climate is hard to distinguish from that caused by the basin infilling, but the initiation of the basin wetland around 2.5 ka as well as the increased wetness around 1.3-1.0 ka reflect a period elevated ground water levels. The increased presence of *Taxodium* pollen around 2.7 ka in the central Florida lake deposits were interpreted as increasingly wet conditions following the gradually rising sea level (Watts and Hansen, 1994). Superimposed on this trend, precipitation patterns potentially also determined the observed wetter conditions (Fig. 8).

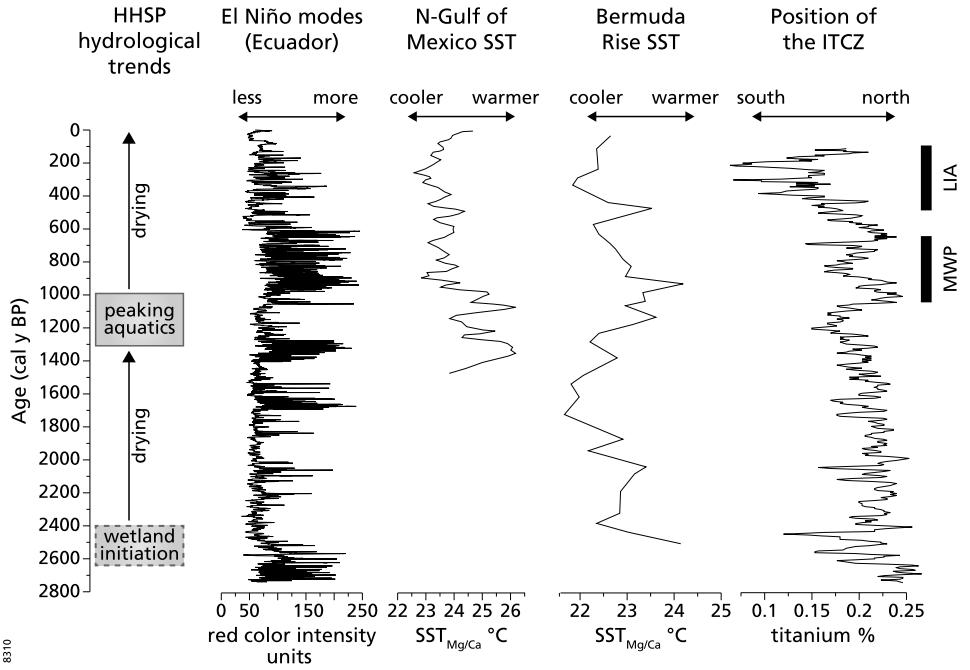

Figure 8. Overview diagram showing a summarized hydrological development at HHSP, reconstructed El Niño activity from Ecuador (Moy et al., 2002), sea surface temperatures (SSTs) from the northwestern Gulf of Mexico (Richey et al., 2007) and the Bermuda Rise (Keigwin, 1996), and migration of the ITCZ (Haug et al., 2001). The black bars on the right indicate the approximate timing of the Medieval Warm Period (MWP) and Little Ice Age (LIA).

Comparison of the HHSP records to other precipitation reconstructions throughout the Florida peninsula show broadly similar patterns. Shifts to wetter conditions around 2.5 ka and 1.1 ka are inferred from $\delta^{18}O$ in ostracods from Little Salt Spring (Alvarez Zarikian et al., 2005) and from deposition rates in stalagmites from Briars Cave (Van Beynen et al., 2008), both located on the eastern Gulf coast. The development of tree islands in the Everglades is related to a lowered water table and thus drier conditions (Willard et al., 2006; Bernhardt, 2011). The apparent pause in tree island initiation and maturation of tree islands between ~1.1 and 0.8 can be interpreted as generally wetter conditions. A pollen record from Fakahatchee Strand Preserve SP, southern Florida, reflects the development of cypress swamp forest in a former prairie landscape (Donders et al., 2005a). Although the sample resolution over the past millennia is low, strong increases in *Taxodium* after ~2.5 and ~1.3 ka potentially indicate a more rapid development of the swamp, related to wetter conditions. Exact dates of the above named wetter phases including HHSP are offset, but this is more likely caused by dating uncertainties combined with sampling resolution.

The late Holocene trend towards wetter conditions observed in Fakahatchee Strand Preserve SP has been related to the intensification of the El Niño- Southern Oscillation after ~3.5 to ~3.1 ka (Donders et al., 2005a). Increased winter precipitation related to El Niño phases leads to wetter conditions and prolonged hydroperiods. Persistent El Niño modes around 2.7 ka and around 1.3 ka are inferred from Ecuador lake deposits (Moy et al., 2002) and may have triggered the initiation of the wetland and the later expansion of aquatic species, respectively (Fig. 8). However, this Ecuador lake record also indicates increased El Niño activity at times when a drying trend is observed in the HHSP records. Therefore, modes of the ENSO do not (fully) explain the hydrological trends in the central Florida wetland.

The initiation of the wetland also co-occurs with a regional increase in tropical storm activity, broadly between 3.1-1.9 ka (Lane et al., 2011; Chapter 3). Besides strong winds, tropical storms can deliver temporary extreme amounts of precipitation, even when it passes at some distance (Franklin et al., 2006). However, there is no direct evidence in the HHSP records of storm related vegetation damage, or aeolian input reflected by sand layers, that can support the impact of tropical storms on the area with certainty.

Long-term precipitation patterns in the Caribbean and Gulf of Mexico are strongly linked to the migration of the Intertropical Convergence Zone (ITCZ), in response to insolation changes (Hodell et al., 1991; Poore et al., 2003). During the northern hemisphere summer, sea surface temperatures (SSTs) in the Atlantic Warm Pool (including the Gulf of Mexico) rise and the ITCZ precipitation belt migrates northward (Ziegler et al., 2008). Late Holocene SST reconstructions based on Mg/Ca ratios in foraminifera from the Bermuda Rise (northeast of Florida) (Keigwin, 1996) and from the Gulf of Mexico (Richey et al., 2007) indicate increased temperatures around 2.5 ka and 1.1 ka (Fig. 8). They relate the high SSTs around 1.1 ka and subsequent cooling to the early Medieval Warm Period and the Little Ice Age, respectively, forced by insolation variability. The offset between the HHSP, regional SSTs

and ITCZ migration records falls within the age uncertainty of the age model (± 100 years). The consequent more northward summer position of the ITCZ and increased convective precipitation during these 'warm' phases have likely led to the wetter conditions observed in Florida. Although the local drying trend observed over the last millennium can arguably also be caused by basin infilling, the strong and concurrent shift in diatom and vegetation assemblages is consistent with Northern Hemisphere wide extreme climatic changes, related to the Little Ice Age. This supports the proposed strong link between (sub)millennial-scale high and low latitude climate variability during the late Holocene (deMenocal et al., 2000).

6. Conclusions

The studied peat record from Highlands Hammock SP in central Florida shows distinct hydrological variability over the past ~2.5 ka. Differences in the timing of change between the pollen and diatom records are likely related to varying sensitivity to hydrological change and spatial range they describe. However, an overall consistent environmental development could be deduced. The expansion of broadleaf marsh taxa and increased diatom inferred hydroperiod around ~2.5 ka indicate wetter conditions and the initiation of the wetland. The following drying trend reflected in the vegetation associations can be related to natural wetland succession, due to gradual basin infilling. A distinct increase in aquatic plants indicate increased wetness between ~1.3 and 1.0 ka, superimposed on the general drying trend. After ~0.7 ka vegetation and diatom assemblages consistently show an abrupt transition to drier conditions. Both, the initiation of the wetland and the intermittent wet phase are likely forced by increased precipitation. These are explained by temporary northward migration of the ITCZ related to increased SSTs in the Gulf of Mexico and the Bermuda Rise. The wet phase and subsequent strong drying in the last millennium can be linked to the Medieval Climate Anomaly and Little Ice Age respectively. Both the diatom and pollen records reflect the 20th century alterations to the landscape when the park was built. The development of the current baygall swamp is likely the result of fire exclusion of the area, allowing tree seedlings to take over the former natural more open wetland.

170 x 240 mm

Chapter 5

Global CO_2 rise leads to reduced maximum stomatal conductance in Florida vegetation

Abstract

A principle response of C3 plants to increasing concentrations of atmospheric carbon dioxide (CO_2) is to reduce transpirational water loss by decreasing stomatal conductance (g_s) and simultaneously increase assimilation rates. Via this adaptation, vegetation has the ability to alter hydrology and climate. Therefore, it is important to determine the adaptation of vegetation to the expected anthropogenic rise in CO_2. Short-term stomatal opening – closing responses of vegetation to increasing CO_2 are described by free-air carbon enrichments growth experiments, and evolutionary adaptations are known from the geological record. However, to date the effects of decadal to centennial CO_2 perturbations on stomatal conductance are still largely unknown. Here we reconstruct a 34% (± 12%) reduction in maximum stomatal conductance (g_{smax}) per 100 ppm CO_2 increase as a result of the adaptation in stomatal density (D) and pore size at maximal stomatal opening (a_{max}) of nine common species from Florida over the past 150 y. The species-specific g_{smax} values are determined by different evolutionary development, whereby the angiosperms sampled generally have numerous small stomata and high g_{smax}, and the conifers and fern have few large stomata and lower g_{smax}. Although angiosperms and conifers use different D and a_{max} adaptation strategies, our data show a coherent response in g_{smax} to CO_2 rise of the past century. Understanding these adaptations of C3 plants to rising CO_2 after decadal to centennial environmental changes is essential for quantification of plant physiological forcing at timescales relevant for global warming, and they are likely to continue until the limits of their phenotypic plasticity are reached.

1. Introduction

Land plants play a crucial role in regulating our planet's hydrological and energy balance by transpiring water through the stomatal pores on their leaf surfaces. A fundamental response of C3 plants to increasing atmospheric carbon dioxide concentration (CO_2) is to minimize transpirational water loss by reducing diffusive stomatal conductance (g_s) and simultaneously increasing assimilation rates (Cowan and Farquhar, 1977). The resulting increased intrinsic water-use efficiency (*iWUE*: the ratio of assimilation to g_s) improves the vegetation's drought resistance and reduces the cost associated with the leaf's water transport system like leaf venation (Raven, 2002; Beerling and Franks, 2010). On a regional to global scale, decreasing rates of transpiration concurrently affect climate through reduced cloud formation and precipitation (Bonan, 2008) and with this exert a physiological feedback on climate and hydrology on top of the radiative forcing of increasing CO_2 (Betts et al., 2007; Andrews et al., 2010; Cao et al., 2010). In the light of continuing anthropogenic climate change, it is therefore imperative to determine how plants adapt to rising atmospheric CO_2.

During their 400 million year history, land plants have been exposed to large variations in environmental conditions that prompted genetic adaptations toward mechanisms that optimize individual fitness. Over this period, plant adaptation to CO_2 is apparent as periods with high CO_2 favored species with few relatively large stomata and low g_s, whereas periods with low CO_2 (as at present) favored species with many relatively small stomata and higher g_s (Franks and Beerling, 2009a). Moreover, decreasing CO_2 after ~100 million years likely triggered the evolutionary development of a more extensive leaf vein network in angiosperms, giving them the advantage of potentially higher g_s than gymnosperms with low vein density (Brodribb and Feild, 2010). At shorter timescales, plants have the ability to adjust their phenotype to optimize gas exchange. In response to short (seconds to hours) perturbations in CO_2, plants open and close their stomata (Farquhar et al., 1978; Katul et al., 2010), whereas in response to CO_2 changes at decadal to centennial timescales, plants adjust leaf stomatal density (D) and/or maximum stomatal dimensions (a_{max}) (Woodward, 1987; Kürschner et al., 1996; Wagner et al., 1996, 2004). This process of epidermal structural adaptation is in part controlled by a signaling mechanism from mature to developing leaves, optimizing stomatal density and size to the changed environmental conditions (Lake et al., 2002). These epidermal characteristics determine the anatomical maximum stomatal conductance to water vapor (g_{smax}, mol·m^{-2}·s^{-1}) of fully opened stomata and can be calculated as (Franks and Farquhar, 2001; Franks and Beerling, 2009a):

$$g_{s\,max} = \frac{\frac{d_w}{v} \cdot D \cdot a_{max}}{l + \frac{\pi}{2}\sqrt{a_{max} \,/\pi}} \qquad (1)$$

in which stomatal density [D (number of stomata·m^{-2})], the size of the fully opened stomata a_{max} (m^2), and depth of the stomatal tube l (m) are the determining variables. The diffusivity of

water vapor dw ($m^2 \cdot s^{-1}$) and the molar volume of air v ($m^3 \cdot mol^{-1}$) are constants. Values of a_{max} and l are derived from the stomatal pore length L (m). Maximum stomatal conductance to CO_2 is $g_{smax}/1.6$ (Farquhar and Sharkey, 1982).

The most comprehensive analyses of plant adaptation to elevated CO_2 in (semi-) natural environments are available from free-air carbon enrichments (FACE) growth experiments (Long et al., 2004). Although decreases in D of C3 plants did occur in some studies (Reid et al., 2003), the observed reduction in g_s was found to be caused by instantaneous adaptation only (Ainsworth and Rogers, 2007). Apparently, the run-time of these growth experiments of <5 y might be too short to trigger statistically significant epidermal structural adaptation (Royer, 2001). Consequently, the subtle adaptation of vegetation to continuously increasing CO_2 can only be elucidated from material covering periods long enough to deduce quantifiable structural adaptation. Because CO_2 has already increased by ~100 ppm over the past 150 y,

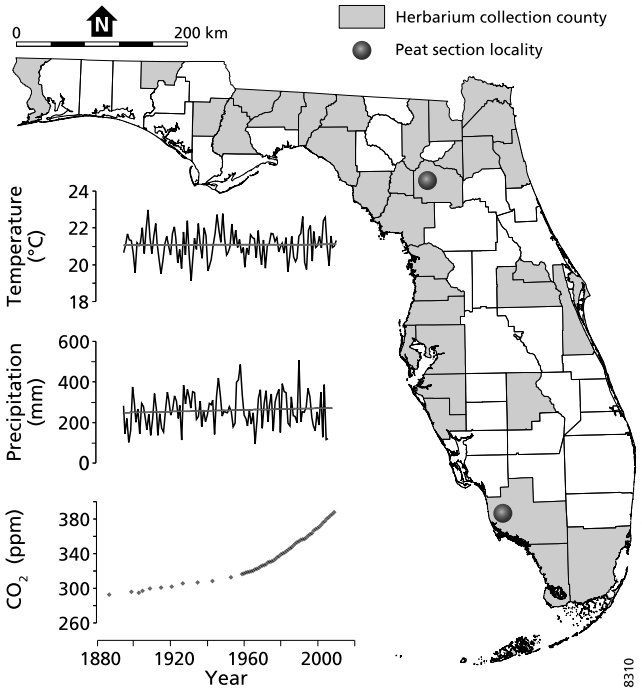

Fig. 1. Locations of leaf material collection sites in Florida: state counties covered by herbarium material (gray) and subfossil leaf fragment sites (gray circles). Florida averaged growing season (March, April and May) temperature and cumulative precipitation (ncdc.noaa.gov), and global atmospheric CO_2 concentration (Siple station: (Neftel et al., 1994); Mauna Loa: (Keeling and Whorf, 2003)) from A.D. 1880 to present are given. The various sites are situated approximately at sea level. Black lines in the temperature and precipitation graphs are long term means of ~21°C and ~260 mm, respectively.

historical leaves preserved in sediments and stored in herbarium collections offer an excellent opportunity to study the adaptation of g_{smax} to the gradual rise in CO_2.

Because the leaf epidermal properties D and a_{max} are also influenced by other environmental factors such as light, temperature, and water availability (Poole and Kürschner, 1999; Franks et al., 2009; Wagner-Cremer et al., 2010), it is necessary to use leaf material from plants that grew under conditions in which the global CO_2 rise is the dominant variable factor. This prerequisite is met in Florida, where the vegetation has been exposed to the global ≈100 ppm CO_2 increase under near constant average growth season temperatures and precipitation rates over the past 150 y (Fig. 1). Moreover, structural adaptation to increasing CO_2 by decreasing D has already been demonstrated for a number of Florida forest taxa (Wagner et al., 2005, 2007).

Here we present a high-resolution historical record of nine C3 species that adapted g_{smax} to the 100 ppm rise in CO_2 since approximately 1880 A.D. Species studied are the woody angiosperms *Acer rubrum* (Aceraceae), *Morella cerifera* (Myricaceae), *Ilex cassine* (Aquifoliaceae), *Quercus laurifolia* (Fagaceae), and *Quercus nigra* (Fagaceae), the conifers *Pinus elliottii* (Pinaceae), *Pinus taeda* (Pinaceae), and *Taxodium distichum* (Cupressaceae), and the fern *Osmunda regalis* (Osmundaceae). This selection embraces species with deciduous and evergreen leaf types, growing in wet to well-drained sites in upper to lower canopy layers (Table S1). The cuticle material analyzed originates from subfossil leaf fragments retrieved from well-dated young peat deposits (Donders et al., 2004; Wagner et al., 2005) as well as herbarium and modern material collected from various sites in Florida (Fig. 1).

In the present study we aim to quantify how these species have adapted g_{smax} in response to the industrial rise in CO_2. Moreover, the present selection includes multiple angiosperm and coniferous species, of which the leaves are characterized by a high and low leaf vein density, respectively. Because angiosperms have invested more in an elaborate leaf hydraulic system (Brodribb et al., 2005), we raise the hypothesis that they will benefit more by reducing g_{smax} stronger to rising CO_2. The data we present here allow for quantification of plant physiological adaptation at timescales relevant for anthropogenic climate change and provide much needed data for parameterization and validation of climate models that include these physiological feedbacks.

2. Results

A consistent decrease in g_{smax} over the anthropogenic rise in CO_2 is observed in all species studied ($P < 0.05$) (Fig. 2). The inferred g_{smax} values of these nine species range between ~0.4 (mol $m^{-2} \cdot s^{-1}$) to ~4 (mol $\cdot m^{-2} \cdot s^{-1}$), with the highest values for the angiosperm canopy species *Q. nigra*, *Q. laurifolia*, and *A. rubrum* and the lowest values for the fern *O. regalis*. Despite the large differences in absolute values of g_{smax} between species, relative sensitivities in g_{smax} over ≈100 ppm CO_2 rise are highly comparable, with a mean slope of −34% (± 12%) per 100 ppm

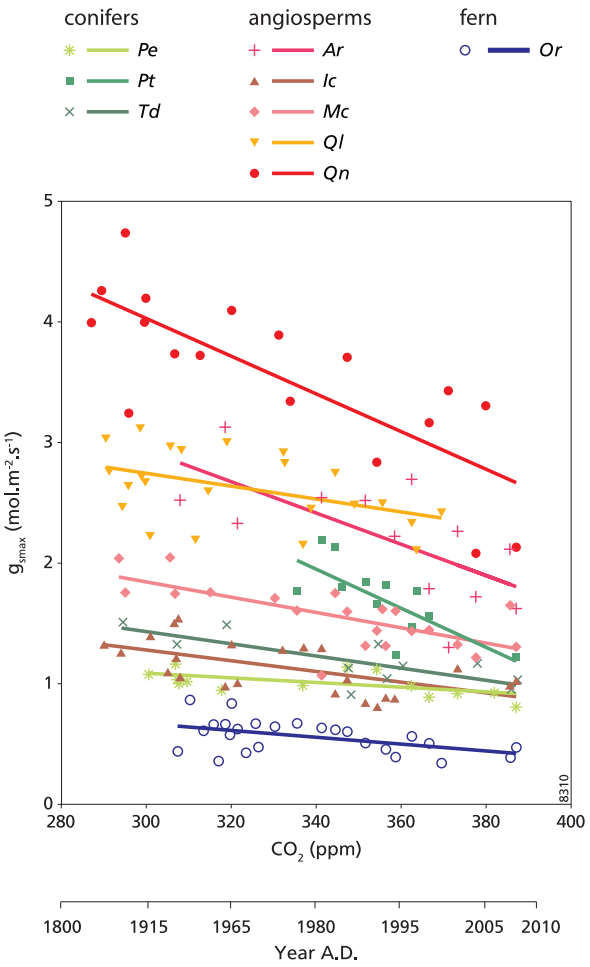

Fig. 2. Species-specific relation between g_{smax} and CO_2 over the past 150 years. Symbols are average g_{smax} [mol·m^{-2}·s^{-1}] for each species per CO_2 level [ppm] studied, and accompanying year A.D. (n= 160) (species names and abbreviations are given in Table 1). Solid lines show linear regressions between CO_2 and g_{smax} for each species, r^2 and relative sensitivity are given in Table 1. The functions and RMSE for each species are provided in Table S2.

(Table 1). The weakest responses occur in *P. elliottii* and *Q. laurifolia*, with a relative sensitivity of only −17% and −18% per 100 ppm, whereas *P. taeda* shows the strongest sensitivity in g_{smax}, with −55% per 100 ppm. Despite these differences in response rate, the total change exceeds the maximum intrinsic variability quantified as the root mean square error (RMSE) in all species (Table S2). The CO_2-induced phenotypic decrease in g_{smax} on decadal timescales resembles evolutionary g_{smax} adaptation over geological timescales (Franks and Beerling, 2009b), reflecting the permanent attempt of plants to optimize individual fitness.

Species		Average g_{smax}		Average stomatal density D		Average pore size a_{max}	
	Species Code	Relative sensitivity (%·ppm^{-1})	r^2	Relative sensitivity (%·ppm^{-1})	r^2	Relative sensitivity (%·ppm^{-1})	r^2
Acer rubrum	Ar	-0.41*	0.45	-0.29*	0.30	-0.27*	0.40
Ilex cassine	Ic	-0.30*	0.36	-0.26*	0.38	-0.13	0.04
Morella cerifera	Mc	-0.36*	0.49	-0.31*	0.40	0.01	<0.001
Osmunda regalis	Or	-0.42*	0.24	-0.27	0.09	-0.31*	0.31
Pinus elliottii	Pe	-0.17*	0.36	-0.23*	0.55	0.13	0.15
Pinus taeda	Pt	-0.55*	0.54	-0.42*	0.56	-0.25	0.25
Quercus laurifolia	Ql	-0.18*	0.21	-0.09	0.13	-0.14	0.07
Quercus nigra	Qn	-0.37*	0.61	-0.28*	0.44	-0.21	0.18
Taxodium distichum	Td	-0.33*	0.58	-0.35*	0.52	0.06	0.06

Table 1. Relative sensitivity of g_{smax}, D and a_{max} to CO_2 increase for the species sampled (intercept, 100% at 280 ppm CO_2), with r^2 of the linear regressions used. *Statistical significance for the regression as well as the change, with ($P < 0.05$).

As on geological timescales (Franks and Beerling, 2009a), combined values of D and a_{max} on which the calculation of g_{smax} is based here are negatively correlated and follow a power law relationship in which high values of D are accompanied by low a_{max} values, and *vice versa* (Fig. 3). For individual species, however, D and a_{max} are confined to specific ranges forming clusters distributed along this power law, where significant negative correlations are also apparent in five out of nine individual clusters (*P. elliottii, T. distichum, Q. laurifolia, M. cerifera*, and *O. regalis*; Table S3). This implies that the clusters represent the phenotypic plasticity of the various species, showing adjustments of both D and a_{max} that occurred in response to the complex of environmental perturbations to which the sampled vegetation was exposed, including CO_2.

Within the total dataset, the most prominent difference exists between the angiosperm clusters with many small stomata that display large diversity in D and the conifers and fern clusters with few large stomata that display large diversity in a_{max}. The position of individual species on this power law curve likely represents their different evolutionary history (Dilcher, 2000; Henry, 2005), with an earlier design for conifers and ferns and a more innovative design for angiosperms. Nevertheless, different combinations of D and a_{max} can lead to the same g_{smax} (Fig. 3) and the same decrease in g_{smax} in response to rising CO_2 (Table 1).

Testing the CO_2 sensitivity of D and a_{max} individually, we observe that the plastic response of D is always negative and more pronounced than in a_{max} (Table 1). This consistent decrease of D

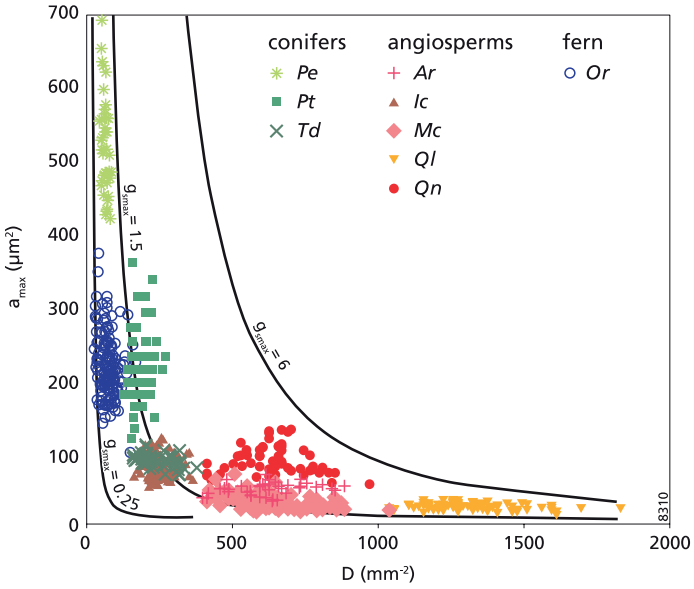

Fig. 3. The measured stomatal density (D [mm^{-2}]) and pore size (a_{max} [µm^2]) of 9 common plant species in Florida (n=667) (species names and abbreviations as in Table 1). The clusters depict a phenotypical range of D and a_{max} for each species under changing conditions of the past 150 years. Approximate lower limits are D= ~20 mm^{-2} and a_{max} = ~15 µm^2. Multiple combination of D and a_{max} can lead to the same g_{smax} value [mol·m^{-2}·s^{-1}], indicated by the black curved lines.

under rising CO_2 has already been reported for the angiosperm and fern species in our dataset (Wagner et al., 2005, 2007). We now complement the range of species known to reduce D in response to rising CO_2 by including the conifers *P. elliottii, P. taeda,* and *T. distichum*. Over the sampled CO_2 rise, the relative sensitivity in D varies from maximal −42% per 100 ppm in *P. taeda* to minimal −9% per 100 ppm in *Q. laurifolia* (Table 1) ($P < 0.05$ for all but *O. regalis* and *Q. laurifolia*, with $P = 0.12$ and $P = 0.10$, respectively). The total change in D exceeds the maximum intrinsic variability quantified as the RMSE in all species except *O. regalis* and *Q. laurifolia* (Table S4). These rates are broadly consistent with decreases in D reported for European tree species grown under anthropogenic CO_2 increase (Woodward, 1987; Kürschner, 1997; Wagner et al., 1996, 2004).

Focusing on the changes in a_{max} over the sampled CO_2 increase, weak and unidirectional relations are observed. Significant relations were only found for *A. rubrum* and *O. regalis*, which show reductions in a_{max} of −27% and −31% per 100 ppm, respectively (Table 1). Moreover, the changes in our a_{max} data series only exceed the RMSE for five of the species studied (Table S5). This variable response is different from changes in a_{max} to anthropogenic CO_2 rise reported earlier for two European tree species, for which a weak increase was

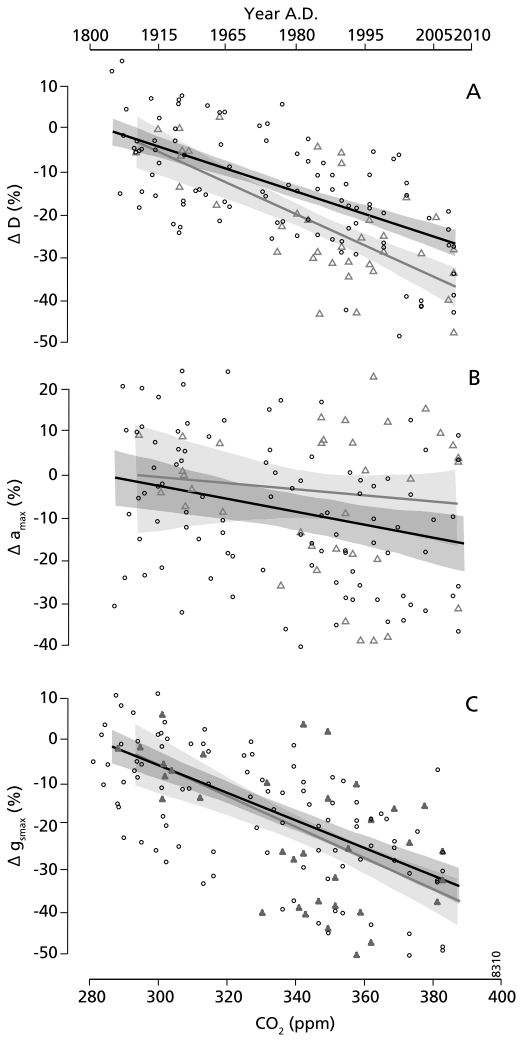

Fig. 4. Relative sensitivity in *D* (A), a_{max} (B) and g_{smax} (C) of the grouped angiosperm species (black line, black dots) and coniferous species (gray line, gray triangles) over the sampled CO_2 increase since the industrial revolution. Shaded areas depict 95% confidence intervals for angiosperms (darker gray) and conifers (lighter gray). SE, r^2 and *p-values* given in table S5. Only the relative sensitivity of *D* is significantly different between angiosperms and conifers ($p < 0.001$).

observed (Wagner et al., 1996; Garcia-Armorena et al., 2006). From these observations it is apparent that *D* is highly sensitive to rising CO_2, whereas changes in a_{max} are variable between species and seem to be governed independently.

Because it is hypothesized that the different leaf structures, in particular leaf vein density, of angiosperms and conifers (Brodribb et al., 2005) result in different epidermal structural responses to rising CO_2, we compared the general relative sensitivities of the two plant groups in our dataset. Results show that coniferous species seem to respond with a significantly stronger decrease in D (slope, −35% per 100 ppm) than angiosperms (slope, −27% per 100 ppm) (Fig. 4A and Table S6). Conversely, angiosperms respond with an apparent but not significantly stronger decrease in a_{max} (slope, −15% per 100 ppm) compared with the conifers (slope, −7% per 100 ppm). Conifers also display a much larger range of variability, indicated by the broader confidence interval (Fig. 4B). Despite these differences, a highly comparable overall decrease in g_{smax} to a rise of CO_2 from pre-industrial to present in angiosperms (slope, −33% per 100 ppm) and conifers (slope, −37% per 100 ppm) emerges from this combination (Fig. 4C). Summarizing, our data show that both angiosperms and conifers exhibit a similar response in g_{smax} to the anthropogenic rise in CO_2.

3. Discussion

The presented data reveal that the nine species from Florida reduce their g_{smax} in response to the industrial CO_2 rise via D and a_{max} adaptation within their phenotypic plasticity. This likely represents the plants' adaptation to increase *iWUE* by optimizing carbon gain to water loss (Katul et al., 2010; Chapter 6). We demonstrate that adaptation of g_{smax} is achieved by species-specific strategies to alter D and/or a_{max}. The overall decrease in g_{smax} is predominantly the result of a general and significant reduction of D in response to rising CO_2 in all species, whereas a_{max} seems to adapt to other environmental conditions as well, because no consistent relation with CO_2 was observed. However, the importance of including D as well as a_{max} in the reconstruction of g_{smax} is emphasized by the generally improved correlation of g_{smax} with CO_2, compared with D and a_{max} separately (Table 1). The observed change in a_{max} opposes the positive relation between pore size and CO_2 found over geological timescales (Franks and Beerling, 2009a). This discrepancy can be explained by considering that on the timescale studied here plants adapt within their phenotype and not genotype to reduce g_{smax}, which is most efficiently done by reducing rather than increasing pore size. This suggests that plants can and do adapt to changing conditions by fine-tuning D and a_{max} plastically to optimize their individual fitness.

Despite the consistent trend observed in g_{smax}, considerable variability characterizes the individual D and a_{max} data series, and consequently g_{smax}, because climatic and site-specific environmental factors such as light, temperature, and water availability affect D and a_{max} as well (Royer, 2001; Franks et al., 2009; Wagner-Cremer et al., 2010). Even though the long-term mean temperature and precipitation in Florida have not changed over the past 150 y, strong inter-annual temperature and precipitation fluctuations (Fig. 1) caused by the El Niño-Southern Oscillation (ENSO) and Atlantic Multidecadal Oscillation teleconnections (Donders et al., 2005a; Curtis, 2008) may in part have caused D and a_{max} variability. Indeed, short-term

changes in epidermis morphology in *Q. laurifolia* have been linked to ENSO-tied winter precipitation (Wagner-Cremer et al., 2010). Together with D and a_{max} diversity throughout the canopy and even within the same leaf (Poole et al., 1996), these environmental factors produce substantial scatter in the data. Consequently, sampling on low temporal resolution might explain the lack of evidence for CO_2-induced *iWUE* adaptation as in herbarium studies covering 2 to 5 selected years only (Miller-Rushing et al., 2009). The present study therefore emphasizes the necessity of sufficiently high-resolution as well as multi-decadal data series to elucidate the long-term subtle response of g_{smax} to changing CO_2.

The large variation in reconstructed g_{smax} values reflect the difference in leaf vascular architecture, whereby the high vein density typical for angiosperms allows for high g_{smax} and the low vein density in ferns and conifers is reflected by low g_{smax} (Brodribb et al., 2005; McKown et al., 2010). The differences in the leaf hydraulic systems between angiosperms and conifers are also expressed in their position on the power law relation between D and a_{max}. Angiosperms reach high g_{smax} with numerous small stomata, and conifers reach lower g_{smax} with fewer large stomata (Franks and Beerling, 2009a). These findings can be placed against an evolutionary background, where ferns and conifers evolved in a higher-than-present CO_2 world, in which lower g_{smax} would be perfectly sufficient to maintain high photosynthesis. The late Cretaceous drop in CO_2 likely triggered the expansion of the leaf-vascular network in angiosperms (Brodribb and Feild, 2010), allowing them to attain higher photosynthesis rates than conifers and ferns but at the cost of high carbon and transpirational water loss (Beerling and Franks, 2010). This water loss in angiosperms might be minimized as small stomata are faster to close than large stomata under desiccating conditions (Hetherington and Woodward, 2003). Moreover, a consequence of the associated high water loss is the resulting evaporative cooling, which maintains an optimal leaf temperature (Upchurch and Mahan, 1988). Our data thus show that species specific g_{smax} is determined in part by evolutionary adaptation to conditions in which they evolved.

When exposed to decadal variability the species studied adapt within the limits of their phenotypic plasticity, by adjusting D and a_{max}. Despite the large differences in D and a_{max} between species, even within the same genus they all exhibit highly comparable adaptation of g_{smax} to increasing CO_2. Comparing the general adaptation of the angiosperms and conifers as groups, however, a different strategy to reduce g_{smax} was observed, depending on their position on the power law curve. Although only the relative change in D between angiosperms and conifers is significantly different, the tendency towards an opposite response in D and a_{max} does illustrate that variable adaptations lead to the same reduction in g_{smax}. These results can be explained by the different position on the power law curve, whereby species reduce g_{smax} most efficiently by changing either D and a_{max} to get the steepest gradient in g_{smax} (Fig. 2). Because the construction of an extended vascular network is coupled to high carbon costs (Beerling and Franks, 2010; McKown et al., 2010), it was hypothesized before that angiosperms reduce g_{smax} more than conifers and ferns. However, our data show a highly comparable sensitivity to the industrial CO_2 rise in all groups sampled and thereby demonstrate the underlying principle

that plants generally optimize their leaf structure in response to rising CO_2, apparently irrespective of their leaf architecture.

Having discussed the responses and possible underlying mechanisms, the potential further development of g_{smax} under future increasing CO_2 can be evaluated. The *iWUE* responses measured in short-term growth experiments over below-present to present CO_2 levels are also found to be comparable in angiosperms, conifers, and ferns, but the trends diverge from present to elevated CO_2, where the response in conifers and ferns levels off (Brodribb et al., 2009). Our results of structural adaptation from ~280 ppm to 387 ppm CO_2 does not bear any evidence for a diverging response between plant lineages. Whether any g_{smax} off-leveling will occur under continuing CO_2 enrichment, and at what CO_2 concentration this will happen, should be estimated by modeling exercises incorporating adaptation within the species specific phenotypic plasticity (Chapter 6).

In conclusion, our results point to a common mechanism in C3 plants to reduce maximum stomatal conductance via adjustment of stomatal density and pore size within the limits of their phenotypic plasticity on a decadal timescale. As atmospheric carbon dioxide concentration is rising, plants can and do reduce water loss by reducing maximal stomatal conductance while maintaining carbon uptake (Beerling and Franks, 2010; Brodribb et al., 2005). Further decreases in stomatal conductance have been observed at CO_2 rising above present levels in FACE short-term experiments (Ainsworth and Rogers, 2007) and in fossil leaves over geological timescales (Franks and Beerling, 2009a). Both lines of evidence, however, fall beyond or below the timescales of the projected rate of continuing CO_2 increase, which is likely to surpass the time needed for adaptation via natural selection. Consequently, the adaptation within the phenotypic plasticity is likely to constrain epidermis structural adaptation in the near future when phenotypic response limits are reached (Kürschner, 1997; Chapter 6). Current increase in CO_2 and the coinciding reduction in plant transpiration already results in increased continental run-off (Gedney et al., 2006), and climate models predict surface temperature increases arising from reduced evaporative cooling (Andrews et al., 2010; Cao et al., 2010). The mechanisms of optimization of carbon gain to water loss described here could be used to better estimate this physiological forcing for the past and future CO_2 but should be considered within the framework of species-specific phenotypic plasticity (Chapter 6).

4. Materials and Methods

Sample Preparation and Analysis

The leaf fragments were treated in 4% sodium hypochlorite ($NaClO_2$) at 40 °C for several minutes up to 24 h, after which the stomata-bearing abaxial cuticle could be peeled off from the mesophyll, dyed with saffranine, and mounted in glycerine jelly. Because *Pinus* has an approximately equal amount of stomata on the abaxial as well as the adaxial surface, the entire cuticle was processed. Standardized, computer-aided analysis of the epidermal properties was

performed on Leica Quantimet 500C/500+ and AnalySIS image analysis systems. Stomatal density (D; number of stomata·m^{-2}) was measured on 5 – 10 alveoles of each leaf sample and averaged. Because of different epidermis cell patterning, *Pinus* is measured with the stomatal rows running diagonally in the image. Pore length (L; µm) is determined by averaging measurements of ~25 stomata for each sample. Data are available upon request.

Calculating g_{smax} to Water Vapor

To determine the stomatal conductance to water vapor g_{smax} (mol·m^{-2}·s^{-1}), the equation provided by Franks and Farquhar (2001) is applied, using a two-way end correction accounting for the diffusion shells (Franks and Beerling, 2009a) (Eq. 1). Maximum pore surface area a_{max} (m^2) is defined as an ellipse and quantified as $\pi \cdot L^2/8$, with L being stomatal pore length (m). Stomatal pore depth l (m) is assumed to be equal to the guard cell width of the stomata when the guard cell is fully inflated (Franks and Beerling, 2009a). Quantification of l follows from the significant positive linear relations between pore length and guard cell width for each species, with exception of *P. taeda*, for which a constant value is taken (Table S7). Values used for gas constants d and v are those for 25 °C. For the determination of the long-term relative sensitivities of the measured D and a_{max}, and consequent g_{smax}, the regressions are performed on values averaged per sampled year.

Statistical Analyses

The significance of the observed regressions presented here is tested in three steps, with P values of <0.05 considered statistically significant. First, the significance of each regression plotted through the data series was tested. Second, using a Student t-test on the slopes of these regressions, it was determined whether the observed changes were significantly larger than 0. Finally, to test whether the average responses in D, a_{max}, and g_{smax} were significantly different between angiosperms and conifers, a t-test (two samples assuming unequal variances) was performed on the pooled data of each group within the CO_2 interval of 360 – 387 ppm.

5. Supporting information

Table S1. Sample selection and species growth specifics

Species				Dataset		
				No. of samples		
	Growth type	Canopy layer	Hydrological preference	Subfossil	Collected	CO_2 range (ppm)
Acer rubrum	BD	Upper	Cosmopolitan	23	17	308-387
Ilex cassine	BE	Middle	Moist/wet	39	49	290-387
Morella cerifera	BE	Middle	Cosmopolitan	48	40	294-387
Osmunda regalis	BD	Lower	Moist	65	83	307-387
Pinus elliottii	NE	Upper	Moist	-	41	300-387
Pinus taeda	NE	Upper	Cosmopolitan	59	3	335-387
Quercus laurifolia	BD	Upper	Moist/wet	89	-	290-371
Quercus nigra	BD	Upper	Cosmopolitan	-	57	287-387
Taxodium distichum	ND	Upper	Wet	21	33	294-387

Table S1. The *Acer rubrum, Ilex cassine, Morella cerifera, Osmunda regalis*, and *Pinus taeda* subfossil material is extracted from a peat core taken in 1998 A.D. in a hardwood swamp forest near Gainesville, FL (Alligator Crossing: 29°39'35"N, 82°15'14"W) (Wagner et al., 2005). Subfossil leaf fragments of *Taxodium distichum* and *Quercus laurifolia* are extracted from two peat cores taken in 1998 A.D. and 2002 A.D., respectively, in a cypress swamp forest of the Fakahatchee Strand Preserve State Park (25°95'N, 81°49'W) (Donders et al., 2004). For all cores age models are constructed with an accuracy of 2 – 5 y. The herbarium samples, obtained from the University of Florida and State Park Headquarters District 4 herbaria, have been collected during the 19th and 20th century from various sites across Florida. Only leaves picked between August and January have been selected to ensure that leaves were fully developed. Self-collected material is available from 1998 A.D. onward. Details of the 9 analyzed species, the origin and amount of samples, and the CO_2 range covered by the samples are given. BD, broadleaved deciduous; BE, broadleaved evergreen; NE, needle-leaved evergreen; ND, needleleaved deciduous; –, no material analyzed.

Table S2: Linear regressions of maximum stomatal conductance g_{smax} (mol·m^{-2}·s^{-1}) vs. CO_2 (ppm)

Species	Function	CV(RMSE) (%)	r^2	P
Acer rubrum	$g_{smax} = -0.013 \cdot [CO_2] + 6.77$	14	0.45	0.01*
Ilex cassine	$g_{smax} = -0.004 \cdot [CO_2] + 2.59$	14	0.36	0.002*
Morella cerifera	$g_{smax} = -0.006 \cdot [CO_2] + 3.72$	11	0.49	<0.001*
Osmunda regalis	$g_{smax} = -0.003 \cdot [CO_2] + 1.51$	20	0.24	0.01*
Pinus elliottii	$g_{smax} = -0.002 \cdot [CO_2] + 1.66$	8	0.36	0.02*
Pinus taeda	$g_{smax} = -0.016 \cdot [CO_2] + 7.41$	9	0.54	0.006*
Quercus laurifolia	$g_{smax} = -0.005 \cdot [CO_2] + 4.31$	12	0.21	0.03*
Quercus nigra	$g_{smax} = -0.016 \cdot [CO_2] + 8.65$	10	0.61	<0.001*
Taxodium distichum	$g_{smax} = -0.005 \cdot [CO_2] + 2.93$	10	0.58	0.006*

Table S2. For easier interspecies comparison, the range of variability is normalized and presented as the variability coefficient of the root mean squared errors CV(RMSE), in %.

*All statistically significant regressions ($P < 0.05$) also have significantly different slopes.

Table S3: Stomatal density *D* (number of stomata ·mm^{-2}) vs. pore size a_{max} (µm^2)

Species	Function	r^2	*P*
Acer rubrum	a_{max} = 0.019·[*D*]+34.6	0.07	0.09
	log10 a_{max} = 0.278·[log10 *D*] + 0.9	0.08	0.08
Ilex cassine	a_{max} = 0.017·[*D*]+72.6	0.002	0.69
	log10 a_{max} = 0.063·[log10 *D*] + 1.7	0.002	0.66
Morella cerifera	a_{max} = -0.041·[*D*]+55.9	0.25	<0.001*
	log10 a_{max} = -0.852·[log10 *D*] + 3.8	0.27	<0.001*
Osmunda regalis	a_{max} = -0.391·[*D*]+246.9	0.06	0.004*
	log10 a_{max} = -0.161·[log10 *D*] + 2.6	0.07	0.001*
Pinus elliottii	a_{max} = -3.101·[*D*]+736.3	0.20	0.003*
	log10 a_{max} = -0.406·[log10 *D*] + 3.5	0.20	0.003*
Pinus taeda	a_{max} = 0.171·[*D*]+186.1	0.01	0.42
	log10 a_{max} = 0.197·[log10 *D*] + 1.9	0.02	0.29
Quercus laurifolia	a_{max} = -0.008·[*D*]+31.5	0.06	0.02*
	log10 a_{max} = -0.475·[log10 *D*] + 2.8	0.06	0.02*
Quercus nigra	a_{max} = -0.017·[*D*]+97.2	0.01	0.45
	log10 a_{max} = -0.065·[log10 *D*] + 2.1	0.003	0.68
Taxodium distichum	a_{max} = -0.075·[*D*]+106.5	0.20	<0.001*
	log10 a_{max} = -0.207·[log10 *D*] + 2.4	0.20	<0.001*
Angiosperms	a_{max} = -0.049·[*D*]+ 84.1	0.42	<0.001*
	log10 a_{max} = -0.724·[log10 *D*] + 3.6	0.51	<0.001*
Conifers	a_{max} = -1.995·[*D*]+ 598.9	0.72	<0.001*
	log10 a_{max} = -1.162·[log10 *D*] + 4.8	0.72	<0.001*
Complete dataset	log10 a_{max} = -0.853·[log10 *D*] + 4.0	0.79	<0.001*

Table S3. For each species studied the linear as well as the log-linear relation between *D* and a_{max} are given. Accompanying coefficients of determination (r^2) and probability (*P*) are also given.

* Statistical significance for the regression. Although a negative power law relation between stomatal density and size is generally known, comparison between the linear and logarithmic relations shows that our species data series do not have this power relation. From these results weak and unidirectional relations are apparent, and only negative relations are statistically significant (*M. cerifera, O. regalis, P. elliottii, Q. laurifolia,* and *T. distichum*). However, the pooled angiosperm and conifer data series, as well as the complete dataset, are best described by a log-transformed linear regression.

Table S4: Linear regressions of stomatal density *D* (number of stomata ·mm^{-2}) vs. CO_2 (ppm)

Species	Function	CV(RMSE) (%)	r^2	*P*
Acer rubrum	$D = -2.23 \cdot [CO_2] + 1398$	13	0.30	0.05*
Ilex cassine	$D = -0.77 \cdot [CO_2] + 509$	11	0.39	0.001*
Morella cerifera	$D = -2.39 \cdot [CO_2] + 1446$	12	0.40	0.002*
Osmunda regalis	$D = -0.33 \cdot [CO_2] + 194$	22	0.09	0.15
Pinus elliottii	$D = -0.19 \cdot [CO_2] + 134$	7	0.55	0.002*
Pinus taeda	$D = -1.14 \cdot [CO_2] + 591$	6	0.56	0.005*
Quercus laurifolia	$D = -1.21 \cdot [CO_2] + 1650$	12	0.13	0.09
Quercus nigra	$D = -2.08 \cdot [CO_2] + 1316$	8	0.44	0.002*
Taxodium distichum	$D = -1.08 \cdot [CO_2] + 613$	12	0.52	0.01*

Table S4. For easier interspecies comparison, the range of variability is normalized and presented as the variability coefficient of the root mean squared errors CV(RMSE), in %.

*All statistically significant regressions ($P < 0.05$) also have significantly different slopes.

Table S5: Linear regressions of pore size a_{max} (µm^2) vs. CO_2 (ppm)

Species	Function	CV(RMSE) (%)	r^2	*P*
Acer rubrum	$a_{max} = -0.156 \cdot [CO_2] + 101$	5%	0.40	0.02*
Ilex cassine	$a_{max} = -0.108 \cdot [CO_2] + 116$	9%	0.04	0.35
Morella cerifera	$a_{max} = 0.005 \cdot [CO_2] + 29$	3%	<0.001	0.94
Osmunda regalis	$a_{max} = -0.8 \cdot [CO_2] + 497$	7%	0.31	0.004*
Pinus elliottii	$a_{max} = 0.607 \cdot [CO_2] + 310$	4%	0.15	0.17
Pinus taeda	$a_{max} = -1.016 \cdot [CO_2] + 579$	5%	0.25	0.10
Quercus laurifolia	$a_{max} = -0.032 \cdot [CO_2] + 32$	9%	0.07	0.21
Quercus nigra	$a_{max} = -0.209 \cdot [CO_2] + 156$	7%	0.18	0.08
Taxodium distichum	$a_{max} = 0.051 \cdot [CO_2] + 71$	3%	0.06	0.46

Table S5. For easier interspecies comparison, the range of variability is normalized and presented as the variability coefficient of the root mean squared errors CV(RMSE), in %.

*All statistically significant regressions ($P < 0.05$) also have significantly different slopes.

Table S6: Relative sensitivities in g_{smax}, D and a_{max} of angiosperms and conifers to CO_2 (ppm) increase

Species	Slope (% ppm^{-1})	SE (% ppm^{-1})	r^2	P
Angiosperm				
g_{smax}	-0.33	0.04	0.35	<0.01*
D	-0.28	0.03	0.41	<0.01* †
a_{max}	-0.15	0.06	0.06	0.02*
Conifers				
g_{smax}	-0.37	0.09	0.33	<0.01*
D	-0.35	0.06	0.49	<0.01* †
a_{max}	-0.07	0.11	0.01	0.53

Table 6.
Intercept = 100% at CO_2 280 ppm, with slope, SE, r^2, and P of linear regressions.

* Statistically significant for the regression to CO_2, and slope significantly different from 0 ($P < 0.05$).
† *Change* in *D* between angiosperms and conifers is significantly different.

Table S7: Pore length/guard cell width linear relations

Species	Mean Cw [µm]	SD [µm]	n	Linear regression	r^2
Acer rubrum	6.79	0.94	36	C_w =0.36·[*L*]+2.90	0.49
Ilex cassine	10.26	1.33	27	C_w =0.28·[*L*] +6.19	0.57
Morella cerifera	7.84	1.10	25	C_w =0.41·[*L*] +3.57	0.62
Pinus elliottii	16.24	2.22	28	C_w =0.27·[*L*] +6.66	0.62
Pinus taeda	11.51	1.22	33	C_w= 11.5 µm	
Quercus laurifolia	6.72	0.77	22	C_w =0.27·[*L*] +4.57	0.49
Quercus nigra	7.29	1.21	27	C_w =0.26·[*L*] +3.55	0.56
Taxodium distichum	9.79	1.57	20	C_w =0.55·[*L*] +1.52	0.72

Table S7. Species-specific relations between pore length (*L*) and guard cell width (*Cw*) are used to derive pore depth (*l*), based on the assumption that *l* is equal to *Cw* (Franks and Beerling, 2009a). Species-specific regressions between *Cw* and *L* are highly significant ($P < 0.001$), with exception of *P. taeda*. We therefore derive *l* from these species-specific regressions, except for *P. taeda*, for which a constant value is applied. The species-specific regressions are used to calculate g_{smax} for each species.

170 x 240 mm

Chapter 6

Climate forcing due to optimization of maximal leaf conductance in subtropical vegetation under rising CO_2

Abstract

Plant physiological adaptation to the global rise in atmospheric carbon dioxide concentration (CO_2) is identified as a crucial climatic forcing. To optimize their functioning under rising CO_2, plants reduce the diffusive stomatal conductance of their leaves (g_s) dynamically by closing their stomata and structurally by growing leaves with altered stomatal densities and pore sizes. The structural adaptations reduce maximal stomatal conductance (g_{smax}) and may constrain the dynamic responses of g_s. Here, we develop and validate models that simulate structural stomatal adaptations based on diffusion of CO_2 and water vapor through stomata, photosynthesis, and optimization of carbon gain under the constraint of a plant physiological cost of water loss. We hypothesize that the ongoing optimization of g_{smax} will eventually be constrained by species specific limits to phenotypic plasticity. Our model reproduces observed structural stomatal adaptations and predicts that adaptation will continue beyond double CO_2. Owing to their distinct stomatal dimensions, angiosperms are expected to reach their phenotypic response limits on average at 740 ppm, and conifers on average at 1250 ppm CO_2. Further, our simulations predict that doubling today's CO_2 will decrease the annual transpiration flux of subtropical vegetation in Florida by approximately 60 $W \cdot m^{-2}$. We conclude that plant adaptation to rising CO_2 is currently altering the freshwater cycle and climate, and will continue to do so throughout this century.

1. Introduction

Plants respond to the complex of environmental signals they perceive by plastic changes in their phenotype in order to increase individual fitness (Trewavas, 2009). The most apparent environmental change that induces phenotypic adaptations in plants is the global increase in atmospheric carbon dioxide concentration (CO_2) (Hetherington and Woodward, 2003). In response to this rise in CO_2 plants reduce the diffusive stomatal conductance of their leaves [g_s (mol·m^{-2}·s^{-1})] to increase drought resistance (Cowan and Farquhar, 1977) and reduce physiological costs associated with water transport (Beerling and Franks, 2010). Plants can reduce g_s by dynamically closing their stomata within minutes (Darwin, 1898; Farquhar and Sharkey, 1982), and structurally within the life span of an individual by growing leaves with altered stomatal density [D (number of stomata·m^{-2})] and pore size at maximal stomatal opening [a_{max} (m^2)] (Royer, 2001; Chapter 5). Structural adaptations thereby reduce maximal stomatal conductance [g_{smax} (mol·m^{-2}·s^{-1})], which critically reduces actual g_s, especially when stomata are fully open during times with ample light and water (Wullschleger et al., 2002).

Reduction of g_s via structural adaptation of g_{smax} has the potential to reduce transpiration fluxes. Plant responses to rising CO_2 may thereby lead to land surface warming in addition to changes in the hydrological cycle (Betts et al., 2007). This climatic effect is termed the physiological forcing of CO_2, which acts beside and independent of the radiative forcing of CO_2. Despite advances to quantify this physiological forcing with global climate models (Andrews et al., 2010, Cao et al., 2010), these models rely on semi-empirical relations to simulate g_s from environmental variables (Ball et al., 1987; Leuning, 1995). Alternative models have been proposed on the concept that stomatal adaptations optimize carbon gain under the constraint of a cost of water loss (Konrad et al., 2008; Katul et al., 2010). Because of their more mechanistic representation of stomatal responses, optimization models are potentially suitable to simulate canopy gas exchange under changing CO_2. However, optimization models implicitly assume that plants will continue to adapt g_s optimally to future rises in CO_2. Whether this assumption holds for the current rate of CO_2 increase is unknown, but structural stomatal responses might be constrained by limits to phenotypic plasticity (Kürschner et al., 1997; Ghalambor et al., 2007) and diffusion through stomatal pores (Wynn, 2003).

To quantify the physiological forcing of CO_2 on past and future climate, two challenges must therefore be addressed. First we test if the observed structural adaptation of g_{smax} to rising CO_2 can be explained by optimization of carbon gain under the constraint of a cost of water loss. Second we predict at what level of CO_2 this structural adaptation may cease due to limits to phenotypic plasticity. Recent advances in stomatal modeling provide possibilities to tackle the first challenge, because the hypothesis that plants adapt g_{smax} structurally to rising CO_2 in order to optimize carbon gain with water loss can be tested mathematically (Konrad et al., 2008; Katul et al., 2010). However, limited experimental data is available for model validation because experiments are generally too short to measure structural stomatal adaptation in forests that take decades or longer to fully adapt to elevated CO_2 (McMurtie et al., 2001). A

unique dataset provides measurements of structural adaptation of g_{smax} to the CO_2 rise of the past century in eight C3 canopy species from natural subtropical vegetation in Florida (see Table 1 for species names) (Chapter 5). Because these species are representative for vegetation in subtropical climates, the observations are crucial to validate models of stomatal adaptations for this climate zone.

The second challenge is more difficult to overcome because, ideally, species specific limits to structural stomatal adaptations should be observed in natural vegetation under rising CO_2. However, no historic analogue of the current high rate of CO_2 increase can be found in the 400-million year history of vascular plants (Berner, 2006; Franks and Beerling, 2009b). The fossil record does show that CO_2 has been driving genetic adaptation that allowed plants to develop ranges of phenotypic plasticity to optimize functioning under changing CO_2 (Franks and Beerling, 2009a, 2009b). Despite these shifts in phenotype at geologic timescales, structural adaptation of g_{smax} was always constrained by interdependence of D and a_{max} in the form of a power law relationship (Fig. 1A). Although D and a_{max} are not the only variables to determine g_{smax}, the constraint on their combined values does suggest a control on the range of g_{smax}, which is calculated as (Franks and Beerling, 2009a):

$$g_{s\,max} = \frac{\frac{d_w}{v} \cdot D \cdot a_{max}}{l + \frac{\pi}{2}\sqrt{a_{max}\ /\pi}} \qquad (1)$$

where d_w ($m^2 \cdot s^{-1}$) is the diffusivity of water vapor and v ($m^3 \cdot mol^{-1}$) is the molar volume of air. The a_{max} is approximated from pore length [L (m)] on the premise that species studied here have ellipse-shaped stomatal apertures at a_{max} with width $W = L/2$. Pore depth l (m) is calculated from a species specific relation with guard cell width and pore length (Chapter 5) (see SI, Table S1). Note that g_s and g_{smax} are expressed as conductance to water vapor ($mol \cdot m^{-2} \cdot s^{-1}$). Additionally, D and a_{max} together express the percentage of leaf surface area allocated to fully opened stomatal pores as: $A_{\%} = 100 \cdot D \cdot a_{max}$. Fig. 1A shows how combined values of D and a_{max} relate to values of equal g_{smax} and equal $A_{\%}$, which is distributed lognormally (Fig. 1B).

The lognormal distribution of $A_{\%}$ allows for the estimation of species specific limits to structural adaptation of g_{smax}, because $A_{\%}$ is bounded on the lower side by a generic value of 0.6% independent of g_{smax}, defined here as $A_{\%low}$ (Fig. 1B). While the species independent power law relationship between D and a_{max} is bound by $A_{\%low}$, each species uses a specific strategy to reduce g_{smax} linearly with $A_{\%}$ (Fig. 1C). So, if a species were to decrease g_{smax} indefinitely, $A_{\%}$ would eventually surpass $A_{\%low}$ and beyond the range of historic observations. We therefore hypothesize that structural response limits are determined by consistent species specific strategies to reduce g_{smax} via adaptation of D and a_{max} along the linear relation between g_{smax} and $A_{\%}$, until $A_{\%low}$ is reached.

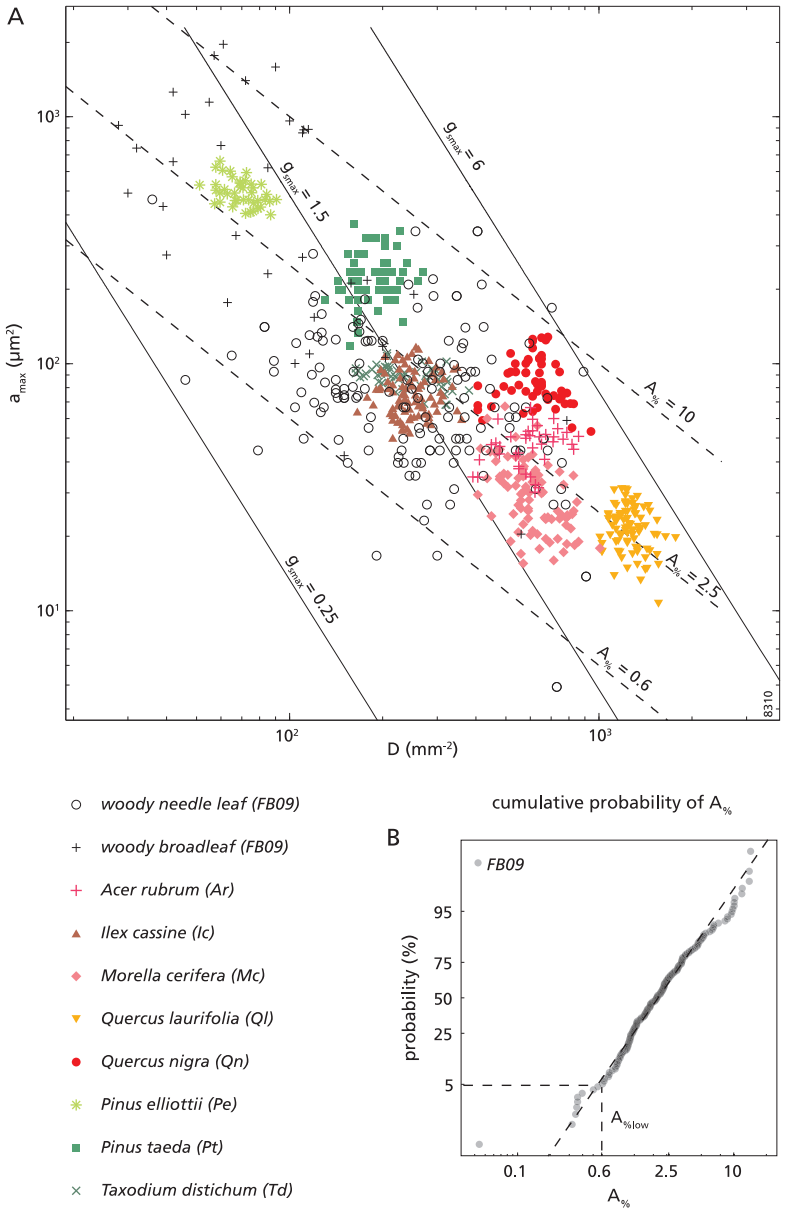

Figure 1. An overview of observed relationships between stomatal density (*D*), pore size at maximal stomatal opening (a_{max}), and the resulting maximal stomatal conductance (g_{smax}) and leaf surface area allocated to fully opened stomatal pores ($A_{\%}$). (A) Power law relationship between *D* and a_{max} are plotted together with lines of equal g_{smax} (solid lines) and $A_{\%}$ (dashed lines). See Equation (1) and Table SI 1 in Supporting Information for calculations of g_{smax}. Note that logarithmic axes are used. (B) Cumulative probability of $A_{\%}$ for woody angiosperm and conifer species fitted to a lognormal distribution. The value of 0.6 indicates the estimated lower bound (5% probability) on $A_{\%}$ defined here as $A_{\%low}$. Note that a logarithmic x-axis is used.

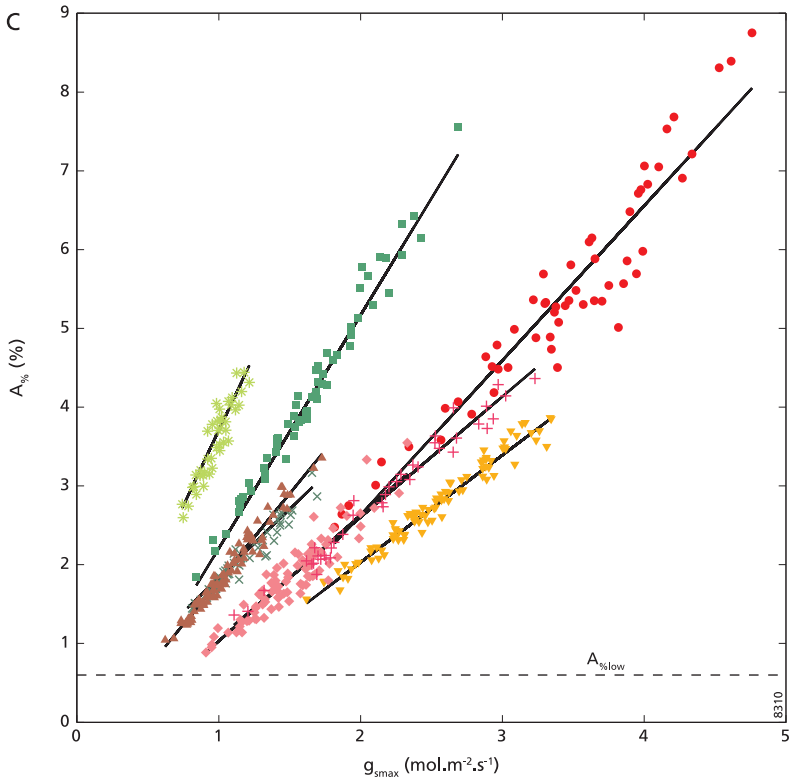

Figure 1 (continued). (C) Species specific strategies to adapt g_{smax} linearly with $A_{\%}$. The dashed line denotes $A_{\%low}$. Lines of linear least squares regressions are indicated per species and used to determine the intersect with $A_{\%low}$ to predict the lowest attainable g_{smax} for each species, defined as g_{low}. The r^2 values are: 0. 97 (Ar), 0.96 (Ic), 0.86 (Mc), 0.96 (Ql), 0.91 (Qn), 0.85 (Pe), 0.98 (Pt) and 0.94 (Td) with $p < 0.001$ for all. Data FB09 are from Franks and Beerling (2009a), others from Chapter 5. Species names and their abbreviations are defined in the legend.

With a model of stomatal optimization and an empirical method to estimate response limits at hand, we may now quantify the physiological forcing of past and future CO_2 in a subtropical climate at decadal to centennial timescales. We first simulate how stomatal optimization reduces g_{smax} with rising CO_2 and validate these results against observations of eight C3 canopy species (Chapter 5) that responded structurally to the CO_2 rise of the past century. As we suggest that these adaptations may be constrained by limits to phenotypic plasticity, we estimate the upper stomatal response limit for each species in terms of CO_2. Finally, we use the stomatal optimization model with structural stomatal response limits to calculate the physiological forcing of CO_2 rising from pre-industrial (280 ppm) through present (385 ppm), and up to double present levels (770 ppm).

2. Results

Our simulations of stomatal optimization are consistent with observations that report a 17-55% decrease in g_{smax} from pre-industrial to present CO_2 (Fig. 2) (Chapter 5). Our model simulates g_{smax} for all species within the variability of observed g_{smax} (Inset Fig. 2) as a consequence of adaptations to the complex of environmental factors determining D and a_{max}, including CO_2 (Wagner-Cremer et al., 2010) (see SI, Fig. S1). Although not all variability in observed g_{smax} can be explained from adaptation to CO_2, the consistent decreases of g_{smax} observed at decadal to centennial timescales are accurately reproduced by our model. These results indicate that structural adaptations of g_{smax} to CO_2 rising from pre-industrial to present levels can be explained from optimization of carbon gain under the constraint of a cost of water loss.

Furthermore, our simulations show that g_{smax} continues to decrease with CO_2 rising beyond present values (Fig. 2). Interpreting these model results, we find this ongoing decrease in g_{smax} unlikely because with the current rate of CO_2 increase, plants are likely to reach the limits of their phenotypic plasticity (Kürschner et al., 1997; Ward and Kelly, 2004; Ghalambor et al., 2007). We therefore predict structural response limits on the premise that the species specific adaptation strategies observed remain unchanged at elevated CO_2 and will eventually be limited by $A_{\%low}$ at the lowest attainable g_{smax}, defined here as g_{low} (Fig. 1C). With our simulations of structural adaptation, we predict that values of g_{low} will be reached in a CO_2 range between 635 and 1,465 ppm (Table 1). Consistent with observations of stomatal adaptations at evolutionary timescales (Franks and Beerling, 2009a), the angiosperms in our dataset (Ar, Ic, Mc, Ql and Qn) have notably lower response limits than conifers (Pe, Pt and Td) (740 and 1250 ppm CO_2

Table 1. Species-specific limits of structural stomatal adaptations to rising CO2

Species names and abbreviations	g_{low} (mol·m^{-2}·s^{-1})	CO_{2lim} (ppm)
Angiosperm average	0.76	740
Acer rubrum (Ar)	0.69	830
Ilex cassine (Ic)	0.46	770
Morella cerifera (Mc)	0.73	670
Quercus laurifolia (Ql)	0.95	635
Quercus nigra (Qn)	0.97	775
Conifer average	0.31	1250
Pinus elliottii (Pe)	0.19	1465
Pinus taeda (Pt)	0.46	1060
Taxodium distichum (Td)	0.29	1210

Table 1. Species specific limits of the structural stomatal adaptation to rising CO_2, denoted by the lower limit on g_{smax} (defined as g_{low}) and CO_2 when mean g_{smax} reaches g_{low} (defined as CO_{2lim}).

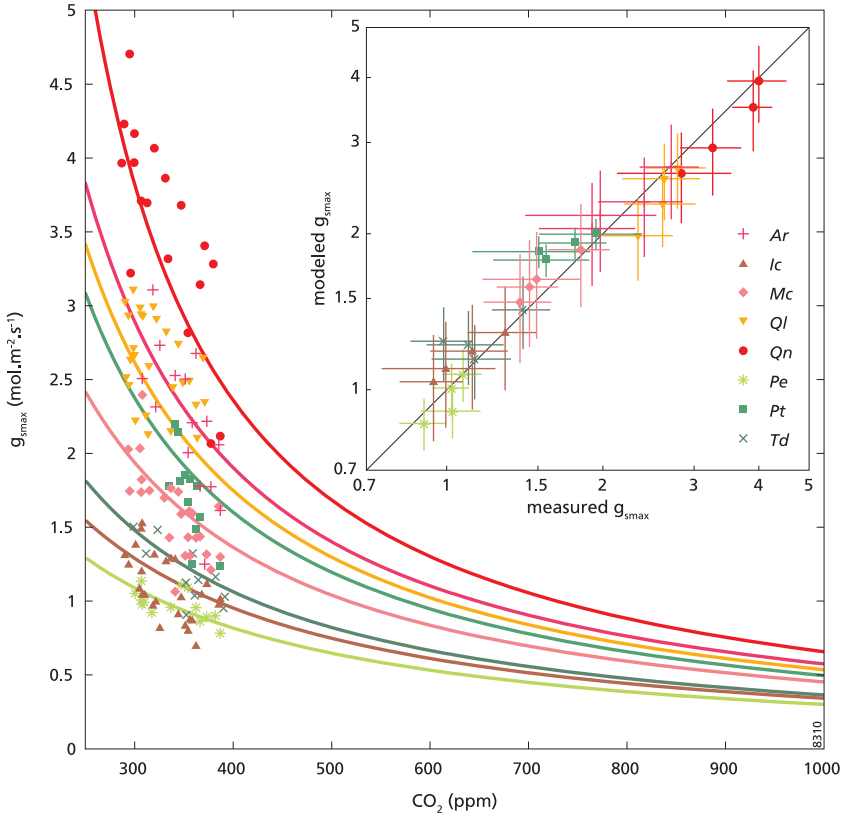

Figure 2. Modeled structural adaptations of g_{smax} to CO_2 for each species (solid colored lines), compared to measured g_{smax} averaged at each measured CO_2. Insert shows direct comparison between modeled and measured g_{smax} averaged over CO_2 quartiles of the data. Error bars indicate standard deviations of modeled (vertical) and measured (horizontal) g_{smax} in each quartile.

on average, respectively). This difference might be related to the distinct leaf vascular designs of angiosperms and conifers, which are intrinsically linked to the gas exchange capacity of their leaves (Beerling and Franks, 2010). Angiosperms evolved towards densely veined leaves which require highly conductive leaf surfaces with many small stomata to maximize gas exchange under low CO_2 (Brodribb and Feild, 2010). Contrastingly, conifers have less conductive leaf surfaces with fewer and larger stomata, matching the lower water transport capacity of the simpler leaf vascular design suited for higher CO_2 (Brodribb et al., 2005).

Structural stomatal adaptations may potentially alter photosynthesis and canopy gas exchange because g_{smax} crucially constrains g_s, especially when assimilation rates reach their daily maximum and stomata are fully open. To determine how photosynthesis and leaf gas exchange is altered by structural stomatal adaptation, we perform three model ensemble simulations: one

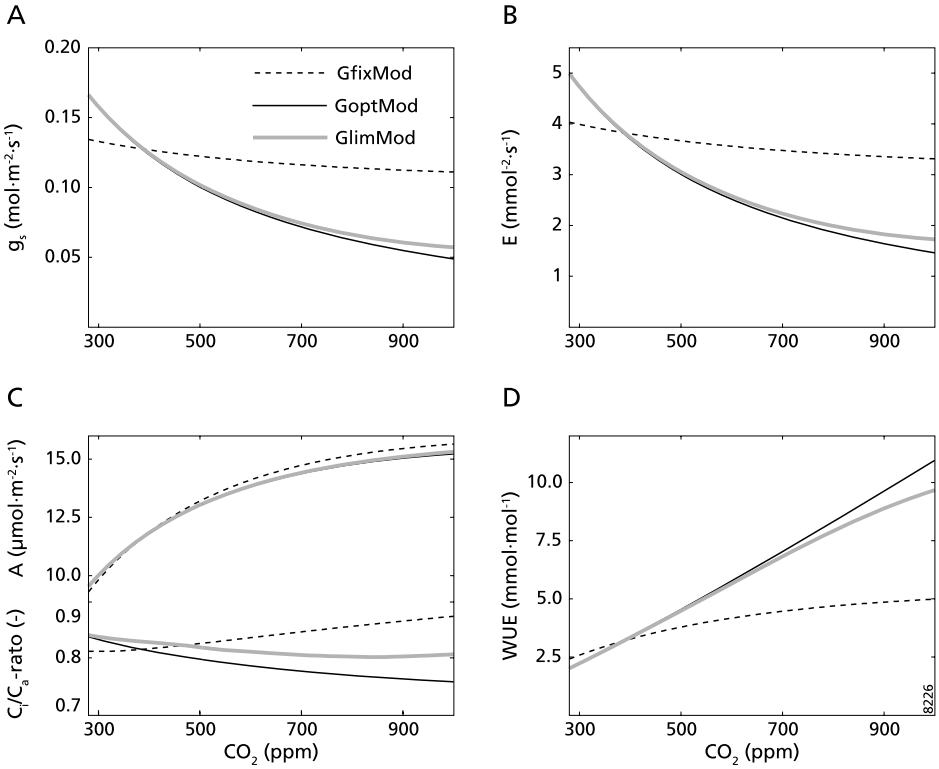

Figure 3. Overview of modeled daily average gas exchange at the leaf level for ensembles with dynamic stomatal adaptation only (GfixMod), with structural and dynamic adaptation (GoptMod) and with CO_2 response limits included (GlimMod). (A) Simulated stomatal conductance (g_s), (B) transpiration (E), (C) assimilation (A) and C_i/C_a-ratio at maximum photosynthesis, and (D) water use efficiency (WUE) expressed in mmol (CO_2)·mol $(H_2O)^{-1}$.

with dynamic adaptation superimposed on constant pre-industrial g_{smax} (GfixMod), one with structural and dynamic adaptation (GoptMod) and one with CO_2 response limits imposed at g_{low} (Table 1) (GlimMod), each of which consists of 8 species members.

The differences in simulated g_s between GfixMod, and GoptMod and GlimMod ensemble averages show that structural adaptation of g_{smax} constrains daily average g_s (Fig. 3A). From pre-industrial to present CO_2, daily average g_s decreases by 20% in the GlimMod and GoptMod ensembles and by 5% in the GfixMod ensemble. From present to double CO_2, g_s decreases by 40% in the GlimMod and GoptMod ensembles and by 10% in the GfixMod ensemble. Because transpiration (E) is controlled by g_s and humidity deficit in the lower atmosphere, E decreases in line with g_{smax} at increasing CO_2. Simulated E decreases with 1.0 mmol·m^{-2}·s^{-1} from pre-industrial to present, and with 1.8 mmol·m^{-2}·s^{-1} from present to double CO_2 in the GlimMod

and GoptMod ensembles (Fig. 3B). The GfixMod ensemble shows considerably less change in E with a decrease of 0.15 mmol·m^{-2}·s^{-1} from pre-industrial to present CO_2 and a decrease of 0.35 mmol·m^{-2}·s^{-1} from present to double CO_2. The change in E is less in the GfixMod simulations because only dynamic adaptation reduces g_s, while g_{smax} remains at its pre-industrial value in this model ensemble.

Contrasting the large differences in transpiration between the three ensemble runs, it is clear that they all show a similar increase in assimilation (A) from 9 µmol·m^2·s^{-1} at pre-industrial CO_2 to 15 µmol·m^2·s^{-1} at double CO_2 (Fig. 3C). This indicates that g_{smax} does not strongly control A, but rather that A is controlled by CO_2 via changes in leaf interior CO_2 concentrations (C_i) (Fig. 3C shows the ratio of internal to atmospheric CO_2 concentration, or C_i/C_a-ratio). The C_i therefore increases in line with CO_2 in the GfixMod ensemble and remains relatively constant over a wide range of CO_2 levels in the GoptMod and GlimMod ensembles. The latter response is commonly observed in C3 species and protects these plants from the adverse effects of photorespiration at low CO_2, while it increases the ratio of water loss versus carbon gain (termed water-use efficiency or WUE) with rising CO_2 (Fig. 3D) (Ainsworth and Rogers, 2007). In addition to reduced leaf level transpiration, the changes in C_i/C_a-ratio and photosynthesis underline the advantage plants gain from adapting stomatal conductance in response to CO_2 (Beerling and Franks, 2010).

The strength of physiological forcing ultimately depends on the change of canopy transpiration (ΔLE) under rising CO_2. When stomatal adaptations occur at the canopy scale, reduced leaf level transpiration might reduce humidity in the lower atmosphere and in turn increase transpiration due to an increased humidity gradient. To determine how transpiration is altered by structural stomatal adaptation, we upscale our model to the canopy scale and include the feedback with moisture in the lower atmosphere. With this canopy scale model, we repeat the GfixMod, GoptMod and GlimMod ensembles and estimate physiological forcing of the CO_2 rise from pre-industrial to present levels and of doubling current CO_2.

The GoptMod and GlimMod ensembles both show a ΔLE of -30 W·m^{-2} due to the CO_2 rise from pre-industrial to present levels and a ΔLE of -60 W·m^{-2} if CO_2 doubles (Fig. 4). The GfixMod ensemble includes only the effects of dynamic adaptation, so here ΔLE is just -15 W.m^{-2} from pre-industrial to double CO_2. The angiosperms in our dataset (Ar, Ic, Mc, Ql and Qn) reach their response limits between 635 and 830 ppm CO_2 (Table 1), so ΔLE is slightly less (5 W·m^{-2}) in the GlimMod compared to GoptMod ensemble at double CO_2. The conifers in our dataset (Pe, Pt and Td) reach their response limits at higher CO_2 (1,250 ppm on average) and therefore show no difference in ΔLE between the GlimMod and GoptMod ensembles. These results suggest that structural stomatal adaptations exert a continuing physiological forcing on climate.

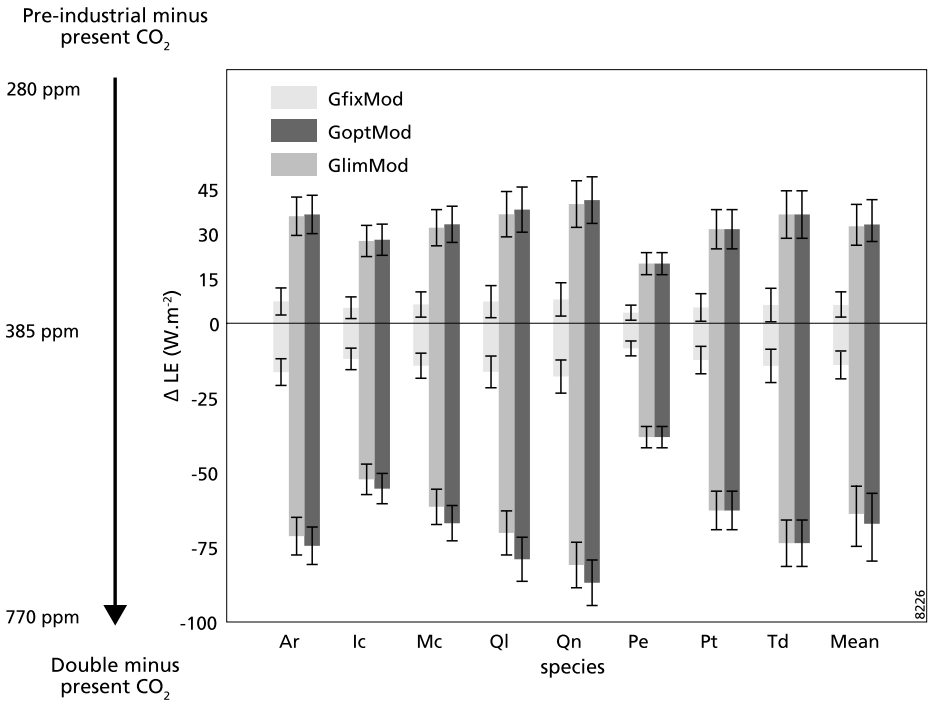

Figure 4. Changes in annual canopy transpiration [Δ*LE* (W·m^{-2})] between pre-industrial, present and double CO_2 for ensembles with dynamic stomatal adaptation only (GfixMod), with structural and dynamic adaptation (GoptMod) and with CO_2 response limits included (GlimMod). Error bars for individual species denote standard deviations in daily average transpiration for pre-industrial and double CO_2, error bars for mean values denote standard deviations between species averages.

3. Discussion

Our results suggest that structural adaptations of g_{smax} constrain the dynamic stomatal responses regulating g_s. These structural stomatal adaptations may thereby reduce the annual transpiration flux from natural subtropical vegetation in Florida under rising CO_2. Our hypothesis is supported by model simulations based on optimization of carbon gain under the constraint of a plant physiological cost of water loss that reproduce the observed adaptation of g_{smax} (which decreased with 17-55% from pre-industrial to present CO_2) (Chapter 5). We further expect that plants will continue to adapt structurally until they reach the limits of their phenotypic plasticity. Because CO_2 is likely doubled by the end of this century (IPCC, 2007) and response limits are generally reached around or above double present CO_2 levels, structural

stomatal adaptation in subtropical vegetation may continue to amplify the climatic forcing of CO_2 throughout this century.

Our simulations with the stomatal optimization model predict that a doubling of present CO_2 will decrease the annual transpiration flux from subtropical vegetation in Florida by approximately 60 $W \cdot m^{-2}$. This decrease is considerable as the current annual evapotranspiration flux in Florida is approximately 120 $W \cdot m^{-2}$ and canopy transpiration contributes for approximately 50% to this regional-scale total (Cao et al., 2010; Douglas et al., 2009). Feedbacks at regional and continental scales could potentially compensate for reduced canopy transpiration and shift the fractional contribution away from transpiration (McNaughton and Jarvis, 1991). Accounting for these feedbacks and the contribution of transpiration to total surface latent heat flux, a comparable decrease in latent heat flux of 30 $W \cdot m^{-2}$ has been simulated over subtropical forests with the Hadley Centre global climate model (Andrews et al., 2010; Boucher et al., 2009), which uses a semi-empirical stomatal response model (Ball et al., 1987). The finding that stomatal adaptations are currently reducing canopy transpiration is supported by independent empirical data from river runoff that reflect reduced continental-scale evapotranspiration over the past century (Gedney et al., 2006). We therefore conclude that plant adaptation to CO_2 is currently altering the hydrological cycle and climate and may continue to do so under further rising CO_2.

Despite this evidence for the climatic effects of stomatal adaptations, changes in transpiration could be compensated if forests respond to rising CO_2 by growing taller and denser and thus increase leaf area index (LAI) (Norby et al., 2005). However, in dense subtropical forests, self-shading and down regulation of photosynthetic capacity often limits this effect of CO_2 fertilization (Millard et al., 2007), so only forest-floor species are likely to benefit from rising CO_2 and these have little impact on canopy transpiration (Naumberg and Ellsworth, 2000). Moreover, increased photosynthesis might also increase turnover rates, leading to a more dynamic forest with unchanged biomass and LAI (Mahli et al., 2009). Simulations with a global vegetation model, which takes these considerations into account, indicate that in subtropical forests LAI increases by a maximum of 10% after a doubling of CO_2 (Kergoat et al., 2002). This increase in LAI can increase canopy transpiration by approximately 5%, which is not sufficient to compensate for reduced transpiration at the leaf level. Decreased transpiration therefore appears a robust response to increasing CO_2 in subtropical forests.

To estimate physiological forcing due to future CO_2 increase, it is essential to validate response limits to structural adaptation. We based estimates of response limits on the hypothesis that plant species adapt g_{smax} by altering D and a_{max} until they reach a generic value of $A_{\%low}$. Although the physiologic relevance of $A_{\%low}$ is not yet fully understood, it might represent a tradeoff between leaf interior CO_2 transport and the structural costs associated with the required leaf water transport system (Warren, 2008; Beerling and Franks, 2010). Since angiosperms and conifers have different leaf hydraulic systems (Brodribb et al., 2005), it could be argued that they also have different limits on $A_{\%}$ and that a generic $A_{\%low}$ overestimates

phenotypic plasticity for either growth type (Kürschner et al., 1997; Strand and Weisner, 2004). However, our analysis does not show significant differences in the lower ranges of $A_{\%}$ between angiosperms and conifers (see supporting information, Fig. S2). Therefore we cannot reject the hypothesis that $A_{\%low}$ is a generic lower limit of $A_{\%}$ and thus the use of equal $A_{\%low}$ for angiosperms and conifers is considered appropriate. Response limits based on $A_{\%low}$ might therefore represent upper limits of ambient CO_2 to which the design of the water transport system of each species is optimized. Our prediction indicates that response limits are lower for angiosperms than conifers (on average 740 and 1250 ppm CO_2, respectively), roughly reflecting the ambient CO_2 under which these lineages evolved (Dilcher, 2000; Henry, 2005).

Comparable differences in stomatal adaptation between angiosperms and conifers have been noted in free-air carbon enrichment (FACE) and greenhouse experiments under elevated CO_2 (Ainsworth and Rogers, 2007; Brodribb et al., 2009). These studies indicate that angiosperms respond with a higher sensitivity in g_s to elevated CO_2 than conifers. Our results suggest that differences in CO_2 response could result from the plant physiological cost of water loss, represented by the Lagrangian multiplier (λ) (see SI, Table S2) in the optimization procedure (Konrad et al., 2008). According to the optimization hypothesis, angiosperm species with a low λ can resort to high values of g_{smax} to function under low CO_2, while conifer species with a high λ cannot. Conversely, a rise in CO_2 reverses this adaptation and therefore shows an (initial) stronger response in angiosperms than conifers. However, as conifers are expected to have higher response limits than angiosperms, they might continue to optimize g_{smax} at CO_2 levels when angiosperms have reached their limit of phenotypic plasticity.

Because CO_2 is currently rising at exceptional rates, plants face the challenge of increasing individual fitness with plastic responses in their phenotype. While modern plants have adapted their physiology to the historically low CO_2 by increasing the diffusive conductance of their leaves over the past million years (Franks and Beerling, 2009a), the current rise in CO_2 allows a reversal of this adaptation. This makes individual plants more productive and drought resistant but also has the climatic consequence of reduced transpiration and associated changes in surface energy balance and the hydrological cycle (Betts et al., 2007; Gedney et al., 2006). With CO_2 continuing to increase, it is crucial to estimate the global magnitude of this climatic forcing via plant physiological responses and the two-way coupling between vegetation and climate (Kleidon, 2004; Dekker et al., 2010). Furthermore, the ongoing rise in CO_2 might give competitive advantage to plant lineages that evolved under high CO_2 and thereby allow a shift of existing vegetation composition favoring plant lineages tied to an earlier time (Ward and Kelly, 2004).

4. Materials and Methods

Model Equations

A biochemical model of photosynthesis (Farquhar et al., 2001) is used to simulate assimilation of CO_2 [(A (mol·m^{-2}·s^{-1})]:

$$A = \left(1 - \frac{\Gamma}{C_i}\right) \cdot \min(W_c, W_j) - R_d \qquad (2)$$

with

$$W_c = V_{c\max} \frac{C_i}{C_i + K_c(1 + \frac{p_0}{K_0})} \qquad (3) \qquad \text{and} \qquad W_j = \frac{2}{9} J \frac{C_i}{C_i + \frac{7}{3}\Gamma} \qquad (4)$$

in which Γ (mol·mol^{-1}) is the CO_2 compensation point in absence of dark respiration R_d (mol·m^{-2}·s^{-1}), C_i (mol·mol^{-1}) is the intercellular CO_2 concentration, W_c and W_j (mol·m^{-2}·s^{-1}) are the Rusbisco and RuBP limited rates of carboxylation, V_{cmax} (mol·m^{-2}·s^{-1}) is the maximum carboxylation capacity, K_c (mol·mol^{-1}) and K_o (mol·mol^{-1}) are the Michaelis-Menten constants for carboxylation and oxygenation and p_o (mol·mol^{-1}) is the partial pressure of oxygen. The rate of electron transport [J (mol·m^{-2}·s^{-1})] depends on the photon flux density [Q (mol·m^{-2}·s^{-1})], the rate and maximum rate of electron transport (Konrad et al., 2008) and temperature response of photosynthesis parameters (Bernacchi et al., 2003). Furthermore, V_{cmax} and J_{max} exhibit down-regulation in response to rising CO_2 (Franks and Beerling, 2009b) (see SI for details on parameter values).

Structural stomatal adaptations to changes in atmospheric CO_2 concentrations [CO_2 (mol·mol^{-1})] are simulated from optimization of carbon gain under the constraint of a plant physiological cost of water loss (Konrad et al., 2008). The underlying assumption of this approach is that plants cannot transpire more water than they can transport from the soil, through their roots and stem up to their leaves (Baldocchi and Xu, 2007). As maximum transpiration generally occurs during maximum photosynthesis, this model calculates an optimal g_{smax} [defined as g_{sopt} (mol·m^{-2}·s^{-1})] according to daily maximum photosynthesis and water availability at this time:

$$g_{sopt} = \frac{\sqrt{\frac{q(K+\Gamma)[CO_2(q-R_d)-(q\Gamma+KR_d)]}{(CO_2+K-\lambda a w_d)\lambda a w_d}}(CO_2+K-2\lambda a w_d)+(q-R_d)CO_2-(q\Gamma+KR_d)-q(K+\Gamma)a}{(CO_2+K)^2} \qquad (5)$$

in which

$$q = \begin{cases} V_{cmax} & if\ W_c \le W_j \\ \frac{2}{9} J & if\ W_c > W_j \end{cases} \qquad (6) \qquad \text{and} \qquad K = \begin{cases} K_c\left(1 + \frac{p_o}{K_o}\right) & if\ W_c \le W_j \\ \frac{7}{3}\Gamma & if\ W_c > W_j \end{cases} \qquad (7)$$

and the Lagrangian multiplier [λ (mol·mol^{-1})] represents a species specific empirical constant for the cost of water loss (see SI, Table S2), w_d (mol·mol^{-1}) is the water vapor deficit calculated from relative and saturated atmospheric humidity [w_{rel} (-) and w_{sat} (mol·mol^{-1})] as $w_d = w_{sat}$ (1 – w_{rel}) in which a (-) is the ratio between diffusivity of CO_2 and water vapor [d_c and d_w (m^2·s^{-1})]. Saturation value of water vapor and diffusivities of CO_2 and water vapor are calculated depending on ambient temperature (Konrad et al., 2008; Nobel, 1999).

We obtain g_{smax} for every 5 ppm CO_2 interval from 280-2000 ppm from maximum g_{sopt} by prescribing an average diurnal cycle of environmental boundary conditions for the season when leaves are formed (March, April and May in Florida). Meteorological data are obtained from the AmeriFlux database (Powell et al., 2008) (see SI, Fig. S1). For each species, λ is calibrated on the highest CO_2 quartile of species specific g_{smax} observations.

Dynamic stomatal responses are simulated with a stomatal response model (Buckley et al., 2003) superimposed on the model of structural adaptation. This model simulates dynamic adaption of g_s to environmental boundary conditions from changes in osmotic gradients in guard cells as a function of water availability and photosynthesis. Simulated actual g_s is the product of g_{smax} and the closure related to guard cell turgor (f_t [-]):

$$g_s = f_t \cdot g_{s\,\max} \qquad (8) \qquad \text{with} \qquad f_t = \frac{\alpha - \gamma}{\alpha + K_g} \qquad (9)$$

in which γ (-) is the hydroactive compensation point, K_g (-) is the Michaelis constant for the guard cell advantage [α (-)], which is calculated as a function of guard cell turgor related to water availability and photosynthesis (Buckley et al., 2003).

To solve the model for leaf level gas exchange, we first obtain values for g_{smax} at each CO_2 level and then force the dynamic and structural adaptation models with a diurnal cycle of annual average environmental boundary conditions (Fig. S1).

We upscale the leaf level simulations to canopy scale by considering photosynthesis at different heights in the canopy and the feedback between transpiration and moisture in the lower atmosphere. Differences in light conditions within the canopy are simulated from light interception. For this, we use a simple exponential light decay scheme (Beer's law) over 5 layers of equal LAI (Jogireddy et al., 2006):

$$Q(L_c) = Q(0)\, e^{-kL_c} \qquad (10)$$

where $Q(L_c)$ (mol·m^{-2}·s^{-1}) is the photosynthetically active radiation calculated from cumulative LAI [L_c (-)] above the considered location in the canopy, photosynthetically active radiation at the canopy top $Q(0)$, and the light extinction coefficient k (-). The feedback between transpiration and moisture in the lower atmosphere is included considering moisture redistribution in the planetary boundary layer (McNaugton and Jarvis, 1984).

To solve the model for canopy scale gas exchange over one year, the humidity of the upper atmosphere is iteratively calculated by forcing the model with an annual cycle of environmental boundary conditions (Powell et al., 2008) (Fig. S1). Then, g_s and E are calculated for every CO_2 level in each layer of the canopy.

As A depends on the total leaf conductance [g_t (mol·m^{-2}·s^{-1})] but in turn controls g_s, C_i is expressed as a function of CO_2, A and g_t:

$$C_i = C_a - \frac{Aa}{g_t} \qquad (11) \qquad \text{where} \quad g_t^{-1} = g_{bl}^{-1} + g_s^{-1} + g_i^{-1} \qquad (12)$$

The g_{bl} (mol·m^{-2}·s^{-1}) is the conductance of the leaf boundary layer (Vesala, 1998) and g_i (mol·m^{-2}·s^{-1}) is the internal conductance, assumed here as $g_i = ½ \cdot g_s$ (Warren, 2008).

5. Supporting information

Table S1: Species specific relations between pore length and guard cell width.

Species	Mean Cw [µm]	σ [µm]	n	Linear regression	r^2
Acer rubrum	6.79	0.94	36	C_w =0.36·[*L*]+2.90	0.49
Ilex cassine	10.26	1.33	27	C_w =0.28·[*L*] +6.19	0.57
Morella cerifera	7.84	1.10	25	C_w =0.41·[*L*] +3.57	0.62
Pinus elliottii	16.24	2.22	28	C_w =0.27·[*L*] +6.66	0.62
Pinus taeda	11.51	1.22	33	C_w= 11.5 µm	
Quercus laurifolia	6.72	0.77	22	C_w =0.27·[*L*] +4.57	0.49
Quercus nigra	7.29	1.21	27	C_w =0.26·[*L*] +3.55	0.56
Taxodium distichum	9.79	1.57	20	C_w =0.55·[*L*] +1.52	0.72

Table S1. Species specific relations between pore length (*L*) and guard cell width (C_w) are used to derive pore depth (*l*), based on the assumption that *l* is equal to C_w (Farquhar et al., 2001). The standard deviation (σ) and number of measurements (n) are indicated, alongside the linear regressions and r^2 values. Species specific regressions between C_w and *L* are highly significant (P < 0.0001, indicated by *) with exception of *P. taeda*. We therefore derive *l* from these species specific regressions, except for *P. taeda* for which a constant value is applied. The average slope of these regressions is used to calculate lines of equal g_{smax} in Figure 1A.

Table S2. Species specific model parameters

Species	λ	LAI	V_{cmax25}	J_{max25}	R_{d25}	derived from	M_a*	Reference
Ar	72	5.5	75.0	94	1.1	Foliar N		(Williams et al., 1996)
Ic	134	5.5	55.5	79.2	0.8	Foliar N	127(15)	(Saha et al., 2009)
Mc	99	5.5	62.5	89.1	0.9	Foliar N	101(35)	(Saha et al., 2009)
Pe	244	2	60.9	86.9	0.9	Foliar N		(Saha et al., 2009)
Pt	87	2	47.0	77.1	0.7	A/C_i curves		(Niinemets et al.,1997)
Ql	62	5.5	54.0	77.0	0.8	Foliar N	102(34)	(Moorhead et al., 1996)
Qn	58	5.5	64.8	92.4	1.0	Foliar N	96(10)	(Moorhead et al., 1996)
Td	55	3	30.0	49.2	0.5	A/C_i curves		(Niinemets et al., 1997)

Table S2. Species specific model parameters. Lagrangian multiplier [λ (µmol·mol^{-1})], leaf area index [*LAI* (-)] and photosynthesis parameters V_{cmax25}, J_{max25} and R_{d25} (µmol·m^{-2}·s^{-1}) and how photosynthesis parameters are derived. If photosynthesis parameters are based on foliar nitrogen (N) concentrations on a leaf mass base, measurements of leaf mass with area [M_a (g·m^{-2})] and their standard deviations are indicated. LAI values for conifers (Vose et al., 1995; Liu et al., 1997) are doubled in the model to account for their amphistomatic leaves.

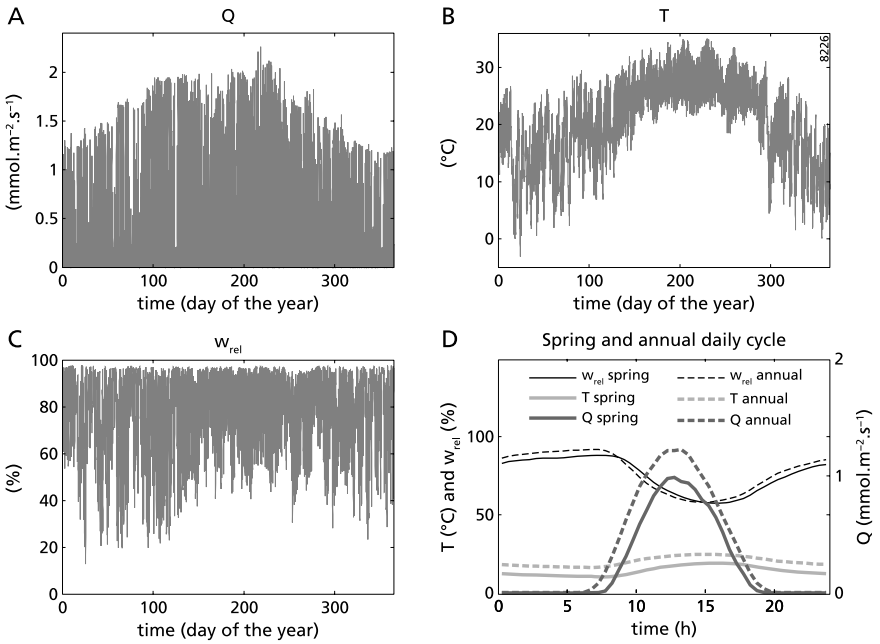

Figure S1. Environmental boundary conditions used to force the stomatal adaptation models. Annual cycles of climatic boundary conditions of photosynthetic active radiation [Q (mmol·m^{-2}·s^{-1})] (A), ambient air temperature [T (°C)] (B), and relative humidity [w_{rel} (%)] (C) measured over a pine flatwoods ecosystem near Gainesville, FL, during the year 2003 (Clark et al., 2004; Powell et al., 2008). (D) Average diurnal cycles for Q, T, and w_{rel} during leaf development (March, April, and May) are prescribed to the optimization models to determine g_{smax}. Annual average diurnal cycles of these boundary conditions are prescribed to calculate gas exchange at the leaf level. A complete annual cycle of these boundary conditions is prescribed to calculate changes in annual canopy transpiration.

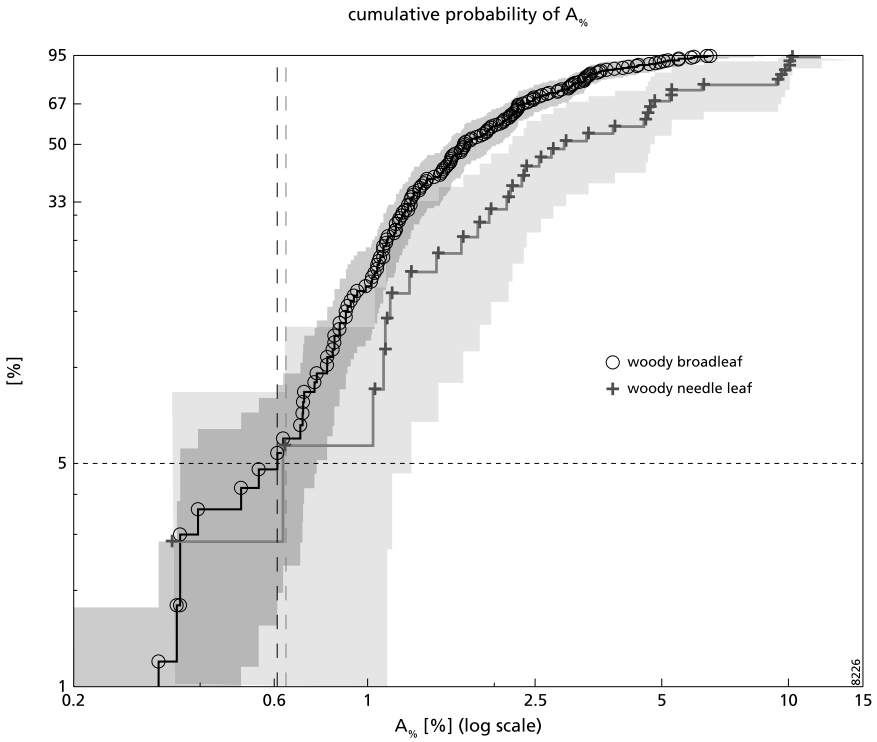

Figure S2. Empirical cumulative probability of $A_{\%}$ for woody broadleaf and woody needle leaf species. Data are from Franks and Beerling (2009a). Circles and crosses denote data points; connecting lines denote the fit of the empirical distribution. The 95% confidence level of each distribution is indicated by shading. Dashed lines denote the lower 5% limit of $A_{\%}$. On average, stomata occupy less space on leaves of woody broadleaf species than on leaves (needles) of woody needle leaf species. However, the 5% lower limit of $A_{\%}$ (defined as $A_{\%low}$) for both distributions cannot be distinguished. Note that a logarithmic x axis is used.

Supplementary methods

The biochemical model of photosynthesis (Farquhar et al., 2001) requires three species-specific photosynthesis parameters (at 25 °C) to be known: maximum carboxylation capacity [V_{cmax25} (mol·m^{-2}·s^{-1})], maximum rate of electron transport [J_{max25} (mol·m^{-2}·s^{-1})] and mitochondrial respiration rate R_{d25} (mol·m^{-2}·s^{-1}) (Table S2). For *Pinus taeda* (Pt) and *Taxodium distichum* (Td), we derived these values from published *A/Ci* curves (Ellsworth et al., 2004) and the empirical relation among V_{cmax25}, J_{max25}, and R_{d25} (Wullschleger, 1993; Baldocchi and Wilson, 2001):

$$J_{\max 25} = (29.1 + 1.64 \cdot 10^{6} \cdot V_{c\ \max 25}) \cdot 10^{-6} \qquad \text{(SI 1)}$$

and

$$R_{d25} = 0.015 \cdot V_{c\ \max 25} \qquad \text{(SI 2)}$$

For the other species *[Acer rubrum* (Ar), *Ilex cassine* (Ic), *Morella cerifera* (Mc), *Quercus laurifolia* (Ql), *Quercus nigra* (Qn), *Pinus elliottii* (Pe), and *Pinus taeda* (Pt)], we derived V_{cmax25} and J_{max25} from foliar nitrogen content (Niinemets and Tenhunen, 1997) and R_{d25} from Eq. SI.2:

$$V_{c\ \max 25} = 6.25 \cdot V_{cr} M_A N_m P_R \cdot 10^{-6} \qquad \text{(SI 3)}$$

where 6.25 is the ratio of weight of Rubisco to the weight of nitrogen in Rubisco (g·g^{-1}), V_{cr} is the specific activity of Rubisco at 25 °C [20.7 (μmol·g^{-1}·s^{-1})], M_A is the leaf mass (g·m^{-2}), N_m is leaf nitrogen content per leaf dry mass (g·g^{-1}) and P_R (-) is the fraction of nitrogen allocated to Rubisco, estimated at 0.15, and:

$$J_{\max 25} = 8.06 \cdot J_{mc} M_A N_m P_B \cdot 10^{-6} \qquad \text{(SI 4)}$$

where 8.06 is the minimal nitrogen investment in cytochrome bioenergetics [μmol of cytochrome·(g of N)$^{-1}$], the potential rate of photosynthetic electron transport per unit cytochrome (J_{MC}) is estimated at 156 μmol electrons·(μmol of cytochrome·s)$^{-1}$ at 25 °C and P_B (g of N in cytochrome) is the fraction of N allocated to RuBP estimated at 0.035.

Down-regulation of the photosynthesis parameters V_{cmax25} and J_{max25} in response to rising CO_2 (Ainsworth and Rogers, 2007; Franks and Beerling, 2009b) is simulated with an exponential decay function:

$$V_{\max 25}(CO_2) = V_{\max 25}(385) \cdot e^{-\kappa(CO_2 - 385)} \qquad \text{(SI 5)}$$

and

$$J_{\max 25}(CO_2) = J_{\max 25}(385) \cdot e^{-\kappa(CO_2 - 385)} \quad \text{(SI 6)}$$

where $V_{cmax25}(385)$ and $J_{max25}(385)$ represent the photosynthesis parameters V_{cmax25} and J_{max25} at their present day values (Table S2) and κ is a decay constant for the CO_2 response of V_{cmax25} and J_{max25}. A value of $2 \cdot 10^{-4} \cdot ppm^{-1}$ is chosen for κ to match estimated down-regulation of photosynthesis parameters at geological timescales (Franks and Beerling, 2009b). Furthermore, species specific values of leaf area index [LAI (-)] are derived from literature (Table S2) (Vose et al., 1995; Liu et al., 1997).

References

Ainsworth, E.A. and A. Rogers (2007). The response of photosynthesis and stomatal conductance to rising [CO_2]: mechanisms and environmental interactions. *Plant, Cell and Environment,* vol. 30, no. 3, pp. 258-270.

Alexander, T.J. and A.G. Crook (1974). Recent vegetational changes in Southern Florida. In: Environments of South Florida: Present and Past. Ed. P.J. Gleason. The Miami Geological Society, Miami, pp.61-72.

Alvarez Zarikian, C.A., P.K. Swart, J.A. Gifford and P.L. Blackwelder (2005). Holocene paleohydrology of Little Salt Spring, Florida, based on ostracod assemblages and stable isotopes. *Palaeogeography, Palaeoclimatology, Palaeoecology,* vol. 225, no. 1-4, pp. 134-156.

Andrews, T., M. Doutriaux-Boucher, O. Boucher and P.M. Forster (2011). A regional and global analysis of carbon dioxide physiological forcing and its impact on climate. *Climate Dynamics,* vol. 36, no. 3-4, pp. 783-792.

Baldocchi, D.D. and L. Xu (2007). What limits evaporation from Mediterranean oak woodlands – the supply of moisture in the soil, physiological control by plants, or the demand by the atmosphere? *Advances in Water Resources,* vol. 30, pp. 2113-2122.

Baldocchi, D.D. and K.B. Wilson (2001). Modeling CO_2 and water vapor exchange of a temperate broadleaved forest across hourly to decadal timescales. *Ecological Modelling,* vol. 142, pp. 155-184.

Ball, J.T., I.E. Woodrow and A. Berry (1987). Progress in Photosynthesis Research, Vol. IV. Martinus Nijhoff, Dordrecht.

Banner, J.L., M. Musgrove, Y. Asmerom, R.L. Edwards and J.A. Hoff (1996). High resolution temporal record of Holocene ground-water chemistry: tracing links between climate and hydrology. *Geology,* vol. 24, no. 11, pp. 1049-1053.

Battarbee, R.W. (1973). A new method for the estimation of absolute microfossil numbers, with reference especially to diatoms. *Limnology and Oceanography,* vol. 18, no. 4, pp. 647.

Battarbee, R.W., J.P. Smol and J. Meriläinen (1986). Diatoms as indicators of pH: a historical review. In: Diatoms and lake acidity. Eds. J.P. Smol, R.W. Battarbee, R.B. Davis and J. Meriläinen. W. Junk, The Hague, The Netherlands,

Beerling, D.J. and P.J. Franks (2010). Plant science: The hidden cost of transpiration. *Nature,* vol. 464, pp. 495-496.

Bernacchi, C.J., C. Pimentel and S.P. Long (2003). In vivo temperature response functions of parameters required to model RuBP-limited photosynthesis. *Plant, Cell and Environment,* vol. 26, pp. 1419-1430.

Berner, R.A. (2006). GEOCARBSULF: A combined model for the Phanerozoic atmospheric O_2 and CO_2. *Geochimica et Cosmochimica Acta,* vol. 70, pp. 5653-5664.

Bernhardt, C. (2011). Native Americans, regional drought and tree island evolution in the Florida Everglades. *The Holocene,* vol. 21, no. 6, pp. 967-978.

Bernhardt, C.E. and D.A. Willard (2009). Response of the Everglades ridge and slough landscape to climate variability and 20th-century water management. *Ecological Applications,* vol. 19, no. 7, pp. 1723.

Betts, R.A., O. Boucher, M. Collins, P.M. Cox, P.D. Falloon, N. Gedney, D.L. Hemming, C. Huntingford, C.D. Jones and D.M.H. Sexton (2007). Projected increase in continental runoff due to plant responses to increasing carbon dioxide. *Nature,* vol. 448, pp. 1037-1041.

Blaauw, M. (2010). Methods and code for 'classical' age-modelling of radiocarbon sequences. *Quaternary Geochronology,* vol. 5, no. 5, pp. 512-518.

Blum, M.D., T.J. Misner, E.S. Collins, D.B. Scott, R.A. Morton and A. Aslan (2001). Middle Holocene sea level rise and highstand at +2 m, Central Texas coast. *Journal of Sedimentary Research,* vol. 71, no. 4, pp. 581-588.

Boldt, K.V., P. Lane, J.D. Woodruff and J.P. Donnelly (2010). Calibrating a sedimentary record of overwash from Southeastern New England using modeled historic hurricane surges. *Marine Geology,* vol. 275, no. 1-4, pp. 127-139.

Bonan, G.B. (2008). Forests and climate change: forcings, feedbacks, and the climate benefits of forests. *Science,* vol. 320, no. 5882, pp. 1444-1449.

Boucher, O., A. Jones and R.A. Betts (2009). Climate response to the physiological impact of carbon dioxide on plants in the Met Office Unified Model HadCM3. *Climate Dynamics,* vol. 32, pp. 237-249.

Bowen, G.J. (2008). The Online Isotopes in Precipitation Calculator, version 2.2. Available: http://www.waterisotopes.org.

Bowen, G.J., L.I. Wassenaar and K.A. Hobson (2005). Global application of stable hydrogen and oxygen isotopes to wildlife forensics. *Oecologia,* vol. 143, pp. 337-348.

Brodribb, T.J. and T.S. Feild (2010). Leaf hydraulic evolution led a surge in leaf photosynthetic capacity during early angiosperm diversification. *Ecology Letters,* vol. 13, no. 2, pp. 175-183.

Brodribb, T.J., S.A.M. McAdam, G.J. Jordan and T.S. Feild (2009). Evolution of stomatal responsiveness to CO_2 and optimization of water-use efficiency among land plants. *New Phytologist,* vol. 183, no. 3, pp. 839-847.

Brodribb, T.J., N.M. Holbrook, M.A. Zwieniecki and B. Palma (2005). Leaf hydraulic capacity in ferns, conifers and angiosperms: impacts on photosynthetic maxima. *New Phytologist,* vol. 165, no. 3, pp. 839-846.

Brooks, G.R. (2011). Florida Gulf Coast estuaries: Tampa Bay and Charlotte Harbor. In: Gulf of Mexico origin, waters, and biota. Volume 3, Geology. Eds. N.A. Buster and C.W. Holmes. Texas A and M Press, College Station, pp.73-87.

Brooks, G.R., L.J. Doyle, B.C. Suthard, S.D. Locker and A.C. Hine (2003). Facies architecture of the mixed carbonate/siliciclastic inner continental shelf of west-central Florida: implications for Holocene barrier development. *Marine Geology,* vol. 200, pp. 325-349.

Brooks, G.R. and L.J. Doyle (1998). Recent sedimentary development of Tampa Bay, Florida: a microtidal estuary incised into Tertiary platform carbonates. *Estuaries and Coasts,* vol. 21, no. 3, pp. 391-406.

Buckley, T.N., K.A. Mott and G.D. Farquhar (2003). A hydromechanical and biochemical model of stomatal conductance. *Plant, Cell and Environment,* vol. 26, pp. 1767-1785.

Camburn, K.E. and D.F. Charles (2000). Diatoms of low-alkalinity lakes in the Northeastern United States. Academy of Natural Sciences of Philadelphia, Philadelphia.

Cao, L., G. Bala, K. Caldeira, R. Nemani and G. Ban-Weiss (2010). Importance of carbon dioxide physiological forcing to future climate change. *Proceedings of the National Academy of Sciences,* vol. 107, no. 21, pp. 9513-9518.

Clark, K.L., H.L. Gholz and M.S. Castro (2004). Carbon dynamics along a chronosequence of slash pine plantations in North Florida. *Ecological Applications,* vol. 14, pp. 1154-1171.

Cowan, I.R. and G.D. Farquhar (1977). Stomatal function in relation to leaf metabolism and environment. In: Integration of activity in the higher plants. Ed. D.H. Jennings. Cambridge University Press, Cambridge, UK, pp.471-505.

Cremer, H., F. Sangiorgi, F. Wagner-Cremer, V. McGee, A.F. Lotter and H. Visscher (2007). Diatoms (Bacillariophyceae) and dinoflagellate cysts (Dinophyceae) from Rookery Bay, Florida, U.S.A. *Caribbean Journal of Science,* vol. 43, no. 1, pp. 23-58.

Cronin, T.M., N.T. Edgar, G.R. Brooks, D. Hastings, R.A. Larson, A. Hine, S. Locker, B. Suthard, B. Flower, D. Hollander, J. Wehmiller, D. Willard and S. Smith (2007). Sea level rise in Tampa Bay. *Eos,* vol. 88, no. 10, pp. 117-118.

Cronin, T.M., R. Thunell, G.S. Dwyer, C. Saenger, M.E. Mann, C.D. Vann and R.R. Seal II (2005). Multi-proxy evidence of Holocene climate variability from estuarine sediments, eastern North America. *Paleoceanography,* vol. 20, pp. PA4006.

Cronin, T.M., G.S. Dwyer, T. Kamiya, S. Schwede and D.A. Willard (2003). Medieval Warm Period, Little Ice Age and 20th century temperature variability from Chesapeake Bay. *Global and Planetary Change,* vol. 36, no. 1-2, pp. 17.

Cronin, T.M., G.S. Dwyer, S.B. Schwede, C.D. Vann and H. Dowsett (2002). Climate variability from the Florida Bay sedimentary record: possible teleconnections to ENSO, PNA and CNP. *Climate Research,* vol. 19, pp. 233-245.

Curtis, S. (2008). The Atlantic multidecadal oscillation and extreme daily precipitation over the US and Mexico during the hurricane season. *Climate Dynamics,* vol. 30, no. 4, pp. 343-351.

Dale, B. and A. Fjellså (1994). Dinoflagellate cysts as paleoproductivity indicators: state of the art, potential, and limits. In: NATO ASI Series I: Global Environmental Change, 17: Carbon Cycling in the Glacial Ocean: Constraints on the Ocean's Role in Global Change. Eds. R. Zahn, T.F. Pedersen, M.A. Kaminski and L. Labeyrie. Springer, Berlin, pp.521-537.

Dalrymple, R.W., B.A. Zaitl and R. Boyd (1992). Estuarine facies models: conceptual basis and stratigraphic implications. *Journal of Sedimentary Research,* vol. Vol. 62, no. 6, pp. 1130-1146.

Dansgaard, W. (1964). Stable isotopes in precipitation. *Tellus,* vol. 16, no. 4, pp. 436-468.

Darwin, F. (1898). Observations on stomata (abstract). *Proceedings of the Royal Society of London,* vol. 63, pp. 413-417.

Davis, J.H. (1967). General map of natural vegetation of Florida. Florida Agricultural Experiment Station.

Davis, R.E., B.P. Hayden, D.A. Gay, W.L. Phillips and G.V. Jones (1997). The North Atlantic subtropical anticyclone. *Journal of Climate,* vol. 10, pp. 728.

Davis Jr., R.A., S.C. Knowles and M.J. Bland (1989). Role of hurricanes in the Holocene stratigraphy of estuaries: examples from the Gulf Coast of Florida. *Journal of Sedimentary Petrology,* vol. 59, no. 6, pp. 1052-1061.

Dekker, S.C. (2010). Biogeophysical feedbacks trigger shifts in the modelled vegetation- atmosphere system at multiple scales. *Biogeosciences,* vol. 7, pp. 1237-1245.

Dekker, S.C., H.J. de Boer, E.I. Lammertsma, M.J. Wassen and M.B. Eppinga (under review). Holocene peatland initiation in southern Florida.

deMenocal, P., J. Ortiz, T.P. Guilderson and M. Sarnthein (2000). Coherent high- and low-latitude climate variability during the Holocene warm period. *Science,* vol. 288, no. 5474, pp. 2198-2202.

Dilcher, D. (2000). Toward a new synthesis: major evolutionary trends in the angiosperm fossil record. *Proceedings of the National Academy of Sciences of the United States of America,* vol. 97, no. 13, pp. 7030-7036.

Dixon, L.K., G.A. Vargo, J.O.R. Johansson, R.T. Montgomery and M.B. Neely (2009). Trends and explanatory variables for the major phytoplankton groups of two southwestern Florida estuaries, U.S.A. *Journal of Sea Research,* vol. 61, no. 1-2, pp. 95-102.

Donders, T.H., H.J. de Boer, W. Finsinger, E.C. Grimm, S.C. Dekker, G.J. Reichart and F. Wagner-Cremer (2011). Impact of the Atlantic Warm Pool on precipitation and temperature in Florida during North Atlantic cold spells. *Climate Dynamics,* vol. 36, no. 1-2, pp. 109-118.

Donders, T.H., P.M. Gorissen, F. Sangiorgi, H. Cremer, F. Wagner-Cremer and V. McGee (2008). Three-hundred-year hydrological changes in a subtropical estuary, Rookery Bay (Florida): Human impact versus natural variability. *Geochemistry Geophysics Geosystems,* vol. 9, no. 7, pp. Q07V06.

Donders, T.H., F. Wagner, D.L. Dilcher and H. Visscher (2005a). Mid-to late-Holocene El Niño-Southern Oscillation dynamics reflected in the subtropical terrestrial realm. *Proceedings of the National Academy of Sciences of the United States of America,* vol. 102, no. 31, pp. 10904-10908.

Donders, T.H., F. Wagner and H. Visscher (2005b). Quantification strategies for human-induced and natural hydrological changes in wetland vegetation, southern Florida, USA. *Quaternary Research,* vol. 64, no. 3, pp. 333-342.

Donders, T.H., F. Wagner, K. Van der Borg, A.F.M. De Jong and H. Visscher (2004). A novel approach for developing high-resolution sub-fossil peat chronologies with ^{14}C dating. *Radiocarbon,* vol. 46, no. 1, pp. 455-464.

Donnelly, J.P. and L. Giosan (2008). Tempestuous highs and lows in the Gulf of Mexico. *Geology,* vol. 36, no. 9, pp. 751-752.

Donnelly, J.P. and J.D. Woodruff (2007). Intense hurricane activity over the past 5,000 years controlled by El Niño and the West African monsoon. *Nature,* vol. 447, no. 7143, pp. 465-468.

Douglas, E.M., J.M. Jacobs, D.M. Sumner and R.L. Ray (2009). A comparison of models for estimating potential evaporation for Florida landcover types. *Journal of Hydrology,* vol. 373, pp. 366-376.

Edwards, L.E. and D.A. Willard (2001). Dinoflagellate cysts and pollen from sediments samples, Mississippi Sound and Gulf of Mexico. Report no. 01-415, US Geological Survey.

Edwards, L.E. and A.S. Andrle (1992). Distribution of selected dinoflagellate cysts in modern marine sediments. In: Neogene and Quaternary Dinoflagellate Cysts and Acritarchs. Eds. M.J. Head and L.H. Wrenn. AASP Foundation, Dallas, pp.259-288.

Ellsworth, D.S. (2004). Photosynthesis, carboxylation, and leaf nitrogen responses of 16 species to elevated pCO_2 across four free-air CO_2 enrichment experiments in forest, grassland and desert. *Global Change Biology,* vol. 10, pp. 2121-2138.

Ellsworth, D.S. (1999). CO_2 enrichment in a maturing pine forest: are CO_2 exchange and water status in the canopy affected? *Plant, Cell and Environment,* vol. 22, no. 5, pp. 461-472.

Elsner, J.B., K. Liu and B. Kocher (2000). Spatial variations in major U.S. hurricane activity: statistics and a physical mechanism. *Journal of Climate,* vol. 13, no. 13, pp. 2293-2305.

Emanuel, K. (2005). Increasing destructiveness of tropical cyclones over the past 30 years. *Nature,* vol. 436, pp. 686-688.

Enfield, D.B. (1996). Relationship of inter-American rainfall to tropical Atlantic and Pacific SST variability. *Geophysical Research Letters,* vol. 23, no. 23, pp. 3305-3308.

Enfield, D.B., A.M. Mestas-Nuñez and P.J. Trimble (2001). The Atlantic Multidecadal Oscillation and its relation to rainfall and river flows in the continental U.S. *Geophysical Research Letters,* vol. 28, pp. 2077-2080.

Evans, M.W. and A.C. Hine (1991). Late Neogene sequence stratigraphy of a carbonate-siliciclastic transition: southwest Florida. *Geological Society of America Bulletin,* vol. 103, pp. 679-699.

Evans, M.W., A.C. Hine and D.F. Belknap (1989). Quaternary stratigraphy of the Charlotte Harbor estuarine-lagoon system, southwest Florida: Implications of the carbonate-siliciclastic transition. *Marine Geology,* vol. 88, no. 3-4, pp. 319-348.

Fægri, K., J. Iversen, P.E. Kaland and K. Krzywinski (1989). Textbook of pollen analysis. Wiley, Chichester.

Farquhar, G.D., S. von Cammerer and J.A. Berry (2001). Models of photosynthesis. *Plant Physiology,* vol. 125, pp. 42-45.

Farquhar, G.D. and T.D. Sharkey (1982). Stomatal conductance and photosynthesis. *Annual Review of Plant Physiology,* vol. 33, no. 1, pp. 317-345.

Farquhar, G.D., D.R. Dubbe and K. Raschke (1978). Gain of the feedback loop involving carbon dioxide and stomata: theory and measurement. *Plant Physiology,* vol. 62, no. 3, pp. 406-412.

FDEP (2007). Highlands Hammock State Park Unit Management Plan. State of Florida, Department of Environmental Protection, Division of Recreation and Parks.

Fensome, R.A. and G.L. Williams (2004). The Lentin and Williams index of fossil dinoflagellates (2004 Edition). AASP Foundation Contribution Series 42.

Forman, S.L., R. Oglesby, V. Markgraf and T. Stafford (1995). Paleoclimatic significance of Late Quaternary eolian deposition on the Piedmont and High Plains, Central United States. *Global and Planetary Change,* vol. 11, no. 1-2, pp. 35-55.

Franklin, J.L., R.J. Pasch, L.A. Avila, J.L. Beven II, M.B. Lawrence, S.R. Stewart and E.S. Blake (2006). Atlantic hurricane season of 2004. *Monthly Weather Review,* vol. 134, pp. 981-1025.

Franks, P.J., P.L. Drake and D.J. Beerling (2009). Plasticity in maximum stomatal conductance constrained by negative correlation between stomatal size and density: an analysis using *Eucalyptus globulus*. *Plant, Cell and Environment*, vol. 32, no. 12, pp. 1737-1748.

Franks, P.J. and D.J. Beerling (2009a). Maximum leaf conductance driven by CO_2 effects on stomatal size and density over geologic time. *Proceedings of the National Academy of Sciences of the United States of America,* vol. 106, no. 25, pp. 10343-10347.

Franks, P.J. and D.J. Beerling (2009b). CO_2-forced evolution of plant gas exchange capacity and water-use efficiency over the Phanerozoic. *Geobiology,* vol. 7, no. 2, pp. 227-236.

Franks, P.J. and G.D. Farquhar (2001). The effect of exogenous abscisic acid on stomatal development, stomatal mechanics, and leaf gas exchange in *Tradescantia virginiana*. *Plant Physiology,* vol. 125, no. 2, pp. 935-942.

Fujine, K., M. Yamamoto, R. Tada and Y. Kido (2006). A salinity-related occurrence of a novel alkenone and alkenoate in Late Pleistocene sediments from the Japan Sea. *Organic Geochemistry,* vol. 37, pp. 1074-1084.

Gaiser, E.E., M.J. Brooks, W.F. Kenney, C.L. Schelske and B.E. Taylor (2004). Interpreting the hydrological history of a temporary pond from chemical and microscopic characterization of siliceous microfossils. *Journal of Paleolimnology,* vol. 31, pp. 63-76.

Gaiser, E.E., B.E. Taylor, and M.J. Brooks (2001). Establishment of wetlands on the southeastern Atlantic Coastal Plain: paleolimnological evidence of a mid-Holocene hydrologic threshold from a South Carolina pond. *Journal of Paleolimnology*, vol. 26, pp. 373-391.

Gaiser, E.E. and J. Johansen (2000). Freshwater diatoms from Carolina Bays and other isolated wetlands on the Atlantic coastal plain of South Carolina, USA, with descriptions of seven taxa new to science. *Diatom Research,* vol. 15, no. 1, pp. 75-130.

Gaiser, E.E., T.E. Philippi and B.E. Taylor (1998). Distribution of diatoms among intermittent ponds on the Atlantic Coastal Plain: development of a model to preduct drought periodicity from surface-sediment assemblages. *Journal of Paleolimnology,* vol. 20, no. 1, pp. 71.

Garcia-Amorena, I., F. Wagner, T.B. van Hoof and F. Gómez Manzaneque (2006). Stomatal responses in deciduous oaks from southern Europe to the anthropogenic atmospheric CO_2 increase; refining the stomatal-based CO_2 proxy. *Review of Palaeobotany and Palynology,* vol. 141, no. 3-4, pp. 303-312.

Gedney, N., P.M. Cox, R.A. Betts, O. Boucher, C. Huntingford and P.A. Stott (2006). Detection of a direct carbon dioxide effect in continental river runoff records. *Nature,* vol. 439, no. 7078, pp. 835-838.

Gedzelman, S.D. and J.R. Lawrence (1990). The isotopic composition of precipitation from two extratropical cyclones. *Monthley Weather Review,* vol. 118, no. 2, pp. 495-509.

Ghalambor, C.K., J.K. McKay, S.P. Carroll and D.N. Reznick (2007). Adaptive versus non-adaptive phenotypic plasticity ant the potential for contemporary adaptation in new environments. *Functional Ecology,* vol. 21, pp. 394-407.

Gilbes, F., C. Tomas, J.J. Walsh and F.E. Müller-Karger (1996). An episodic chlorophyll plume on the West Florida Shelf. *Continental Shelf Research,* vol. 16, no. 9, pp. 1201-1224.

Givnish, T.J., J.C. Volin, V.D. Owen, V.C. Volin, J.D. Muss and P.H. Glaser (2008). Vegetation differentiation in the patterned landscape of the central Everglades: importance of local and landscape drivers. *Global Ecology and Biogeography,* vol. 17, no. 3, pp. 384.

Gleason, P.J. and P. Stone (1994). Age, origin, and landscape evolution of the Everglades peatland. In: Everglades: the ecosystem and its restoration. Eds. S.M. Davis and J.C. Ogden. St. Lucie Press, Delray Beach, FL, pp.149-197.

Goldenberg, S.B., C.W. Landsea, A.C. Mestas-Nuñez and W.M. Gray (2001). The recent increase in Atlantic hurricane activity: causes and implications. *Science,* vol. 293, pp. 474-479.

Goodbred, S.L.,Jr, E.E. Wright and A.C. Hine (1998). Sea level change and storm-surge deposition in a Late Holocene Florida salt marsh. *Journal of Sedimentary Research,* vol. 68, no. 2, pp. 240-252.

Gray, W.M. (1984). Atlantic Seasonal Hurricane Frequency. Part I: El Niño and 30 mb Quasi-Biennial Oscillation Influences. *Monthly Weather Review,* vol. 112, no. 9, pp. 1649-1668.

Grimm, E.C., (1991-2001). Tilia, TiliaGraph, TGView software.

Grimm, E.C., W.A. Watts, G.L. Jacobson Jr., B.C.S. Hansen, H.R. Almquist and A.C. Dieffenbacher-Krall (2006). Evidence for warm wet Heinrich events in Florida. *Quaternary Science Reviews,* vol. 25, no. 17-18, pp. 2197-2211.

Grimm, E.C., G.L. Jacobson Jr, W.A. Watts, B.C. Hansen and K.A. Maasch (1993). A 50,000-year record of climate oscillations from Florida and its temporal correlation with the Heinrich events. *Science,* vol. 261, no. 5118, pp. 198-200.

Hallett, R.I., (1999). Consequences of environmental change on the growth and morphology of *Lingulodinium polyedrum* (Dinophyceae) in culture. PhD dissertation. University of Westminster, London.

Haug, G.H., K.A. Hughen, D.M. Sigman, L.C. Peterson and U. Röhl (2001). Southward migration of the intertropical convergence zone through the Holocene. *Science,* vol. 293, no. 5533, pp. 1304-1308.

Heiri, O., A.F. Lotter and G. Lemcke (2001). Loss on ignition as a method for estimating organic and carbonate content in sediments: reproducibility and comparability of results. *Journal of Paleolimnology,* vol. 25, no. 1, pp. 101-110.

Henry, R.J. (2005). Plant diversity and evolution: genotypic and phenotypic variation in higher plants. Centre for Plant Conservation Genetics, Southern Cross University, Lismore, Australia.

Hernandez, M., S.N. Miller, D.C. Goodrich, B.F. Goff, W.G. Kepner, C.M. Edmonds and K.B. Jones (2000). Modeling runoff response to landcover and rainfall spatial variability in semi-arid watersheds. *Environmental Monitoring and Assessment,* vol. 64, no. 1, pp. 285-298.

Hetherington, A.M. and F.I. Woodward (2003). The role of stomata in sensing and driving environmental change. *Nature,* vol. 424, no. 6951, pp. 901-908.

Higuera-Gundy, A., M. Brenner, D.A. Hodell, J.H. Curtis, B.W. Leyden and M.W. Binford (1999). A 10,300 ^{14}C yr record of climate and vegetation change from Haiti. *Quaternary Research,* vol. 52, no. 2, pp. 159-170.

Hine, A.C., M.W. Evans, R.A. Davis and D.F. Belknap (1987). Depositional response to seagrass mortality along a low-energy, barrier-island coast; west-central Florida. *Journal of Sedimentary Research,* vol. 57, no. 3, pp. 431-439.

Hodell, D.A., J.H. Curtis, G.A. Jones, A. Higuera-Gundy, M. Brenner, M.W. Binford and K.T. Dorsey (1991). Reconstruction of Caribbean climate change over the past 10,500 years. *Nature,* vol. 352, no. 6338, pp. 790-793.

Hustedt, F. (1930 – 1966). Die Kieselalgen Deutschlands, Österreichs und der Schweiz unter Berücksichtigung der übrigen Länder Europas sowie der angrenzenden Meeresgebiete. In: Kryptogamen-Flora, Band VII, Die Kieselalgen. Ed. Dr. L. Rabenhorsts. Otto Koeltz Science Publishers, Koenigstein,

Hustedt, F. (1955). Marine littoral diatoms of Beaufort, North Carolina. *Duke University Marine Station Bulletin,* vol. 6, pp. 1-67.

Indermühle A., T. F. Stocker, F. Joos, H. Fischer, H. J. Smith, M. Wahlen, B. Deck, D. Mastroianni, J. Tschumi, T. Blunier, R.Meyer and B. Stauffer (1999). Holocene carbon-cycle dynamics based on CO_2 trapped in ice at Taylor Dome, Antarctica. *Nature*, vol 398, pp.121-126.

Ishman, S.E., G.L. Brewster-Wingard, D.A. Willard, T.M. Cronin, L.E. Edwards and C.W. Holmes (1996). Preliminary paleontological report on Core T-24, Little Madeira Bay, Florida. Report no. 96-543, US Geological Survey.

Isphording, W.C., F.D. Imsand and J.C. Flowers (1989). Physical characteristics and aging of Gulf coast estuaries. *Gulf Coast Association of Geological Societies, Transactions,* vol. 39, pp. 387-401.

IPCC: Climate Change 2007, The physical basis. Contribution of Working Group I to the Fourth Assessment Report of the Intergovernmental Panel on Climate Change, edited by Solomon, Manning, Chen, Marquis, Averty, Tignor and Miller.

Jogireddy, V.R., P.M. Cox, C. Huntingford, R.J. Harding and L. Mecardo (2006). An improved description of canopy light interception for use in a GCM land-surface scheme: Calibration and testing against carbon fluxes at coniferous forest. Report Hadley Centre Technical note: 63, The Hadley Centre.

Katul, G., S. Manzoni, S. Palmroth and R. Oren (2009). A stomatal optimization theory to describe the effects of atmospheric CO_2 on leaf photosynthesis and transpiration. *Annals of Botany,* vol. 105, pp. 431-442.

Keeling, C.D. and T.P. Whorf (2003). Atmospheric CO_2 concentrations- Mauna Loa observatory, Hawaii, 1958-2003.

Keigwin, L.D. (1996). The Little Ice Age and Medieval Warm Period in the Sargasso Sea. *Science,* vol. 274, no. 5292, pp. 1503-1508.

Kelly, M.H. and J.A. Gore (2008). Florida river flow patterns and the Atlantic multidecadal oscillation. *River Research and Applications,* vol. 24, no. 5, pp. 598-616.

Kergoat, L. (2002). Impact of doubled CO_2 on global-scale leaf area index and evapotranspiration; conflicting stomatal conductance and LAI responses. *Journal of Geophysical Research,* vol. 107, pp. 4808.

Killops, S.D. and V.J. Killops (2005). Introduction to organic geochemistry. Blackwell Publishing, Oxford.

Kleidon, A. (2004). Optimized stomatal conductance of vegetated land surfaces and its effects on simulated productivity and climate. *Geophysical Research Letters,* vol. 3

Knox, J.C. (2000). Sensitivity of modern and Holocene floods to climate change. *Quaternary Science Reviews,* vol. 19, no. 1-5, pp. 439-457.

Koltermann, C.E. and S.M. Gorelick (1992). Paleoclimatic signature in terrestrial flood deposits. *Science,* vol. 256, no. 5065, pp. 1775-1782.

Konrad, W., A. Roth-Nebelsick and M. Grein (2008). Modelling of stomatal density response to atmospheric CO_2. *Journal of Theoretical Biology,* vol. 253, pp. 638-658.

Kürschner, W.M. (1997). The anatomical diversity of recent and fossil leaves of the durmast oak (*Quercus petraea* Lieblein/*Q. pseudocastanea* Goeppert) – implications for their use as biosensors of palaeoatmospheric CO_2 levels. *Review of Palaeobotany and Palynology,* vol. 96, no. 1-2, pp. 1-30.

Kürschner, W.M., J. van der Burgh, H. Visscher and D.L. Dilcher (1996). Oak leaves as biosensors of late Neogene and early Pleistocene paleoatmospheric CO_2 concentrations. *Marine Micropaleontology,* vol. 27, no. 1-4, pp. 299-312.

Kushlan, J.A. (1990). Freshwater wetlands and aquatic ecosystems: freshwater marshes. In: Ecosystems of Florida. Eds. R.L. Myers and J.J. Ewel. University of Central Florida Press, Orlando, pp.324-363.

Lake, J.A., F.I. Woodward and W.P. Quick (2002). Long-distance CO_2 signalling in plants. *Journal of Experimental Botany,* vol. 53, no. 367, pp. 183-193.

Lane, P., J.P. Donnelly, J.D. Woodruff and A.D. Hawkes (2011). A decadally-resolved paleohurricane record archived in the late Holocene sediments of a Florida sinkhole. *Marine Geology,* vol. 287, no. 1-4, pp. 14-30.

Landsea, C.W. (2005). Meteorology: Hurricanes and global warming. *Nature*, vol. 438, E11-E12.

Lawrence, J.R., S.D. Gedzelman, J. Gamache and M. Black, (2002). Stable Isotope Ratios: Hurricane Olivia. Journal of Atmospheric Chemistry, vol. 41, no. 1, pp. 67-82.

Laws, R.A. (1988). Diatoms (Bacillariophyceae) from surface sediments in the San Francisco bay estuary. *Proceedings of the California Academy of Sciences,* vol. 45, pp. 133-154.

Lea, D.W., D.K. Pak, L.C. Peterson and K.A. Hughen (2003). Synchroneity of tropical and high-latitude Atlantic temperatures over the last glacial termination. *Science,* vol. 301, no. 5638, pp. 1361-1364.

Leigh, D.S. and T.P. Feeney (1995). Paleochannels indicating wet climate and lack of response to lower sea level, southeast Georgia. *Geology,* vol. 23, no. 8, pp. 687-690.

Leuning, R. (1995). A critical appraisal of a combined stomatal-photosynthesis model for C3 plants. *Plant, Cell and Environment,* vol. 18, pp. 339-355.

Levin, I. and B. Kromer (2004). The tropospheric $^{14}CO_2$ level in mid latitudes of the Northern Hemisphere (1959-2003). *Radiocarbon,* vol. 46, pp. 1261-1277.

Lewis, J. and R. Hallett (1997). *Lingulodinium polyedrum* (*Gonyaulax polyedra*) a blooming dinoflagellate. *Oceanography and Marine Biology Annual Review,* vol. 35, pp. 97-161.

Li, Y.X., T.E. Törnqvist, J.M. Nevitt, B. Kohl (2012). Synchronizing a sea level jump, final Lake Agassiz drainage, and abrupt cooling 8200 years ago. *Earth and Planetary Science Letters*, vol 315-316, pp 41-50.

Liu, K. and M.L. Fearn (2000). Reconstruction of prehistoric landfall frequencies of catastrophic hurricanes in northwestern Florida from lake sediment records. *Quaternary Research,* vol. 54, no. 2, pp. 238-245.

Liu, S., H. Riekerk and H.L. Gholz (1997). Leaf litter fall, leaf area index, and radiation transmittance in cypress wetlands and slash pine plantations in north-central Florida. *Wetlands Ecology and Management,* vol. 4, pp. 257-271.

Liu, K. and M.L. Fearn (1993). Lake-sediment record of late Holocene hurricane activities from coastal Alabama. *Geology,* vol. 21, no. 9, pp. 793-796.

Locker, S.D., A.C. Hine and G.R. Brooks (2003). Regional stratigraphic framework linking continental shelf and coastal sedimentary deposits of west-central Florida. *Marine Geology,* vol. 200, no. 1-4, pp. 351-378.

Long, S.P., E.A. Ainsworth, A. Rogers and D.R. Ort (2004). Rising atmospheric carbon dioxide: plants FACE the future. *Annual Review of Plant Biology,* vol. 55, pp. 591-628.

Mahli, Y. (2009). Exploring the likelihood and mechanism of a climate-change-induced dieback of the Amazon forest. *Proceedings of the National Academy of Sciences,* vol. 106, pp. 20610-20615.

Malaizé, B., P. Bertran, P. Carbonel, D. Bonnissent, K. Charlier, D. Galop, D. Imbert, N. Serrand, C. Stouvenot and C. Pujol (2011). Hurricanes and climate in the Caribbean during the past 3700 years BP. *The Holocene,* vol. 21, no. 6, pp. 911-924.

Mann, M.E., J.D. Woodruff, J.P. Donnelly and Z. Zhang (2009). Atlantic hurricanes and climate over the past 1,500 years. *Nature,* vol. 460, no. 7257, pp. 880-883.

Marret, F., J.D. Scourse, G.J.M. Versteegh, F.J.H. Jansen and R. Schneider (2001). Integrated marine and terrestrial evidence for abrupt Congo River palaeodischarge fluctuations during the last deglaciation. *Journal of Quaternary Science,* vol. 16, no. 8, pp. 761-766.

Marret, F. and K.A.F. Zonneveld (2003). Atlas of modern organic-walled dinoflagellate cyst distribution. *Review of Palaeobotany and Palynology,* vol. 125, no. 1-2, pp. 1-200.

McCloskey, T.A. and G. Keller (2009). 5000 year sedimentary record of hurricane strikes on the central coast of Belize. *Quaternary International,* vol. 195, no. 1-2, pp. 53-68.

McCloskey, T.A. and J.T. Knowles (2009). Hurricanes and climate change; migration of the tropical cyclone zone throughout the Holocene. In: Hurricanes and climate change. Eds. J.B. Elsner and T.H. Jagger. Springer US, US,

McKown, A.D., H. Cochard and L. Sack (2010). Decoding leaf hydraulics with a spatially explicit model: principles of venation architecture and implications for its evolution. *American Naturalist,* vol. 175, pp. 447-460.

McMurtie, R.E., B.E. Medlyn and R.C. Dewar (2001). Increased understanding of nutrient immobilization in soil organic matter is critical for predicting the carbon sink strength of forest ecosystems over the next 100 years. *Tree Physiology,* vol. 21, pp. 831-839.

McNoughton, K. and P.G. Jarvis (1991). Effects of spatial scale on stomatal control of transpiration. *Agriculture and Forest Meteorology,* vol. 54, pp. 279-302.

McNoughton, K. and P.G. Jarvis (1984). Using the Penman-Monteith equation predictively. *Agricultural Water Management,* vol. 8, pp. 263-278.

McPherson, B.F., R.L. Miller and Y. Stoker (1996). Physical, chemical, and biological characteristics of the Charlotte Harbor basin and estuarine system in southwestern Florida: a summary of the 1982-89 US Geological Survey Charlotte Harbor assessment and other studies. Report no. 2486, USGS Water Supply.

McPherson, B.F. and R.L. Miller (1990). Nutrient distribution and variability in the Charlotte Harbor estuarine system, Florida. *Journal of the American Water Resources Association,* vol. 26, no. 1, pp. 67-80.

Medlyn, B.E., C.V.M. Barton, M.S.J. Broadmeadow, R. Ceulemans, P. De Angelis, M. Forstreuter, M. Freeman, S.B. Jackson, S. Kellomäki, E. Laitat, A. Rey, P. Roberntz, B.D. Sigurdsson, J. Strassemeyer, K. Wang, P.S. Curtis and P.G. Jarvis (2001). Stomatal conductance of forest species after long-term exposure to elevated CO_2 concentration: a synthesis. *New Phytologist,* vol. 149, no. 2, pp. 247-264.

Mertens, K.N., S. Ribeiro, I. Bouimetarhan, H. Caner, N. Combourieu Nebout, B. Dale, A. De Vernal, M. Ellegaard, M. Filipova, A. Godhe, E. Goubert, K. Grøsfjeld, U. Holzwarth, U. Kotthoff, S.A.G. Leroy, L. Londeix, F. Marret, K. Matsuoka, P.J. Mudie, L. Naudts, J.L. Peña-Manjarrez, A. Persson, S. Popescu, V. Pospelova, F. Sangiorgi, M.T.J. van der Meer, A. Vink, K.A.F. Zonneveld, D. Vercauteren, J. Vlassenbroeck and S. Louwye (2009). Process length variation in cysts of a dinoflagellate, *Lingulodinium machaerophorum*, in surface sediments: Investigating its potential as salinity proxy. *Marine Micropaleontology,* vol. 70, no. 1-2, pp. 54-69.

Millard, P., M. Sommerkorn and G. Grelet (2007). Environmental change and carbon limitation in trees: a biochemical, ecophysiological and ecosystem appraisal. *New Phytologist,* vol. 175, pp. 11-28.

Miller, R.L., T.F. Kraemer and B.F. McPherson (1990). Radium and Radon in Charlotte Harbor estuary, Florida. *Estuarine, Coastal and Shelf Science,* vol. 31, pp. 439-457.

Miller-Rushing, A.J., R.B. Primack, P.H. Templer, S. Rathbone and S. Mukunda (2009). Long-term relationships among atmospheric CO_2, stomata, and intrinsic water use efficiency in individual trees. *American Journal of Botany,* vol. 96, no. 10, pp. 1779-1786.

Milliken, K.T., J.B. Anderson and A.B. Rodriguez (2008). A new composite Holocene sea level curve for the northern Gulf of Mexico. In: Response of upper Gulf Coast estuaries to Holocene climate change and sea level change: the Geological Society of America Special Paper 443. Eds. J.B. Anderson and A.B. Rodriguez. pp.1-11.

Ming, L., L. Zhong, W.C. Boicourt, S. Zhang and D.L. Zhang (2007). Hurricane-induced destratification and restratification in a partially-mixed estuary. *Journal of Marine Research,* vol. 65, no. 2, pp. 169-192.

Montero-Serrano, J.C., V. Bout-Roumazeilles, T. Sionneau, N. Tribovillard, A. Bory, B.P. Flower, A. Riboulleau, P. Martinez and I. Billy (2010). Changes in precipitation regimes over North America during the Holocene as recorded by mineralogy and geochemistry of Gulf of Mexico sediments *Global and Planetary Change,* vol. 74, no. 3-4, pp. 132-143.

Moorhead, K.K. and J. McArthur (1996). Spatial and temporal patterns of nutrient concentrations in foliage of riparian species. *Am Midl Nat,* vol. 136, pp. 29-41.

Morris, J.T., P.V. Sundareshwar, C.T. Nietch, B. Kjerfve and D.R. Cahoon (2002). Responses of coastal wetlands to rising sea level. *Ecology,* vol. 83, no. 10, pp. 2869-2877.

Morton, R.A., J.G. Paine and M.D. Blum (2000). Responses of stable bay-margin and barrier-island systems to Holocene sea level highstands, western Gulf of Mexico. *Journal of Sedimentary Research,* vol. 70, no. 3, pp. 478-480.

Moy, C.M., G.O. Seltzer, D.T. Rodbell and D.M. Anderson (2002). Variability of El Niño/Southern Oscillation activity at millennial timescales during the Holocene epoch. *Nature,* vol. 420, pp. 162-165.

Müller, P.J., G. Kirst, G. Ruhland, I. von Storch and A. Rosell-Melé (1998). Calibration of the alkenone paleotemperature index UK'37 based on core-tops from the eastern South Atlantic and the global ocean (60°N-60°S). *Geochimica et Cosmochimica Acta,* vol. 62, no. 10, pp. 1757-1772.

Myers, R.L. and J.J. Ewel (1990). Ecosystems of Florida. University of Central Florida Press, Orlando.

Naumburg, E. and D.S. Ellsworth (2000). Photosynthetic sunfleck utilization potential of understory saplings growing under elevated CO_2 in FACE. *Oecologia,* vol. 122, pp. 163-174.

Neftel, A., H. Friedli, E. Moor, H. Lötscher, H. Oeschger, U. Siegenthaler and B. Stauffer (1994). Historical CO_2 record from the Siple Station ice core. In: Trends: a compendium of data on global change. Carbon Dioxide Information Analysis Center, Oak Ridge National Laboratory, U.S. Department of Energy, Oak Ridge, Tennessee, USA,

Nes, W. (1974). Role of sterols in membranes. *Lipids,* vol. 9, no. 8, pp. 596-612.

Niinemets, Ü. and J.D. Tenhunen (1997). A model separating leaf structural and physiological effects on carbon gain along light gradients for the shade-tolerant species *Acer saccharum*. *Plant, Cell and Environment,* vol. 20, pp. 845-866.

Nürnberg, D., M. Ziegler, C. Karas, R. Tiedemann and M.W. Schmidt (2008). Interacting Loop Current variability and Mississippi River discharge of the past 400 kyr. *Earth and Planetary Science Letters*, vol. 272, pp. 278-289.

Nobel, P.S. (1999). Physiochemical and environmental plant physiology. Academic Press, San Diego.

Norby, R.J. (2005). Forest response to elevated CO_2 in conserved across a broad range of productivity. *Proceedings of the National Academy of Sciences,* vol. 102, pp. 18052-18056.

Otvos, E.G. (1970). Development and migration of barrier islands, northern Gulf of Mexico. *Geological Society of America Bulletin,* vol. 81, no. 1, pp. 241-246.

Paerl, H.W., J.D. Bales, L.W. Ausley, C.P. Buzelli, L.B. Crowder, L.A. Eby, J.M. Fear, M. Go, B.L. Peierls, T.L. Richardson II and J.S. Ramus (2001). Ecosystem impacts of three sequential hurricanes (Dennis, Floyd, and Irene) on the United States' largest lagoonal estuary, Pamlico Sound, NC. *Proceedings of the National Academy of Sciences,* vol. 98, no. 10, pp. 5655-5660.

Patrick, R. and C.W. Reimer (1966). The diatoms of the United States exclusive of Alaska and Hawaii. vol 1. Fragilariaceae, Eunotiaceae, Achnanthaceae, Naviculaceae. Academy of Natural Sciences of Philadelphia, Philadelphia.

Pearce, C., H. Cremer and F. Wagner-Cremer (2010). *Aulacoseira coroniformis* sp. nov., a new diatom (Bacillariophyta) species from Highlands Hammock State Park, Florida. *Phytotaxa,* vol. 13, pp. 40-48.

Pearce, C., H. Cremer, E. Lammertsma and F. Wagner-Cremer (2011). A 2,500-year record of environmental change in Highlands Hammock State Park (Central Florida, U.S.A.) inferred from siliceous microfossils. *Journal of Paleolimnology,*

Piao, S., P. Friedlingstein, P. Ciais, N. de Noblet-Ducoudre, D. Labat and S. Zaehle (2007). Changes in climate and land use have a larger direct impact than rising CO_2 on global river runoff trends. *Proceedings of the National Academy of Sciences of the United States of America,* vol. 104, no. 39, pp. 15242-15247.

Pierce, R.H., D.L. Wetzel and E.D. Estevez (2004). Charlotte Harbor Initiative: assessing the ecological health of southwest Florida's Charlotte Harbor estuary. *Ecotoxicology,* vol. 13, no. 3, pp. 275-284.

Poole, I. and W.M. Kürschner (1999). Stomatal density and index: the practice. In: Fossil plant and spores: modern techniques. Eds. T.P. Jones and N.P. Rowe. The Geological Society, London, UK, pp.257-260.

Poole, I., J.D.B. Weyers, T. Lawson and J.A. Raven (1996). Variations in stomatal density and index: implications for palaeoclimatic reconstructions. *Plant, Cell and Environment,* vol. 19, no. 6, pp. 705-712.

Poore, R.Z., H. Dowsett, S. Verardo and T.M. Quinn (2003). Millennial- to century-scale variability in Gulf of Mexico Holocene climate records. *Paleoceanography,* vol. 18, no. 2, pp. PA000868.

Powell, T.L. (2008). Carbon exchange of a mature, naturally regenerated pine forest in north Florida. *Global Change Biology,* vol. 14, pp. 2523-2538.

Prahl, F.G. and S.G. Wakeham (1987). Calibration of unsaturation patterns in long-chain ketone compositions for palaeotemperature assessment. *Nature,* vol. 330, no. 6146, pp. 367-369.

Price, R.M., P.K. Swart and H.E. Willoughby (2008). Seasonal and spatial variation in the stable isotopic composition ($\delta^{18}O$ and δD) of precipitation in south Florida. *Journal of Hydrology,* vol. 358, no. 3-4, pp. 193-205.

Quillen, A.K., E.E. Gaiser and E.C. Grimm (2011). Diatom-based paleolimnological reconstruction of regional climate and local land-use change from a protected sinkhole lake in southern Florida, USA. *Journal of Paleolimnology.*

Raven, J.A. (2002). Selection pressures on stomatal evolution. *New Phytologist,* vol. 153, no. 3, pp. 371-386.

Reichart, G., H. Brinkhuis, F. Huiskamp and W.J. Zachariasse (2004). Hyperstratification following glacial overturning events in the northern Arabian Sea. *Paleoceanography,* vol. 19, no. 2, pp. PA2013.

Reid, C.D., H. Maherali, H.B. Johnson, S.D. Smith, S.D. Wullschleger and R.B. Jackson (2003). On the relationship between stomatal characters and atmospheric CO_2. *Geophysical Research Letters,* vol. 30, no. 19, pp. 1983-1986.

Richey, J.N., R.Z. Poore, B.P. Flower and T.M. Quinn (2007). 1400 yr multi-proxy record of climate variability from the northern Gulf of Mexico. *Geology,* vol. 35, no. 5, pp. 423-426.

Rochon, A., J. Lewis, M. Ellegaard and I.C. Harding (2009). The *Gonyaulax spinifera* (Dinophyceae) "complex": perpetuating the paradox? *Review of Palaeobotany and Palynology,* vol. 155, no. 1-2, pp. 52-60.

Rochon, A., A. de Vernal, J.L. Turon, J. Matthiessen and M.J. Head (1999). Distribution of recent dinoflagellate cysts in surface sediments from the North Atlantic Ocean and adjacent seas in relation to sea-surface parameters. AASP Contribution Series 35,

Rodbell, D.T., G.O. Seltzer, D.M. Anderson, M.B. Abbott, D.B. Enfield and J.H. Newman (1999). An ~15,000-year record of El Niño-driven alluviation in southwestern Ecuador. *Science,* vol. 283, pp. 516-520.

Ropelewski, C.F. and M.S. Halpert (1987). Global and regional scale precipitation patterns associated with the El Niño/Southern Oscillation. *Monthly Weather Review,* vol. 115, pp. 1606-1626.

Royer, D.L. (2001). Stomatal density and stomatal index as indicators of paleoatmospheric CO_2 concentration. *Review of Palaeobotany and Palynology,* vol. 114, no. 1-2, pp. 1-28.

Sachs, J.P. and R.F. Anderson (2005). Increased productivity in the subantarctic ocean during Heinrich events. *Nature,* vol. 434, no. 7037, pp. 1118-1121.

Sachse, D., J. Radke and G. Gleixner (2006). δD values of individual n-alkanes from terrestrial plants along a climatic gradient – Implications for the sedimentary biomarker record. *Organic Geochemistry,* vol. 37, no. 4, pp. 469-483.

Sachse, D., J. Radke and G. Gleixner (2004). Hydrogen isotope ratios of recent lacustrine sedimentary n-alkanes record modern climate variability. *Geochimica et Cosmochimica Acta,* vol. 68, no. 23, pp. 4877-4889.

Saha, A.K., L.D. Sternberg and F. Miralles-Wilhelm (2009). Linking water sources with foliar nutrient status in upland plant communities in the Everglades National Park, USA. *Ecohydrology,* vol. 2, pp. 42-54.

Salisbury, E.J. (1928). On the causes and ecological significance of stomatal frequency, with special reference to the woodland flora. *Philosophical Transactions of the Royal Society of London,* vol. 216, pp. 1-65.

Sangiorgi, F., E. Dinelli, P. Maffioli, S. Principato, L. Capotondi, S. Giunta, C. Morigi, K.C. Emeis, A. Negri and C. Corselli (2006). Geochemical and micropaleontological characterisation of a Mediterranean sapropel S5: a case study from core BAN89GC09 (south of Crete). *Palaeogeography, Palaeoclimatology, Palaeoecology,* vol. 235, pp. 192-207.

Scheuer, P.J. (1973). Chemistry of marine natural products. Academic Press, New York.

Schmidt, N., E.K. Lipp, J.B. Rose and M.E. Luther (2001). ENSO influences on seasonal rainfall and river discharge in Florida. *Journal of Climate,* vol. 14, pp. 615-628.

Schmidt, N. and M.E. Luther (2002). ENSO impacts on salinity in Tampa Bay, Florida. *Estuaries and Coasts,* vol. 25, no. 5, pp. 976-984.

Scholl, D.W., F.C. Craighead Sr. and M. Stuiver (1969). Florida submergence curve revised: its relation to coastal sedimentation rates. *Science,* vol. 163, no. 3867, pp. 562-564.

Scholl, D.W. and M. Stuiver (1967). Recent submergence of southern Florida: a comparison with adjacent coasts and other eustatic data. *Geological Society of America Bulletin,* vol. 78, pp. 437-454.

Scileppi, E. and J.P. Donnelly (2007). Sedimentary evidence of hurricane strikes in western Long Island, New York. *Geochemistry Geophysics Geosystems,* vol. 8, no. 6, pp. Q06011.

Scott, D.B., E.S. Collins, P.T. Gayes and E. Wright (2003). Records of prehistoric hurricanes on the South Carolina coast based on micropaleontological and sedimentological evidence, with comparison to other Atlantic Coast records *Geological Society of America Bulletin,* vol. 115, no. 9, pp. 1027.

Scott, T.M., K.M. Campbell, F.R. Rupert, J.D. Arthur, T.M. Missimer, J.M. Lloyd, J.W. Yon and J.G. Duncan (2001). Geologic map of the state of Florida. Report no. 80, Florida Geological Survey.

Sinninghe Damsté, J.S., F. Kenig, M.P. Koopmans, J. Koster, S. Schouten, J.M. Hayes and J.W. De Leeuw (1995). Evidence for gammacerane as an indicator of water column stratification. *Geochimica et Cosmochimica Acta,* vol. 59, no. 9, pp. 1895-1900.

Sionneau, T., V. Bout-Roumazeilles, P.E. Biscaye, B. Van Vliet-Lanoe and A. Bory (2008). Clay mineral distributions in and around the Mississippi River watershed and Northern Gulf of Mexico: sources and transport patterns. *Quaternary Science Reviews,* vol. 27, no. 17-18, pp. 1740-1751.

Siver, P.A., P.B. Hamilton, K. Stachura-Suchoples and J.P. Kociolek (2005). Diatoms of North America: the freshwater flora of Cape Cod, Massachusetts, U.S.A. In: Iconographia Diatomologica. vol. 14. Diatoms of North America. Ed. H. Lange-Bertalot. A.R.G. Gantner Verlag K.G., Ruggell, pp.1 – 463.

Smol, J.P. and Stoermer, E.F. (eds) 2010, The diatoms: applications for environmental and earth sciences. 2nd edition, Cambridge University Press, Cambridge.

Stoker, Y.E. (1992). Salinity distribution and variation with freshwater inflow and tide, and potential changes in salinity due to altered freshwater inflow in the Charlotte Harbor estuary System, Florida. Water Resources Investigations Report 92-4062, USGS.

Strand, J.A. and S.E.B. Weisner (2004). Phenotypic plasticity contrasting species-specific traits induced by identical environments constraints. *New Phytologist,* vol. 163, pp. 449-451.

Stuiver, M., P.J. Reimer and R.W. Reimer (2010). CALIB Radiocarbon Calibration (HTML version 6.0). Available: http://calib.qub.ac.uk/calib/.

Thorsen, T.A. and B. Dale (1997). Dinoflagellate cysts as indicators of pollution and past climate in a Norwegian fjord. *The Holocene,* vol. 7, no. 4, pp. 433-446.

Törnqvist, T.E., J.L. González, L.A. Newsom, K. Van der Borg, A.F.M. De Jong and C.W. Kurnik (2004). Deciphering Holocene sea level history on the US Gulf Coast: a high-resolution record from the Mississippi Delta. *Geological Society of America Bulletin,* vol. 116, no. 7-8, pp. 1026-1039.

Toscano, M.A. and I.G. Macintyre (2003). Corrected western Atlantic sea level curve for the last 11,000 years based on calibrated ^{14}C dates from *Acropora palmata* framework and intertidal mangrove peat. *Coral Reefs,* vol. 22, no. 3, pp. 257-270.

Trenberth, K.E., P.D. Jones, P. Ambenje, R. Bojariu, D. Easterling, A. Klein Tank, D. Parker, F. Rahimzadeh, J.A. Renwick, M. Rusticci, B. Soden, P. Zhai (2007). Observations: surface and atmospheric climate change. In: Solomon et al., (eds) Climate Change 2007, The physical basis. Contribution of Working Group I to the Fourth Assessment Report of the Intergovernmental Panel on Climate Change. Cambridge University Press, Cambridge.

Trewavas, A. (2009). What is plant behaviour? *Plant, Cell and Environment,* vol. 32, pp. 606-616.

Troiani, B.T., A.R. Simms, T. Dellapenna, E. Piper and Y. Yokoyama (2011). The importance of sea level and climate change, including changing wind energy, on the evolution of a coastal estuary: Copano Bay, Texas. *Marine Geology,* vol. 280, no. 1-4, pp. 1-19.

Tyler, D., D.G. Zawada, A. Nayegandhi, J.C. Brock, M.P. Crane, K.K. Yates and K.E.L. Smith (2007). Topobathymetric data for Tampa Bay, Florida. Report no. Open File Report 2007-1051 (revised), USGS.

Upchurch, D.R. and J.R. Mahan (1988). Maintenance of constant leaf temperature by plants – II. Experimental observations in cotton. *Environmental and Experimental Botany,* vol. 28, no. 4, pp. 359-366.

Van Beynen, P.E., L. Soto and J. Polk (2008). Variable calcite deposition rates as proxy for paleo-precipitation determination as derived from speleothems in Central Florida, U.S.A. *Journal of Cave and Karst Studies,* vol. 70, no. 1, pp. 25-34.

Van Beynen, P.E., Y. Asmerom, V. Polyak, L. Soto and J.S. Polk (2007). Variable intensity of teleconnections during the late Holocene in subtropical North America from an isotopic study of speleothem from Florida. *Geophysical Research Letters,* vol. 34, pp. L18703.

Van der Meer, M., F. Sangiorgi, M. Baas, H. Brinkhuis, J.S. Sinninghe Damsté and S. Schouten (2008). Molecular isotopic and dinoflagellate evidence for Late Holocene freshening of the Black Sea. *Earth and Planetary Science Letters,* vol. 267, pp. 426-434.

Van Soelen, E.E., G.R. Brooks, R.A. Larson, J.S. Sinninghe Damsté and G. Reichart (2012). Mid- to late-Holocene coastal environmental changes in southwest Florida, USA. *The Holocene,* vol. 22, no. 8, pp. 929-938.

Versteegh, G.J.M., E. Schefuβ, L. Dupont, F. Marret, J.S. Sinninghe Damsté and J.H.F. Jansen (2004). Taraxerol and *Rhizophora* pollen as proxies for tracking past mangrove ecosystems. *Geochimica et Cosmochimica Acta,* vol. 68, no. 3, pp. 411-422.

Versteegh, G.J.M., H.J. Bosch and J.W. De Leeuw (1997). Potential palaeoenvironmental information of C24 to C36 mid-chain diols, keto-ols and mid-chain hydroxy fatty acids; a critical review. *Organic Geochemistry,* vol. 27, no. 1-2, pp. 1-13.

Vesala, T. (1998). On the concept of leaf boundary resistance for forced convection. *Journal of Theoretical Biology,* vol. 194, pp. 91-100.

Volkman, J.K., S.M. Barrett, G.A. Dunstan and S.W. Jeffrey (1992). C30-C32 alkyl diols and unsaturated alcohols in microalgae of the class Eustigmatophyceae. *Organic Geochemistry,* vol. 18, no. 1, pp. 131-138.

Vose, J.M. (1995). Vertical leaf area distribution, light transmittance, and application of the Beer-Lambert Law in four mature hardwood stands in the southern Appalachians. *Canadian Journal of Forest Research,* vol. 25, pp. 1036-1043.

Wagner-Cremer, F., T.H. Donders and H. Visscher (2010). Drought stress signals in modern and subfossil *Quercus laurifolia* (Fagaceae) leaves reflect winter precipitation in southern Florida tied to El Niño-Southern Oscillation activity. *American Journal of Botany,* vol. 97, no. 5, pp. 753-759.

Wagner, F., H. Visscher, W.M. Kürschner and D.L. Dilcher (2007). Influence of ontogeny and atmospheric CO_2 on stomata parameters of *Osmunda regalis*. *Courier Forschungsinstitut Senckenberg,* vol. 258, pp. 183-189.

Wagner, F., D.L. Dilcher and H. Visscher (2005). Stomatal frequency responses in hardwood-swamp vegetation from Florida during a 60-year continuous CO_2 increase. *American Journal of Botany,* vol. 92, no. 4, pp. 690-695.

Wagner, F., L.L.R. Kouwenberg, T.B. van Hoof and H. Visscher (2004). Reproducibility of Holocene atmospheric CO_2 records based on stomatal frequency. *Quaternary Science Reviews,* vol. 23, no. 18-19, pp. 1947-1954.

Wagner, F., R. Below, P.D. Klerk, D.L. Dilcher, H. Joosten, W.M. Kürschner and H. Visscher (1996). A natural experiment on plant acclimation: lifetime stomatal frequency response of an individual tree to annual atmospheric CO_2 increase. *Proceedings of the National Academy of Sciences of the United States of America,* vol. 93, no. 21, pp. 11705-11708.

Wall, D., B. Dale, G.P. Lohmann and W.K. Smith (1977). The environmental and climatic distribution of dinoflagellate cysts in modern marine sediments from regions in the North and South Atlantic Oceans and adjacent seas. *Marine Micropaleontology,* vol. 2, pp. 121-200.

Walsh, R. and A. Reading (1991). Historical changes in tropical cyclone frequency within the Caribbean since 1500. *Wurz. Geogr. Arz.,* vol. 80, pp. 199-240.

Wang, T., D. Surge and K.J. Walker (2011). Isotopic evidence for climate change during the Vandal Minimum from *Ariopsis felis* otoliths and *Mercenaria campechiensis* shells, southwest Florida, USA. *The Holocene,* vol. 21, no. 7, pp. 1081-1091.

Wang, C., D.B. Enfield, S. Lee and C.W. Landsea (2006). Influences of the Atlantic Warm Pool on Western Hemisphere summer rainfall and Atlantic hurricanes. *Journal of Climate,* vol. 19, no. 12, pp. 3011-3028.

Ward, J.K. and J.K. Kelly (2004). Scaling up evolutionary responses to elevated CO_2: lessons from *Arabidopsis*. *Ecology Letters,* vol. 7, pp. 427-440.

Warren, C.R. (2008). Stand aside stomata, another actor deserves centre stage: the forgotten role of the internal conductance to CO_2 transfer. *Journal of Experimental Botany,* vol. 59, pp. 1475-1487.

Watts, W.A. (1980). The late Quaternary vegetation of south-eastern United States. *Annual Review of Ecology and Systematics,* vol. 11, pp. 387-409.

Watts, W.A. (1975). A late Quaternary record of vegetation from Lake Annie, southcentral Florida. *Geology,* vol. 3, pp. 344-346.

Watts, W.A. (1971). Postglacial and Interglacial vegetation history of southern Georgia and central Florida. *Ecology,* vol. 52, pp. 676-690.

Watts, W.A. (1969). A pollen diagram from Mud Lake, Marion County, North Central Florida. *Geological Society of America Bulletin,* vol. 90, pp. 631-642.

Watts, W.A. and B.C.S. Hansen (1994). Pre-Holocene and Holocene pollen records of vegetation history from the Florida peninsula and their climatic implications. *Palaeogeography, Palaeoclimatology, Palaeoecology,* vol. 109, no. 2-4, pp. 163-176.

Watts, W.A., B.C.S. Hansen and E.C. Grimm (1992). Camel Lake: a 40,000-yr record of vegetation and forest history from northwest Florida. *Ecology,* vol. 73, no. 3, pp. 1056-1066.

Willard, D.A. and C.E. Bernhardt (2011). Impacts of past climate and sea level change on Everglades wetlands: placing a century of anthropogenic change into a late-Holocene context. *Climatic Change,* vol. 107, no. 1-2, pp. 59-80.

Willard, D.A., C.E. Bernhardt, G.R. Brooks, T.M. Cronin, T. Edgar and R. Larson (2007). Deglacial climate variability in central Florida, USA. *Palaeogeography, Palaeoclimatology, Palaeoecology,* vol. 251, no. 3-4, pp. 366-382.

Willard, D.A., C.E. Bernhardt, C.W. Holmes, B. Landacre and M. Marot (2006). Response of Everglades tree islands to environmental change. *Ecological Monographs,* vol. 76, pp. 565-583.

Willard, D.A., C.E. Bernhardt, L. Weimer, S.R. Cooper, D. Gamez and J. Jensen (2004). Atlas of pollen and spores of the Florida Everglades. *Palynology,* vol. 28, no. 1, pp. 175-227.

Willard, D.A., T.M. Cronin and S. Verardo (2003). Late-Holocene climate and ecosystem history from Chesapeake Bay sediment cores, USA. *The Holocene,* vol. 13, no. 2, pp. 201-214.

Willard, D.A., C.W. Holmes and L.M. Weimer 2001 (2001a). The Florida Everglades ecosystem: climatic and anthropogenic impacts over the last two millennia. *Bulletins of American Paleontology,* vol. 361, pp. 41-55.

Willard, D.A., L.M. Weimer and W.L. Riegel (2001b). Pollen assemblages as paleoenvironmental proxies in the Florida Everglades. *Review of Palaeobotany and Palynology,* vol. 113, no. 4, pp. 213-235.

Williams, M. (1996). Modelling the soil-plant-atmosphere continuum in a *Quercus* and *Acer* stand at Harvard Forest: the regulation of stomatal conductance by light, nitrogen, and soil/plant hydraulic properties. *Plant, Cell and Environment,* vol. 19, pp. 911-927.

Wingard, G.L., S. Ishman, T.M. Cronin, L.E. Edwards, D.A. Willard and R.B. Halley (1995). Preliminary analysis of down-core biotic assemblages; Bob Allen Keys, Everglades National Park, Florida Bay. Report no. 95-628, USGS.

Winkler J.G., P.R. Sanford and S.W. Kaplan (2001). Hydrology, vegetation, and climate change in the southern Everglades during the Holocene. *Bulletins of American Paleontology,* vol. 361, pp. 57-97.

Witkowski, A., H. Lange-Bertalor and D. Metzeltin (2000). Diatom flora of marine coasts I. *Iconographia Diatomologica,* vol. 7, pp. 1-925.

Wolin, J.A. and J.R. Stone (2010). Diatoms as indicators of water level change in freshwater lakes. In: The diatoms: applications for environmental and earth sciences. Eds. J.P. Smol and E.F. Stoermer. Cambridge University press, Cambridge, pp.174-185.

Wood, G.D., A.M. Gabriel and J.C. Lawson (1996). Chapter 3. Palynological techniques – processing and microscopy. In: Palynology: principles and applications; American Association of Stratigraphic Palynologists Foundation. Ed. J.a.M. Jansonius D.C. pp. 29-50.

Woodruff, J.D., J.P. Donnelly, D. Mohring and W.R. Geyer (2008). Reconstructing relative flooding intensities responsible for hurricane-induced deposits from Laguna Playa Grande, Puerto Rico. *Geology,* vol. 36, no. 5, pp. 391-394.

Woodward, F.I. (1987). Stomatal numbers are sensitive to increases in CO_2 from pre-industrial levels. *Nature,* vol. 327, pp. 617-618.

Wullschleger, S.D. (1993). Biochemical limitations to carbon assimilation in C3 plants- a retrospective analysis of the A/CI curves from 109 species. *Journal of Experimental Botany,* vol. 44, pp. 907-920.

Wullschleger, S.D., T.J. Tschaplinski and R.J. Norby (2002). Plant water relations at elevated CO_2 implications for water-limited environments. *Plant, Cell and Environment,* vol. 25, pp. 319-331.

Wynn, J.G. (2003). Towards a physically based model of CO_2-induced stomatal frequency response. *New Phytologist,* vol. 157, pp. 394-398.

Xu, L., C.M. Reddy, J.W. Farrington, G.S. Frysinger, R.B. Gaines, C.G. Johnson, R.K. Nelson and T.I. Eglinton (2001). Identification of a novel alkenone in Black Sea sediments. *Organic Geochemistry,* vol. 32, no. 5, pp. 633-645.

Ziegler, M., D. Nürnberg, C. Karas, R. Tiedemann and L. Lourens (2008). Persistent summer expansion of the Atlantic Warm Pool during glacial abrupt cold events. *Nature Geoscience,* vol. 1, no. 9, pp. 601-605.

Zonneveld, K.A.F., G.J.M. Versteegh and G.J. de Lange (1997). Preservation of organic-walled dinoflagellate cysts in different oxygen regimes: a 10,000 year natural experiment. *Marine Micropaleontology,* vol. 29, no. 3-4, pp. 393-405.

170 x 240 mm

Samenvatting

Vanaf het begin van de Industriële Revolutie in de 19e eeuw is de concentratie koolstofdioxide (CO_2) in de atmosfeer buitengewoon snel toegenomen, voornamelijk door de grootschalige verbranding van fossiele brandstoffen en veranderend grondgebruik. Tegelijkertijd is het klimaat op mondiaal niveau sterk opgewarmd, wat nu al heeft geleid tot veranderde weerpatronen en een zeespiegelstijging. De verwachting is dat bij toekomstige maatschappelijke- en industriële ontwikkelingen deze veranderingen zich nog sterker zullen ontwikkelen. Vooral neerslagpatronen worden mogelijk extremer, met minder frequente maar zwaardere buien, maar ook extreme droogte. Daarbij wordt ook verwacht dat door de opwarming van het oceaan oppervlak tropische cyclonen zich tot een grotere kracht en levensduur kunnen ontwikkelen. In toenemende mate wordt erkend dat vegetatie een rol speelt in klimaatverandering en de regulering van de hydrologische cyclus, doordat planten hun transpiratiesnelheid verlagen als CO_2 toeneemt. Hoe sterk deze 'plant fysiologische' sturing is en tot hoe ver in de toekomst dit een rol speelt is echter nog niet goed gekwantificeerd. Omdat deze biosfeer-atmosfeer wisselwerking kan leiden tot niet-lineaire reacties van het klimaat is het van groot belang dit proces ook in beschouwing te nemen naast veranderingen als gevolg van het broeikaseffect.

Vooral in laaggelegen en dichtbevolkte kustgebieden in orkaangevoelige regio's zoals Florida, in het zuidoosten van de Verenigde Staten, kunnen veranderingen in klimaat en de zeespiegel negatieve gevolgen hebben voor de maatschappij en de economie. Door de nu al hoge druk op de beschikbaarheid van zoetwater voor landbouw, stedelijke- en natuurlijke gebieden, is dit gebied zeer gevoelig voor toekomstige veranderingen in het hydrologische 'regime'. Florida heeft een (sub)tropisch klimaat met over het algemeen droge winters en extreem natte zomers, die worden gekarakteriseerd door talrijke onweersbuien en tropische stormen. Vanwege de doorlatende ondergrond van (opgeloste) kalksteen en zand blijft regenwater maar relatief kort aan het oppervlak liggen. Vóór de grootschalige aanpassingen van het landschap door mensen was een grootste deel van het oppervlak begroeid met zogenaamde 'pine flatwoods' en droge eiken-dennen bossen. Uitgebreide moerasgebieden of 'wetlands' ontwikkelden zich waar het grondwater op of boven het oppervlak komt, vooral in de zuidelijke punt van het schiereiland. Schijnbaar onbeduidende verschillen in (grond)waterdiepte, chemische samenstelling van het water en jaarlijkse periode van overstroming ('hydroperiode') kunnen leiden tot duidelijk te onderscheiden ecosystemen. Een beter begrip van toekomstige veranderingen in deze hydrologische kenmerken door zeespiegelstijging en klimaatveranderingen is van groot belang voor zowel het behoud en de restauratie van natuurlijke gebieden, als de planning voor de agrarische- en stedelijke hoofdstructuur.

Terwijl klimaat en landschappelijke veranderingen over de laatste decennia goed zijn gedocumenteerd, moeten de trends van verder in het verleden worden bepaald uit zogenaamde

'proxy data'. Metingen op lange ijskernen geven aan dat CO_2 gedurende het Holoceen, ongeveer de aflopen 11,7 ka (kiloannum = 1000 jaar voor heden), redelijk constant is gebleven tot de 19e eeuw. Daarentegen zijn grootschalige trends in zeespiegel en klimaat gedurende deze periode afgeleid uit verschillende natuurlijke archieven in de Caribische Zee en Golf van Mexico. De relatieve zeespiegel is tientallen meters gestegen na de beëindiging van de laatste ijstijd (vanaf 11,7 ka). Ook was gedurende het vroeg- en midden Holoceen de temperatuur van het zeewater in deze omgeving enkele graden warmer dan tegenwoordig, als gevolg van orbitaal geforceerde sterkere zonne-instraling. Tegelijkertijd was ook zomerpositie van de 'Intertropische Convergentie Zone' regenband meer noordelijk, dichter bij Florida. Er bestaat een sterke teleconnectie tussen Florida en het grootschalige oceaanatmosfeer systeem 'El Niño-Southern Oscillation', wat hier tot uitzonderlijk hoge neerslag in het droge winterseizoen leidt. Onderzoek uit Zuid Amerika geeft aan dat dit systeem pas over de laatste 5000 jaar tot zijn huidige intensiteit is ontwikkeld.

Door te kijken naar hoe organismen en het landschap zich in het verleden aanpasten bij deze veranderingen, kan men zich beter voorbereiden op de verwachte veranderingen in de toekomst. Beschikbare studies in Florida beschrijven vooral veranderingen in hydrologische condities van de moerassen en de ondiepe zee in het zuidelijke deel van de staat, en de hooggelegen Lake Wales Ridge in centraal Florida. Studies op veenkernen uit de moerassen van zuid Florida tonen schommelingen in nattigheid aan met periodes van tientallen tot honderden jaren gedurende de laatste 5000 jaar. Afwisselend nattere-drogere condities op land met periodes van duizenden jaren zijn afgeleid van studies op meerafzettingen uit centraal Florida. De ruimtelijke verdeling over Florida en resolutie in het tijdsbereik van de verschillende studies maken het niet goed mogelijk om een omvattend beeld te vormen van de hydrologische veranderingen gedurende het Holoceen, en de sturende processen erachter. Hiervoor is gedetailleerd onderzoek nodig in gebieden die gevoelig zijn voor klimaat- en zeespiegel gestuurde veranderingen, verspreid over een groter gebied.

Bij het onderzoek dat in dit proefschrift is beschreven, is specifiek gekeken naar veranderingen in 'overgangs' milieus, zoals estuaria en moerassen (wetlands). De meeste biota, of organismen, die daar leven hebben heel specifieke voorwaarden voor hun leefomgeving, waaronder (grond)waterdiepte, hydroperiode, saliniteit, nutriënt beschikbaarheid en waterstroming, welke direct of indirect weer worden bepaald door klimaat en zeespiegel. Sommige overblijfselen van deze organismen blijven goed bewaard in natte afzettingsmilieus waarin of waarbij ze leven, zoals venen, meren en zeebodems. Het analyseren van organische cysten van in het wateroppervlak levende dinoflagellaten (dinocysten) en van de silicaatskeletjes van diatomeeën, heeft zich bewezen een waardevolle methode te zijn voor het beschrijven van hydrologische veranderingen in het aquatisch milieu. Planten zijn direct afhankelijk van zoetwaterbeschikbaarheid, maar er bestaat een grote variatie tussen soorten voor de specifieke condities. Daarom zijn plant-gerelateerde proxies op basis van stuifmeel (pollen) en bladresten uitermate geschikt voor het traceren van veranderingen in hydrologische condities. Veranderingen in de soortensamenstelling van deze organismen over de diepte van

de afzetting geven een indicatie voor veranderingen in de milieuomstandigheden in de tijd. Naast bladresten bewaard in veen, biedt ook historisch bladmateriaal verzameld door herbaria een mogelijkheid meer inzicht te krijgen in de potentiële transpiratiesnelheid van planten. Het toepassen van meerdere proxies om veranderingen in bepaalde milieus te reconstrueren is de sleutel naar een meer robuuste interpretatie van hydrologische variabiliteit.

Samengevat ligt de doelstelling van dit onderzoek op het beschrijven van de 'achtergrond' variatie in hydrologische regimes gedurende het Holoceen. Hiervoor wordt gebruik gemaakt van palynologische, micropaleontologische en (paleo)botanische proxies. De volgende vragen werden gesteld: hoe heeft de Holocene zeespiegelstijging de kust- en binnenlandse milieus beïnvloed? Is er een verband tussen neerslagpatronen in Florida en de zeewatertemperatuur van omliggende zeeën? Bestaat er een patroon in de regionale orkaanactiviteit gedurende het Holoceen? Hoe sterk is de plant fysiologische forcering op het klimaat en de hydrologische kringloop bij toenemende CO_2, en hoe lang speelt dit nog een rol?

In **hoofdstuk 1** worden de milieuveranderingen als gevolg van de stijgende zeespiegel beschreven, aan de hand van biomarker, pollen, dinoflagellaten cysten en diatomeeën samenstellingen in mid tot laat Holocene estuariene afzettingen uit Tampa Bay. Hieruit kan worden opgemaakt dat het bemonsterde gebied ongeveer 7,5 ka is overspoeld en het gebied van een (brakwater) moeras in een ondiepe lagune veranderde. Een verschuiving in de dinocysten en diatomeeën samenstelling naar meer open mariene soorten, toenemende concentraties van mariene biomarkers en een toename in de 'Diol Index' geven aan dat het estuarium in toenemende mate zouter wordt tussen 7.5 ka en nu. Deze studie verfijnt eerdere reconstructies van de landschappelijke ontwikkeling door het gelijktijdig bestuderen van veranderingen op land en in het estuarium.

Ondanks de veelzijdige informatie is de resolutie in tijd van de multi-proxy studie in Tampa Bay te laag om mogelijke klimaatgestuurde veranderingen te bepalen. Zoetwater afvoer naar het estuarium wordt voor een belangrijk deel bepaald door neerslag. In Florida is de regionale overgang van eiken naar dennen gedomineerde vegetatie na ongeveer 6,5 ka over het algemeen geïnterpreteerd als een grootschalige verandering naar nattere condities. Deze 'nattere' vegetatie blijft aanwezig tot de tegenwoordige tijd, terwijl op verschillende locaties in het Caribisch gebied een trend naar drogere condities plaatsvindt na ~4,5 ka. Om deze mid tot laat Holocene dennenvegetatie beter te kunnen interpreteren zijn in **hoofdstuk 2** de regionale vegetatieveranderingen en rivierafvoer patronen gelijktijdig bestudeerd in estuarine afzettingen van Charlotte Harbor. De aanzienlijke afname in eikenpollen na ~7 ka komt overeen met de pollenstudies van Tampa Bay en het binnenland. Deze trend loopt gelijk aan een hogere inspoeling van terrestrisch materiaal en toenemende aanwezigheid van dinocyst *Lingulodinium machaerophorum* in het estuarium, een soort die bloeit bij waterstratificatie en hoge nutriënten inspoeling. Een sterk verminderde inspoeling van terrestrisch materiaal na ~4.5 ka suggereert verminderde waterafvoer, mogelijk door afgenomen neerslag. De samenstelling van dinocysten suggereert echter dat waterafvoer weer toeneemt na ~2.8 ka. Al kan op basis

van deze studie niet met zekerheid worden vastgesteld hoe de waterafvoer verband houdt met neerslagpatronen en de ontwikkeling van het landoppervlak, de hydrologische condities op land lijken meer variabel te zijn dan is voorgesteld door de continue aanwezigheid van de dennenvegetatie.

In Tampa Bay en Charlotte Harbor, beschreven in hoofdstukken 1 en 2, zijn laagjes grover (zand en schelpfragmenten) materiaal aanwezig in het over het algemeen fijne estuariene sediment. In dergelijke milieus worden deze vaak afgezet bij hoog-energetische condities zoals stormgolven, en zijn dus een mogelijke indicator voor tropische stormactiviteit in het verleden. Als over periodes van duizenden jaren de zeespiegel stijgt, veranderen daarbij ook de ondiep mariene afzettingscondities en kan een incompleet beeld ontstaan van vroegere stormactiviteit. In **hoofdstuk 3** wordt beschreven hoe dit probleem mogelijk omzeild kan worden door naast lithologische informatie ook dinocysten samenstelling en waterstof isotopen ratio in terrestrisch organisch materiaal te bestuderen. De eerste wordt beïnvloed door wind/ golf energie in het estuarium, terwijl de laatste de isotopische samenstelling van regenwater weergeeft; beide worden sterk beïnvloed door tropische stormen. Naast clusters van grovere laagjes zijn in het fijne sediment tijdelijke toenames van mariene dinocysten in een anders lagune-achtig milieu geobserveerd. Gelijk met de mariene dinocysten vindt ook een sterke verlichting in de waterstof isotopensamenstelling van plantenwassen plaats. Dat de dinocysten in allebei de estuaria dezelfde veranderingen vertonen is een sterke aanwijzing voor de sturing van een grootschalig proces, mogelijk tropische stormen. Het gecombineerde lithologische, palynologische en geochemische bewijs wijst op periodes met toegenomen stormactiviteit tussen ~6,4-5,5 ka, ~5,0-4,0 ka en ~3,2-1,9 ka, wat grotendeels overeenkomt met andere reconstructies in de Golf van Mexico en Caribische Zee. Verplaatsingen van de zomerpositie van de Bermuda High over periodes van duizenden jaren wordt voorgesteld als belangrijke sturende factor voor dit regionale patroon. Deze studie toont aan dat een completer beeld van vroegere stormactiviteiten kan worden verkregen als er naar meerdere proxies wordt gekeken.

De palynologische studies van meren in centraal Florida en de hierboven beschreven estuaria geven grootschalige veranderingen in vegetatie en waterafvoer. Door het grote stroomgebied zijn deze milieus minder geschikt voor het reconstrueren van kleinschalige hydrologische veranderingen. Palynologisch onderzoek in de wetlands van zuid Florida heeft aangetoond dat zulke milieus heel gevoelig zijn voor kleine veranderingen in lokale hydrologie door neerslag, maar er bestaat onenigheid over de richting van verandering gedurende het laat Holoceen. Om een beeld te krijgen van regionale hydrologische patronen is gedetailleerde informatie van andere locaties nodig, en de wetlands van de Lake Wales Ridge in centraal Florida zijn tot nu toe nog nauwelijks bestudeerd. In **hoofdstuk 4** worden lokale hydrologische veranderingen over de laatste ~2,5 ka beschreven op basis van pollen- en diatomeeën samenstellingen in veenafzettingen van Highlands Hammock State Park. De ontwikkeling van moeras condities rond 2,5 ka wijzen op een eerste vernatting, waarna de geobserveerde trend naar drogere condities kan worden verklaard door een langzame invulling van het moerasbekken. De uitbreiding van waterplanten tussen 1,3-1,0 ka wijst op een tijdelijke vernatting. Zowel de

vorming van het wetland als de uitbreiding van waterplanten zijn waarschijnlijk het gevolg van een toename in neerslag, als gevolg van hogere zeewatertemperaturen van de Golf van Mexico en Atlantische Oceaan. De tweede natte fase en daaropvolgende sterke verdroging in de afgelopen 1300 jaar kunnen worden gekoppeld aan respectievelijk het vroeg Middeleeuws Klimaatoptimum en Kleine IJstijd. Opvallende veranderingen in zowel de vegetatie- als de diatomeeën samenstelling gedurende de 20e eeuw kunnen worden toegeschreven aan de bouw van kanalen en dijken in het park, bedoelt om het gebied te beschermen tegen natuurbranden.

In de eerste 4 hoofdstukken is klimaatsvariabiliteit gereconstrueerd met behulp van de biotische respons op hydrologische veranderingen. Andersom spelen landplanten ook een belangrijke rol in het reguleren van de energie en waterbalans van onze planeet, door het transpireren van water door de poriën of stomata op het bladoppervlak. Een primaire respons van C3 planten op toenemende CO_2 in de atmosfeer is om waterverlies door transpiratie te verminderen en tegelijkertijd assimilatie te verhogen. Daarom is het van groot belang deze aanpassing van planten op de toekomstige toename van atmosferische CO_2 te bepalen. Tot nu toe is het effect van CO_2 toename op stomatale doorlatendheid over periodes van tientallen jaren nog niet goed gekwantificeerd. In **hoofdstuk 5** wordt getoond dat in 9 verschillende plantensoorten uit Florida de maximale 'stomatale doorlatendheid' met 34% (±12%) afneemt als respons op de afgelopen CO_2 stijging van 100 ppm. Dit is het gevolg van een aanpassing in zowel stomatale dichtheid als poriegrootte. De soort-specifieke aanpassing lijkt te worden bepaald door de evolutionaire achtergrond van de soorten. Ook al volgen angiospermen en gymnospermen een andere aanpassingsstrategie, het leidt een coherente verandering van maximale stomatale doorlatendheid over de afgelopen eeuw. De optimalisatie van assimilatie tegenover waterverlies, wat hier wordt beschreven, is essentieel voor het bepalen van de plant fysiologische forcering onder vroegere en toekomstige CO_2 concentraties.

Schattingen van de kracht en duur van deze plantfysiologische CO_2 forcering op het klimaat met verder toenemende CO_2 worden gegeven in **hoofdstuk 6**. Hiervoor zijn modellen ontwikkeld en gevalideerd die structurele stomatale aanpassingen simuleren, gebaseerd op de diffusie van CO_2 en waterdamp door de stomata, fotosynthese, en de optimalisatie van koolstof 'winst' tegenover waterverlies. Het model reproduceert de geobserveerde structurele aanpassing zoals beschreven in hoofdstuk 5 goed, en voorspelt dat planten zich nog voorbij een verdubbeling van de huidige CO_2 zullen aanpassen, tot de grens van hun fenotypische plasticiteit is bereikt. Simulaties laten zien dat bij een verdubbeling van huidige CO_2 de jaarlijkse transpiratieflux boven de bossen van Florida significant zal afnemen. Op basis hiervan wordt geconcludeerd dat de aanpassing van planten op toenemende CO_2 de waterkringloop en het klimaat substantieel veranderd en dat dit proces nog de komende eeuwen zal doorgaan.

170 x 240 mm

Dankwoord/ Acknowledgements

I get by with a little help from my friends
I get high with a little help from my friends
Going to try with a little help from my friends
(with a little help from my frieeeeeeeends!)

(John Lennon and Paul McCartney, 1967)

Toen ik begon met dit PhD-onderzoek/ avontuur leken 4 jaar zeeën van tijd, maar als ik zo terug kijk is het eigenlijk allemaal zo snel voorbij gegaan! Na vele uren achter de microscoop, tripjes naar de USA, congressen en heel veel versies tekst en grafieken (… final, ...final_v2, ...final_new, ...final_final!!!) is dan nu mijn boekje af! Dat was niet gelukt zonder de hulp van heel veel mensen.

Voor de mogelijkheid zoveel te reizen en nieuwe mensen te ontmoeten moet ik directe begeleider dr., bijna prof. dr., Rike Wagner-Cremer bedanken. In 2006 is het High Potential project 'Hurricanes and Global Change' opgezet door Rike, Stefan Dekker en Gert-Jan Reichart, met Florida als thuisbasis voor het onderzoek. Toen ik solliciteerde op deze baan was ik gelijk over de streep door Rike's enthousiasme voor Florida; de fascinerende landschappen en mensen, en natuurlijk ook de cocktails op het strand en het heerlijke 'winter'weer. Rike, dank je wel dat je voor me klaarstond met advies, hulp en een biertje als ik het echt nodig had. Stefan, co-promotor 2, ik vond het heel fijn dat ik altijd bij je binnen mocht wandelen om te praten over werk en niet-werk. En Gert-Jan, bedankt voor je humor en relativeringsvermogen! Andy Lotter is de afgelopen 3 jaar en 11 maanden betrokken geweest bij het onderzoek als mijn promotor, bedankt dat ik altijd met vragen bij je terecht kon. En Hans Middelkoop, bedankt dat jij op de valreep van mijn AiO-tijd mijn tweede promotor wilt zijn!

Voor mij was de goede samenwerking binnen dit project met de andere 'Hurricane' AiO's Els (of Elly?) en Hugo (Uugu Modelboy!) onmisbaar. Els, onze vrijdagmiddag 'mix-and-match' van nieuwe datasets uit Charlotte Harbor en Tampa Bay, onder het genot van chocola en thee, waren altijd de beste afsluiting van de week. En Hugo ik vond het heerlijk om naar jouw gefilosofeer over het 'gedrag' van planten te luisteren (hoe werkt dat??). Zonder jullie vriendschap en samenwerking was dit proefschrift heel anders geworden, en ik ben vereerd bij jullie allebei paranimf te mogen zijn. Go Team Hurricane!

Een multi-proxy onderzoek was nooit gelukt zonder zoveel experts in de buurt! Timme Donders en Francesca Sangiorgi waren mijn trainers in Florida pollen- en dinocystkunde. Bedankt voor alle nuttige discussies en hulp, op de uni, en bij jullie aan de keukentafel onder

het genot van een versgebakken pizza. Ook Holger Cremer, die onze Master studenten begeleidde bij het diatomeeën werk, bedankt voor je advies en vooral nuchtere kijk op dingen!

All this work would not have been possible without the assistance and hospitality of many people in Florida! Gregg Brooks and Rebekka Larson from Eckerd College, thanks for all the help with the estuarine records. Emily Nodine and Evelyn Gaiser, I had a great time visiting you at the FIU in Miami, thanks so much for the discussions and your hospitality. Ken Alvarez and Terry Hingtgen, and all the other Florida State Park people, thank you for the support and showing us around in your amazing Florida natural 'backyard'. Also many thanks to David Dilcher, for the useful discussions on the Florida leaf work. I'll never forget the little walk we did in your private swamp! Thanks to Kent Perkins of the University of Florida herbarium in Gainesville for the assistance in selecting leaf samples. And last but least, and not in Florida, many thanks to Deb Willard, Tom Cronin and Chris Bernhardt of the US Geological Survey in Reston, VA, for the many fruitful discussions and your enthusiasm about Florida, and for making me feel at home during the weeks I visited you guys.

Ik had er nooit aan gedacht een promotieonderzoek te doen als Wim Hoek me niet heel erg enthousiast had gemaakt voor de paleo-wereld gedurende mijn Master! Wim, jouw humor en je vertrouwen in mij heeft me nog ver na mijn Master-tijd gesteund, bedankt!

Over de aflopen 4 jaar heb ik toch de meeste (wakkere) uren op het lab van 'Pal en Pal' doorgebracht, voor heel veel werken maar ook heel veel lol! Dat laatste is voor een belangrijk deel te danken aan de geweldige groep AiO's (lotgenoten) die de LPP altijd weet te verzamelen. Van de oude ploeg: Emi, Peter S., Maarten, Frederike, Judith, Nina and Micha, met jullie was er altijd iemand waarbij ik steun kon vinden, of om een biertje(s) mee te drinken. Ik ben zo blij dat we elkaar nog steeds zien voor een hapje en drankje, die gezelligheid vergaat hopelijk nooit! En de nieuwe ploeg: Alex, Joost, Mariska, Mirja, Arjen, Johan and Niels, nu is het jullie beurt deze troep legendarisch te maken! Met het nieuwe futsal-team zijn 'we' in ieder geval aardig onderweg… Tussen 'oud' en 'nieuw' zat ik samen met Sander en Peter. Gegroeid van 'buurmannen' op de zaak naar fantastische vrienden; ik kan me het LPP niet voorstellen zonder jullie, gewoon omdat dat voor mij nooit zo is geweest! Bedankt dat ik (bijna) altijd welkom was in de (Henk's?) Nieuwe Leerstoel, om te kletsen of gewoon stil te werken. Sander, ik blijf de droom vasthouden om later (als we groot zijn) echt een bierbrouwerij met eetcafé in Utrecht te openen!

Something old, something new, (no offense! op de AiO-schaal), mijn lieve paranimfen Frederike en Alex. Jullie hebben elkaar afgewisseld als vaste steunpilaar op werk de afgelopen 4 jaar, en ik ben zo blij met jullie vriendschap! You girls rock!

Henk en Appy, de Big Boys van Marine Palynologie, bedankt voor jullie steun en advies over dino's, en zaken die niks met dino's te maken hebben, op het terras of tijdens een potje poker. En voor de gastvrijheid, Henk, ik hoorde ook een beetje bij jullie groep.

Het LPP zou nooit zo'n goed geoliede machine zijn zonder Marjolein, Jan, Natasja, Hans en ook Leonard; bedankt dat jullie altijd klaar stonden om te helpen! Hiernaast zou het LPP niet hetzelfde zijn zonder al die andere bijzondere mensen, zoals Han en Johan (waar ik altijd met blaadjesvragen terecht kon), Zwier, Roel, Henk Visscher (die altijd goed advies klaar heeft) en Gea. En ook niet zonder alle leuke studenten, waarvan ik Maud (extreme sporten-maatje), Linda (gaan we weer vallende sterren spotten?), Christof (mijn allround favoriete Belg), Floortje (hoe spel je die soortnaam?) en Loes (de rattenvanger van Miami) in het bijzonder wil bedanken voor de samenwerking en/of de vermakelijke tijd samen! Buiten de LPP waren de gezelligheid met Lennart, Marie-Louise, Anna, Jos en Marieke, Gilles en Nelleke van FG, en heel veel anderen voor mij ook onmisbaar. En Margot en Ton van de (carto)grafische vormgeving, bedankt voor de hulp met de figuren, ik ben blij dat jullie bereid waren alle 'opmaak truukjes' twee keer uit te leggen.

Ik wil al mijn vrienden buiten werk vooral bedanken voor hun geduld! Zij herinnerden me er steeds aan dat er een (heel leuk!) leven is naast de uni, als ik dat soms leek te vergeten. De groep van oud studiegenoten Joachim en Lieza, Dirk en Liselotte, Joep en Evelien, Buijs en Merel, en Pieter en Jonna, maar ook mijn oude veldwerkmaatje Saskia, m'n Suuske, Banff-buddy Daan en Maaike, en heel veel anderen die ik nu vast vergeet… Ik heb door de drukte flink gespijbeld bij sociale activiteiten, maar dat is nu gelukkig even voorbij!

Uiteindelijk zijn het mijn ouders die het zaadje hebben geplant voor mijn interesse in aardwetenschappen en biologie: mamma, jouw grote passie voor de natuur en alles wat erin leeft (behalve spinnen!), en pappa, jouw drive om altijd te willen weten hoe iets in elkaar zit, en het letterlijk uit elkaar te halen om erachter te komen hoe het werkt. Heel erg bedankt voor jullie interesse en nooit aflatende vertrouwen in dat wat ik besloot te gaan doen wel goed zou komen. Maris, mijn lieve zusje, bedankt voor je steun en relativeringsvermogen (doe nou maar gewóón!). En bedankt Oma, samen met Opa, voor de verwondering en trots als ik weer met Grote Verhalen aankwam. En ook Peter, Laura, Vincent en Naomi, bedankt voor jullie interesse en gezelligheid.

En natuurlijk nogmaals Peter… collega, goede vriend, en nu ook mijn vriendje. Dank je wel dat je er altijd voor me bent, in alle hiervoor genoemde hoedanigheden. Je hebt me in de afgelopen jaren in meer dingen gesteund dan je misschien beseft. Letterlijk, als ik moeite had een Weense kroeg uit te komen, maar ook met heel veel geduld tijdens de absolute chaos in huis en in mijn hoofd die het proefschrift afronden met zich meebracht. Ik kijk er naar uit nu ook gewoon eens vrije tijd met jou door te brengen!

170 x 240 mm

Curriculum Vitae

Emmy Lammertsma werd op 11 oktober 1982 geboren in Haarlem, Nederland. In 2000 behaalde zij haar VWO Atheneum diploma aan het College Hageveld te Heemstede, waarna ze een jaar gewerkt en gereisd heeft in Spanje en Canada. In 2001 begon zij met de opleiding Aardwetenschappen aan de Universiteit Utrecht. Na behalen van haar propedeuse Aardwetenschappen in 2002 jaar volgde zij de Bachelor opleiding Fysische Geografie (UU), en Master opleiding Kwartair Geologie en Klimaatsverandering (UU). Het Master afstudeeronderzoek verrichte ze bij Dr. Wim Hoek, en omvatte zowel het karteren van de ondergrond in het Niers-Rijn dal in Duitsland, als het reconstrueren van laatglaciale vegetatie en klimaatsveranderingen in dit gebied. Ook liep ze stage bij het TNO Bouw en Ondergrond onder begeleiding van Dr. Frans Bunnik en Dr. Jeroen Schokker. Hier werkte zij aan een reconstructie van laatglaciale tot vroege Holocene rivierterras- en vegetatie ontwikkeling van de Zandmaas vallei, Limburg. Na het behalen van haar Master diploma in 2007 bleef zij werkzaam bij het TNO als palynoloog, tot ze in 2008 begon met haar promotieonderzoek bij de vakgroep Palaeoecologie (UU). Haar onderzoek valt binnen het multidisciplinaire project 'Hurricanes and Global Change', geïnitieerd door Dr. F. Wagner-Cremer, Dr. S.C. Dekker en Dr. G.-J. Reichart, en gefinancierd door het 'High Potential' programma van de Universiteit Utrecht. Haar promotoren zijn Prof. dr. H. Middelkoop en Prof. dr. A.F. Lotter, en haar copromotoren zijn Dr. F. Wagner-Cremer en Dr. S.C. Dekker. De resultaten van haar promotieonderzoek zijn beschreven in dit proefschrift.

170 x 240 mm